DISCOVERY OF A DOUBLE BINARY AND NONRADIAL PULSATIONS IN THE Be STAR OMICRON ANDROMEDAE

By

GRANT MICHAEL HILL

B.Sc., The University of British Columbia, 1986

A THESIS SUBMITTED IN PARTIAL FULFILLMENT OF

THE REQUIREMENTS FOR THE DEGREE OF

MASTER OF SCIENCE

in

THE FACULTY OF GRADUATE STUDIES

Department of Geophysics and Astronomy

We accept this thesis as conforming

to the required standard

THE UNIVERSITY OF BRITISH COLUMBIA

April 1988

In presenting this thesis in partial fulfilment of the requirements for an advanced degree at the University of British Columbia, I agree that the Library shall make it freely available for reference and study. I further agree that permission for extensive copying of this thesis for scholarly purposes may be granted by the head of my department or by his or her representatives. It is understood that copying or publication of this thesis for financial gain shall not be allowed without my written permission.

Department of _Geophysics and Astronomy_

The University of British Columbia
1956 Main Mall
Vancouver, Canada
V6T 1Y3

Date _April 28/88_

Abstract

The multiple star system omicron Andromedae has been studied using high signal-to-noise ratio Reticon spectra. The narrow absorption features superimposed on the rotationally broadened Mg II λ 4481 line of o And A are almost certainly from the spectrum of o And B which is shown to be a double-lined spectroscopic binary with a period of 33 days. The speckle interferometrically measured separations of A–a and A–B indicate that the system contains at least two binaries separated by some 25 AU, based on a parallax of 0.015 ± 0.008 arcseconds. Based on this parallax the A–a separation of is about 4 AU. The two stars which make up the unresolved spectroscopic binary o And B are separated by about 0.4 AU based on an orbital solution. The periods, based on the parallax and reasonable mass estimates, for A–a and Aa–B, are on the order of four and thirty years respectively.

The two stars which constitute o And B are shown to most likely be late B stars of luminosity class V-IV. After compensating for the presence in the spectrum of a contribution from component B, o And A is reclassified as B5IIIe. The spectral type of o And a is not known and no contribution to the spectrum from it is observed.

High signal-to-noise time series of spectra have revealed the presence of nonradial pulsations. An intermediate order, $l = 6$ mode, reveals itself through moving subfeatures in the line profiles. Line width variations are detected which probably arise from an $l = 2$ low order mode. The co-existence of these two modes is capable of explaining the 1.57 day photometric variations. This period is twice that of the line width variations. Rapid radial velocity variations measured from the line wings were found but the

line profile variations and the nature of the light curve do not support the existence of a fifth star. The measured radial velocity variations could be a result of the underlying profile variations as opposed to motion of o And A.

Table of Contents

List of Tables

List of Figures

Acknowledgements

Gordon, Petr, Anne, Stephenson;

Hokey Dinah!   It's been a slice!

Chapter 1. Introduction

1.1 Introduction To Be/shell Stars: Observations

The conventional theory of stellar atmospheres does not predict the presence of emission lines in stellar spectra. A Be star is a B-type star of luminosity classes V, IV, or III whose spectrum has, or had at one time, one or more of the hydrogen Balmer lines in emission. Luminosity classes I and II are excluded for a number of reasons. The most luminous B supergiants, of class Ia, possess emission at $H\alpha$ more often than not. Among supergiants, one rarely observes emission beyond $H\alpha$ in the Balmer series whereas the Be stars can exhibit emission as far up the Balmer series as H20. In addition to emission in the Balmer lines, some Be stars exhibit emission lines arising from singly ionized metals such as Fe II. Some B-type stars have emission lines arising from forbidden transitions; such stars are assigned spectral type classifications Bep or B[e]. The thousands of Be stars known make up about 20 percent of all B stars at type B2-B3. Towards later spectral types the fraction declines, reaching a few percent around B9-A0. Reviews of the Be phenomenon can be found in Underhill and Doazan (1982), the proceedings of IAU Symposium 98 (Jaschek and Groth, 1982) and the proceedings of IAU Colloquium 92 (Slettebak and Snow, 1987).

Be stars are known to exhibit photometric and/or spectroscopic variability on time scales ranging from minutes to years. One form of variability that may be universal among Be stars is transitions between normal B, Be, or shell phases. Time scales for phases transitions range from days to decades. The different phases can be passed

1

through in any order. In the case of Pleione, (Gulliver, 1977), the transition from a shell phase to a Be phase and back to a shell phase took 35 years. For μ Cen, Peters (1986) observed the appearance of significant emission at Hα over the course of only two days. Other examples of observed phase changes in recent years are ς Oph (Ebbets, 1981), η Cen (Baade, 1983; Dachs et al., 1986), α Eri (Dachs et al, 1981, 1986) and λ Eri (Barker, 1983). In a shell phase certain spectral features indicate the presence of a cool optically thick component to the envelope. These features are: (1) hydrogen lines with very deep, narrow absorption cores with the lower members of the Balmer series having emission wings; (2) sharp absorption lines from singly ionized metals. A B/shell spectrum can thus mimic the spectrum of an A supergiant. Examples of stars showing shell features are Pleione (Gulliver, 1977; Kogure and Hirata, 1982), o And (Gulliver et al., 1980), 88 Her (Doazan, 1973; Doazan et al, 1982) and 59 Cyg (Hubert-Delplace and Hubert, 1981; Barker, 1982). The three phases mentioned above are not mutually exclusive. The shell spectrum can be superimposed on a normal B spectrum or on a Be spectrum. For example, one can find B-type stars that appear normal at low resolution but are found to possess weak emission at higher resolution and signal-to-noise. Such a star is α Leo , which occasionally shows faint emission at Hα but is classified as B7V, (Singh, 1982). Some stars may have strong emission lines with superimposed shell features. An example of this situation is EW Lac, (Poeckert, 1980). One often speaks of Be/shell stars to indicate the general characteristic of passing (possibly repeatedly) through the various phases. New Be/shell stars are still being discovered among bright, well observed, apparently normal B stars which suggests that the number of B stars

capable of becoming Be/shell stars may be quite large.

The spectra of Be stars show large variations within a spectral class so that the classical parameters of T_{eff} and g_{eff} are necessary, but not sufficient, parameters for describing the conditions that exist in the photospheres and envelopes of these stars. The emission lines visible in the optical and infrared spectra indicate that a large cool circumstellar envelope exists. In this region there is no evidence for large expansion velocities. The presence of Fe II lines indicates electron temperatures $\sim 10^4$ K. Number densities are $\sim 10^{11}$ to 10^{12} cm^{-3}. In general Be stars have an infrared excess that can be attributed to free-free emission (Woolf et al., 1970). The shape of the infrared excess out to 10 μ m implies temperatures of about 10^3 K for the emitting plasma. The 10 and 20 μ m silicate features are not observed in Be stars, (Gerhz et al., 1974). Before ultraviolet spectra had been obtained the main difference between B and Be stars was thought to be an envelope of cool, fairly dense gas, created by outflow which B stars lacked. In the past twenty years this picture has changed.

Ultraviolet observations of resonance lines in the spectra of B and Be stars reveal the presence of highly superionized regions where electron temperatures are $\sim 10^5$ to 10^6 K (Snow and Morton, 1976; Snow and Marlborough, 1976). Under the condition of radiative equilibrium, the effective temperatures of B-type stars are not compatible with the presence in the spectrum of lines arising from such highly ionized species as N V and O VI. Additionally, profile fitting of the resonance lines by Snow and Marlborough (1976) and Marlborough and Snow (1976) indicate outflow velocities on the order of 10^3 km s^{-1}. It is generally agreed that nonradiative heating and momentum transfer

are implied by these observations. The ultraviolet spectra of both B and Be stars can be highly variable. Line intensities, shifts and profiles can vary, indicating variability in outflow density and velocity.

The picture that has emerged is that both B and Be stars possess extended atmospheres. The radiative flux emerges from the photosphere and the nonradiative energy flux provides additional heating above the photosphere and alters the temperature structure in the outer atmosphere. Above the photosphere are successively, the chromosphere, the corona and a post-coronal region. The shapes of these regions are subjects of debate so that spherical symmetry should not be implicitly assumed. Going outward from the photosphere to the corona, both temperature and wind velocity increase. Beyond the corona, temperatures decrease due to radiative losses. Be stars seem to differ from normal B stars in that they possses a cool low velocity region in the post-corona at about 5 to 15 stellar radii where densities are high enough to form an emission spectrum in the visible and the infrared. It is not yet clear how the line emitting region is formed, what shape it has or what connection, if any, it has with the wind. The geometry of this line emitting region and the conditions within it may vary considerably with time for a given star and from star to star as evidenced by the diversity of emission line strengths and profiles exhibited by Be stars.

The emission in Be stars is always strongest at Hα and decreases in strength with ascension up the Balmer series. When emission first becomes visible during a B to Be phase transition it is always observed first at Hα . This first, weak appearance of emission is always in the form of a double-peaked profile with peak separation $\leq$

2vsin$i$. The amount of emisson can vary from a weak central reversal at Hα (only visible at high resolution and high signal-to-noise ratio), to enough emission to fill in the underlying absorption line and rise to heights ten or twenty times the continuum. The ratio of emission line strength to the strength in the adjacent continuum, is denoted by E/C. Variation of E/C with time is common among Be stars. The time between successive E/C maxima can range from weeks to decades. Variations can be irregular and cycle-to-cycle variations in the value of E/C maxima are also typical. Not only does the strength of emission lines vary with time, but the shapes of emission lines can vary irregularly and quasiperiodically. The most common profile is one with two peaks which are always separated by less than 2vsin$i$. The relative strength of the two peaks is denoted by V/R (short wavelength/long wavelength). V/R variability is a common form of line profile variability among Be stars that possess the double-peaked type of emission lines. The total emission in the line can stay fairly constant even though V/R may be varying. The time scales for V/R variations can range from minutes to decades. The value of V/R can be different for different members of the Balmer series and can differ between the hydrogen lines and metal lines. This would seem to imply temperature and density structure within the line emitting region. Other common emission line profiles include ones with single peaks or triple peaks, and ones with deep narrow shell absorptions superimposed. Profiles can be quite asymmetric and when observed at high resolution inflexions on the flanks are sometimes observed. Reviews of emission line shapes and variability can be found in Underhill and Doazan (1982) and Dachs (1987).

In addition to emisson line variablity, Be stars are known to exhibit considerable variability in the underlying absorption lines and the continuum. Summaries of rapid spectroscopic and photometric variations of Be stars can be found in Slettebak (1982a) and Percy (1986,1987). The incidence of rapid line profile variability amongst Be stars is common. These variations have been variously ascribed to nonradial pulsations (NRP), spots or patches on the star carried across the line of sight by rotation, and binarity. The most widely accepted explanation is nonradial pulsation. In his study of 25 rapidly rotating B and Be stars Penrod (1986) found evidence for high degree NRP in all the B stars and most of the Be stars. All the Be stars were found to possess a long period $l = 2$ mode as well. Starting with ς Oph (Walker, Yang, and Fahlman 1979; Vogt and Penrod 1983), rapid periodic or quasi-periodic line profile variations attributed to NRP have been reported for a growing list of Oe and Be stars. Some recent examples are ω CMa (Baade 1982a,1982b), 10 CMa (Baade 1984a), μ Cen (Baade 1984b), HR 4074 (Baade 1984a), λ Eri (Smith, Gies, and Penrod 1987) and γ Cas (Yang,Ninkov and Walker 1988). Photometric variability is observed on both short and long time scales. During emission and shell phases, Be stars often become redder and sometimes brighten. Rapid periodic photometric variations, with low amplitude, have been observed for a growing list of Be stars, and again star spots, binarity and NRP have been invoked as possible explanations. Among Be/shell stars, variations in the height and location of the Balmer discontinuity have been observed. Sometimes the shortward side of the discontinuity is actually observed in emission. Occasionly two discontinuities are observed, one typical of a dwarf star and the other typical of a

6

supergiant.

1.2 Introduction To Be/shell Stars: Models

Explanations of the Be phenomenom usually use ad hoc models which attempt to incorporate certain observational facts. The models attempt to explain how a line emitting region is created and what its conditions and geometry are. The line and continuum variability is a necessary feature of the models given its ubiquity among the Be stars. Struve (1931) proposed the first model for Be stars in which the emission lines arose from an ionized circumstellar envelope. At the time of Struve's model it was known that, unlike Wolf-Rayet stars, the optical spectra of Be stars did not imply expansion velocities large enough to explain the formation of extended envelopes. It was also suspected that on average Be stars rotate faster than normal B stars. This latter property has since been confirmed. The average vsin$i$ of Be stars is 200 to 250 km s^{-1} with values ranging up to 400 km s^{-1} observed (Slettebak, 1982b). In Struve's model, Be stars rotate at their critical velocity and an equatorial disk is formed by matter ejected by rotational instability. Struve's model is able to explain the diversity of emission line profiles as an inclination effect. Viewing a star equator-on produces a shell spectrum superimposed on an emission spectrum. Viewing a star pole-on produces narrow single peaked emission lines (since the dominant motion in the disk is rotation). Intermediate angles produce double-peaked emission lines. The main failures of Struve's rotational model are that it fails to predict variability, and no Be star is observed to be rotating at its critical velocity. Moreover, rotational ejection is not capable of displacing matter out to the distances (5-20 stellar radii) that line emitting regions are believed

to extend to. We now know through ultraviolet observations that a mass flux does exist. Rotation is no longer believed to be the sole mechanism by which a line emitting region is formed but is likely to somehow play a role since on average Be stars possess a larger vsin$i$ than normal B stars.

In the past twenty years a number of models for Be stars have been proposed. In the binary model (Kriz and Harmanec 1975), all Be stars are assumed to be interacting binaries. Reviews of the binary hypothesis can be found in Harmanec and Kriz (1976), and Harmanec (1982,1987). In the binary model a mass losing secondary fills its Roche-lobe and an accretion disk forms around the primary (Be) star. Long term E/C variations arise from variations in the mass transfer rate. Long term V/R variations result from a temporarily non-symmetrical and rotating accretion disk formed by a mass transfer burst. The accretion disk is the line emitting region in the binary model, in agreement with the finding that most emission line profiles can be modeled quite well by emission from an equatorial disk. It is argued that long orbital periods, broad spectral lines and low radial velocity semiamplitudes have enabled most Be stars to evade detection of their binarity.

A connection between NRP and the Be phenomenon has been suggested in recent years by Vogt and Penrod (1983), Penrod and Smith (1985), Penrod (1986,1987) and Baade (1987). The best documented cases of a correlation between pulsation amplitudes and Be events is for λ Eri (Bolton 1982, Penrod 1986,1987) and ς Oph (Vogt and Penrod (1983). Other examples may be o And and 2 Vul (Penrod 1987). Penrod and Smith (1985) note that the $l = 2$ NRP mode contains more energy than higher-l

modes. They speculate that the low-l mode may act as a reservoir of stored energy and that during Be outbursts high-l modes are excited. These high-l modes may have large amplitudes but contain little energy (due to their confinement to the surface). If the non-linearities associated with the large amplitudes lead to shocks, Penrod and Smith suggest that this may cause the ejection of some atmospheric material into orbit. Penrod (1986) suggests that an $l = 2$ mode may increase the scale height of the atmosphere and thus combine with radiation pressure and rotation to further lower the effective gravity making it easier for shocks to eject material and form a circumstellar disk. Some other possible mechanisms by which NRP may contribute to the Be phenomenon are presented by Wilson (1986) and Osaki (1986). It is interesting to note that one of the problems facing the study of NRP in rapidly rotating early-type stars is the question of what mechanism drives the pulsation. The presence of a low mass companion could generate low order pulsations through tidal coupling. In this sense the NRP model and the binary model of the Be phenomenon may not be mutually exclusive.

Another model that has been suggested in recent years is the magnetic loop model (Underhill 1987). This model consists of an equatorial disk formed by magnetohydrodynamic interactions with the circumstellar material. Plume-like structures supported by field lines are postulated to wrap up as the star rapidly rotates. The magnetic fields allow energy and momentum to be non-radiatively transported above the photosphere. The stellar wind emanates mainly from coronal-hole–type structures above and below the stellar equatorial region. As field lines are distorted by MHD interactions and rota-

tion, they sometimes tangle, break and recombine allowing for bursts of increased mass loss and wind variability. The rotating structured disk explains the rapid photometric variability. Phase changes (such as from B to Be) are postulated to occur when changes in a subsurface convection zone alter the magnetic flux.

The models discussed above implicitly assume the line emitting region (LER) is disklike. There exists another large class of models in which the LER is assumed to be spheroidal. These models often attempt to create the necessary environment for the creation of a variable emission line spectrum by variations of the stellar wind and the resulting variations in the circumstellar envelope. Since both normal B and Be stars possess winds the variability of Be star winds versus the steady outflow of normal B stars is invoked as the distinguishing characteristic of the former. The stellar wind is assumed to possess spherical symmetry and to increase in velocity outward. The LER is formed by the wind first accelerating then decelerating as it collides with the interstellar medium or from a wind varying in velocity and density interacting with itself. In other variations the wind is rotationally enhanced so that although not disklike the LER is concentrated toward the equatorial plane. Reviews of these wind based models can be found in Doazan (1987) and Marlborough (1987).

1.3 Omicron Andromedae As A Be/shell Star

The bright Be/shell star o Andromedae (HR 8762, HD 217675-6,B6 IIIpe) has been the object of spectroscopic and photometric observations for nearly a century. More recently it has become apparent that the star is at least triple. Interferometric and micrometric studies (Blazit et al. 1977; Heintz 1978; McAlister 1979; Tokovinin

1983; McAlister and Hartkopf 1984; Tokovinin 1985; Bonneau et al. 1986; McAlister et al. 1987) have revealed the presence of two companions, at separations of about 0.05 (Aa) and 0.3 (AB) arc seconds. The AB position angle changed steadily by about 10° between 1975 and 1985 with a decrease in separation from about 0.375 to 0.266 arc seconds. As B is only 0.5 to 1.0 magnitudes fainter than the primary (McAlister, private communication) it may contribute up to 40 percent of the total flux from the system.

A variety of photometric variations is known or suspected to exist. The double wave light curve has a 1.571272 day period but varies in both amplitude and shape (Harmanec 1984; Stagg et al. 1985; Stagg 1987; Harmanec et al. 1987). Harmanec (1984) suspects that the time scale for the variation in shape of the light curve is 11-15 days and that the amplitude of the 1.57 day light curve may vary in conjunction with a 3100 day periodic variation. The amplitude of the 3100 day periodic variations is about 0.1 magnitude and at maximum light (V=3.61) the amplitude of the 1.57 day light curve is almost zero while during the minima the amplitude of the short-term variations reaches a maximum of about 0.1 magnitude.

Spectroscopic investigations can be divided roughly into searches for short-term radial velocity variations (about a day) and long-term (years) variations in radial velocity and shell strength. After analysing radial velocities from 1900 to 1976, Fracassini and Pasinetti (1977) and Fracassini et al. (1977) reported the presence of a 23.5 year period and a 1.5845 day period. Horn et al. (1982) using a partially different set of radial velocities found a period of 25.9 years but found no periods in the range 0.5 to

1000 days. Gulliver and Bolton (1978) searched for radial velocity periods in the range 0.5 to 1000 days with only a quasi-periodicity of 0.84 days being found. A period search by Baade et al. (1982) using plates taken during 1981 and 1982 found no periodicity in radial velocity.

Schmidt (1959), Pasinetti (1967,1968), and Fracassini and Pasinetti (1975) have suggested that there are shell outbursts every 31 years. The occurrence of outbursts at more frequent intervals than 31 years has since made this period seem less likely than the 8.5 year (3100 day) period suggested by Harmanec (1984). Gulliver, Bolton and Poeckert (1980) and Koubsky (1984) have shown that the overall behaviour of the shell may be more complicated than simply periodic.

In some sense o And may represent a prototype Be star in that it has at times exhibited the spectrum of a normal B star, passed through phases of Balmer emission and gone through shell phases many times in the almost 100 years it has been observed spectroscopically (Koubsky 1984, Harmanec 1984, Bossi et al. 1982). Unexplained variations of the Mg II λ 4481 line profile of o And have been known for quite some time. Gulliver, Bolton and Poeckert (1980) showed that the narrow components superimposed on the broad underlying profile survived the disappearance of the shell and varied in velocity, but they found no periodicity in these variations. Recently (1982-83) o And possessed a shell and HI emission lines (Baade et al. 1982, Bossi et al. 1982). At this time the V amplitude of the 1.57 day light curve reached a maximum of about 0.1 magnitude, (Stagg 1987, Harmanec et al. 1987). In 1984-85 o And possessed a normal B absorption spectrum and the amplitude of the light variations declined (Harmanec

et al. 1987). In August and October 1986 our spectra showed no evidence of a shell or emission at $H\gamma$. At this time some emission was observed at $H\alpha$ by Tarasov (private communication). In July and August 1987 we saw some evidence for a weak shell at $H\alpha$. At this time $H\beta$ and $H\gamma$ looked normal. In September 1987 we saw no evidence of emission or a shell at $H\gamma$.

In light of the multiple nature of o And and its rapid photometric variations we undertook a spectroscopic investigation of (a) long term variations that might arise due to its multiplicity and, (b) rapid variations related to the photometric variations. The presence of NRP if found, combined with the multiple nature of o And and its long history of observation, may represent an excellent opportunity to test two of the many theories advanced to explain the Be phenomenon, namely the binary hypothesis and the NRP model. By determining the orbital parameters and geometry of the system a correlation with Be/shell episodes may be found. Similarly, future Be/shell events may be found to relate to the amplitude of NRP.

Chapter 2. Omicron Andromedae As A Multiple System

2.1 Introduction

In order to study the medium term (months) spectroscopic variations of o And, a monitoring program using the University of British Columbia 0.42m telescope was undertaken. The purpose of this study was to search for radial velocity variations and to monitor the narrow components known to be superimposed on the broad underlying profile of Mg II λ 4481.

2.2 Observations and Radial Velocity Measurements

The University of British Columbia 0.42 m telescope was used to obtain 70 spectra on 63 nights between May 7 and September 1 1987. The observers were the author and/or Nadine Dinshaw an undergraduate summer research assistant. An additional 6 spectra were obtained on June 1,2,3 of 1986 by the author. The spectra were taken with a liquid-nitrogen-cooled RL1872F/30 Reticon on the coudé spectrograph. A description of the detector and data reduction procedures can be found in Walker, Johnson, and Yang (1985). The spectrograph was used in the second order of the 1200 line/mm grating which gave a reciprocal dispersion of 17 Å/mm corresponding to about 0.26 Å per diode with a spectral coverage of 488 Å centered at 4460 Å. The exposure times were between 1.5 and 2 hours. For all spectra the signal-to-noise per diode was 200 or greater. Figure 1 shows the region of the lines of Mg II λ 4481 and He I λ 4471 for all the 1987 UBC spectra. All the He I λ 4388 profiles obtained at UBC in 1987 are

Fig. 1a — Reticon spectra obtained with the UBC 0.42m telescope showing He I λ 4471 and Mg II λ 4481.The resolution is 0.7 Å. The S/N ratios are ≥ 200. The midexposure time from BJD 2,446,500 is indicated for each spectrum. Where two consecutive spectra were obtained on one night, the average is presented.

486.897
488.891
489.885
490.891
491.894
492.891
493.898

497.891
498.911

500.884

504.880
505.842
506.819

508.821
509.875
510.770

512.802
513.812
514.799
515.866

522.856

524.882
525.854
526.843
527.846
528.843
529.747
530.864
531.835

534.953

538.900
539.939

4%

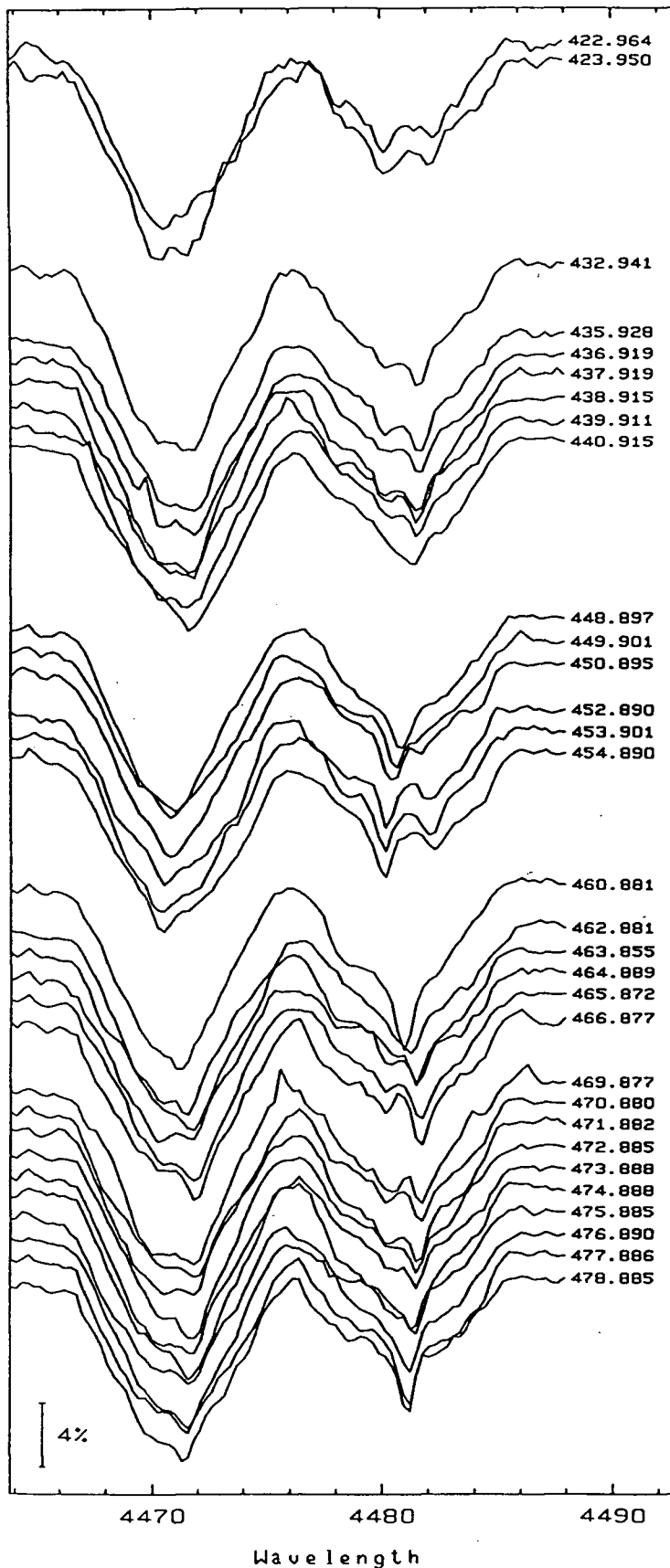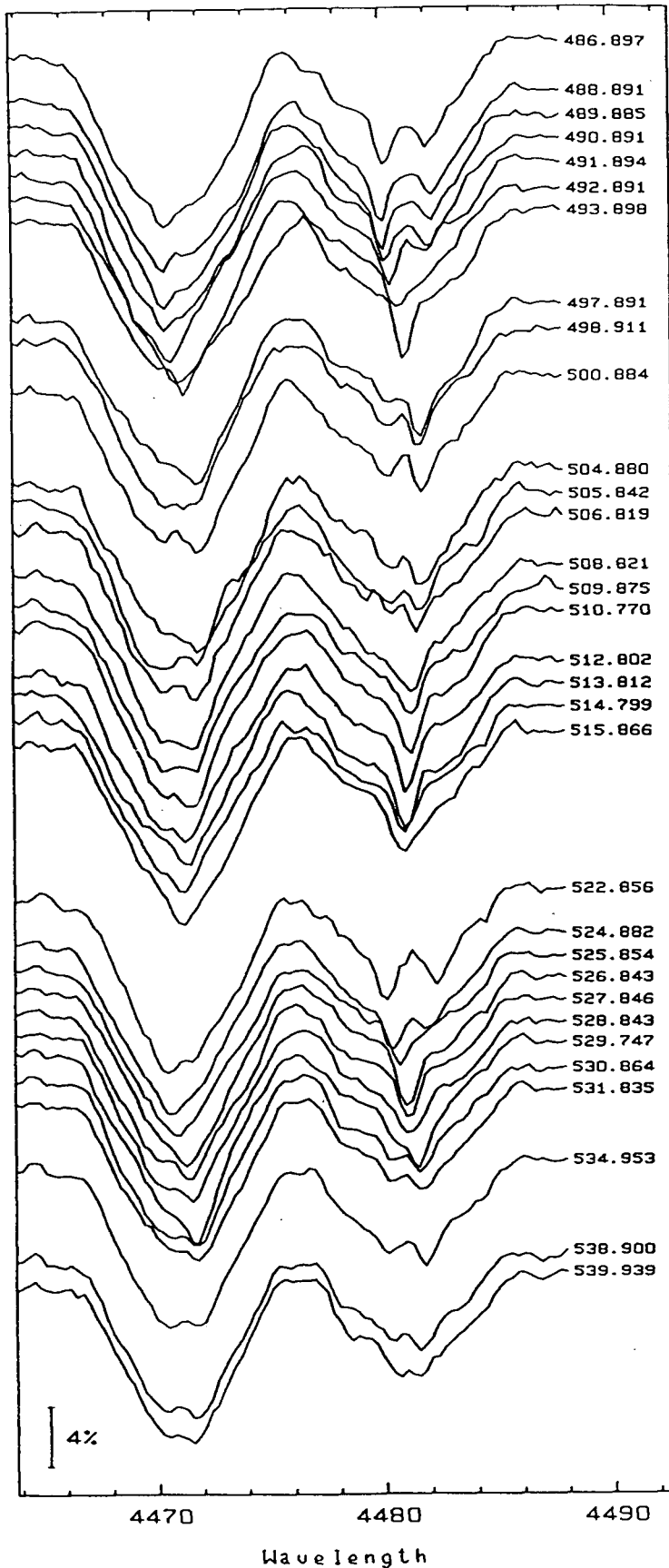4470   4480   4490

Wavelength

Fig. 1b — Reticon spectra obtained with the UBC 0.42m telescope showing He I λ 4471 and Mg II λ 4481. The resolution is 0.7 Å. The S/N ratios are $\geq$ 200. The midexposure time from BJD 2,446,500 is indicated for each spectrum. Where two consecutive spectra were obtained on one night, the average is presented.

shown in Figure 2. The spacing of the spectra along the vertical axis is scaled by the barycentric Julian dates of their midexposure times.

In addition to the UBC observations, we obtained spectra of higher time and wavelength resolution with the Cassegrain spectrograph of the DAO 1.83 m telescope at 10 Å/mm (0.15 Å per diode) using an identical Reticon. Altogether 84 spectra were obtained on 4 nights in August and 3 nights in October of 1986. The observers were the author, P. Harmanec, G.A.H. Walker, and S. Yang.

The principle lines present in both the DAO and UBC spectra are C II λ 4267, Hγ λ 4340 , He I λ λ 4388, 4471 and Mg II λ 4481. The spectra are dominated by the rotationally broadened (vsin$i$ $\sim$ 225 km/sec) lines of the B6 III primary (o And A). The presence of C II λ 4267 indicates the spectral type may be slightly earlier than B6III but we shall forestall a discussion of the spectral type until chapter 3. Superimposed upon these are the narrower lines of a spectroscopic binary, which we shall show to almost certainly be B, the more distant of the two interferometrically resolved companions. These narrower components are most clearly visible in the Mg II λ 4481 profile where their presence was first noted by Gulliver and Bolton (1978).

Only the Mg II lines of the spectroscopic binary were used for radial velocity measurements. The He I lines of the binary are visible but not as strong or sharp compared to the underlying broad profile. The C II lines were not measured due to their weakness. The Hγ lines of the spectroscopic binary were only barely visible on the highest signal-to-noise spectra. The Stark broadening of the Hγ lines prevented accurate measurement of radial velocities for the double-lined binary.

Fig. 2a — Reticon spectra obtained with the UBC 0.42m telescope showing He I λ 4388. The resolution and S/N are the same as Fig. 1. The midexposure time from BJD 2,446,500 is indicated for each spectrum. Where two consecutive spectra were obtained on one night, the average is presented.
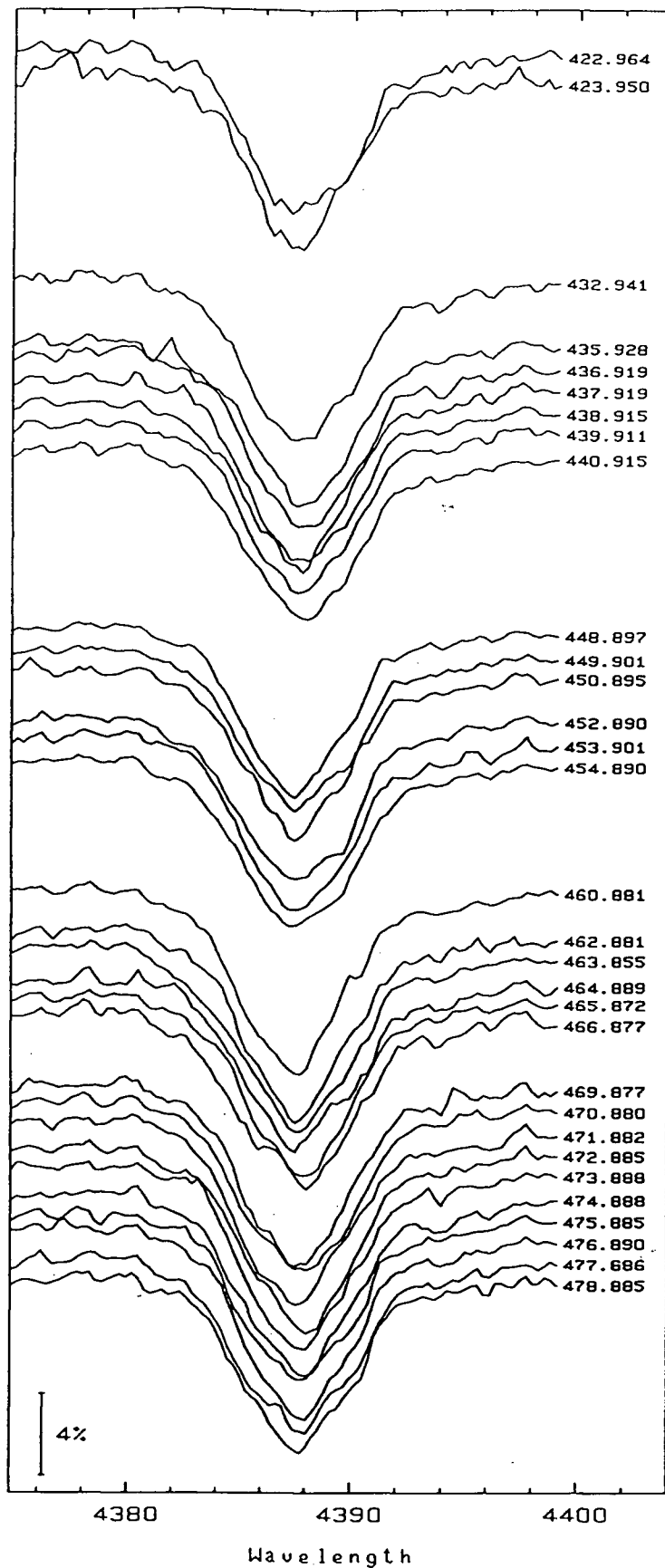
18

Fig. 2b — Reticon spectra obtained with the UBC 0.42m telescope showing He I λ 4388. The resolution and S/N are the same as Fig. 1. The midexposure time from BJD 2,446,500 is indicated for each spectrum. Where two consecutive spectra were obtained on one night, the average is presented.
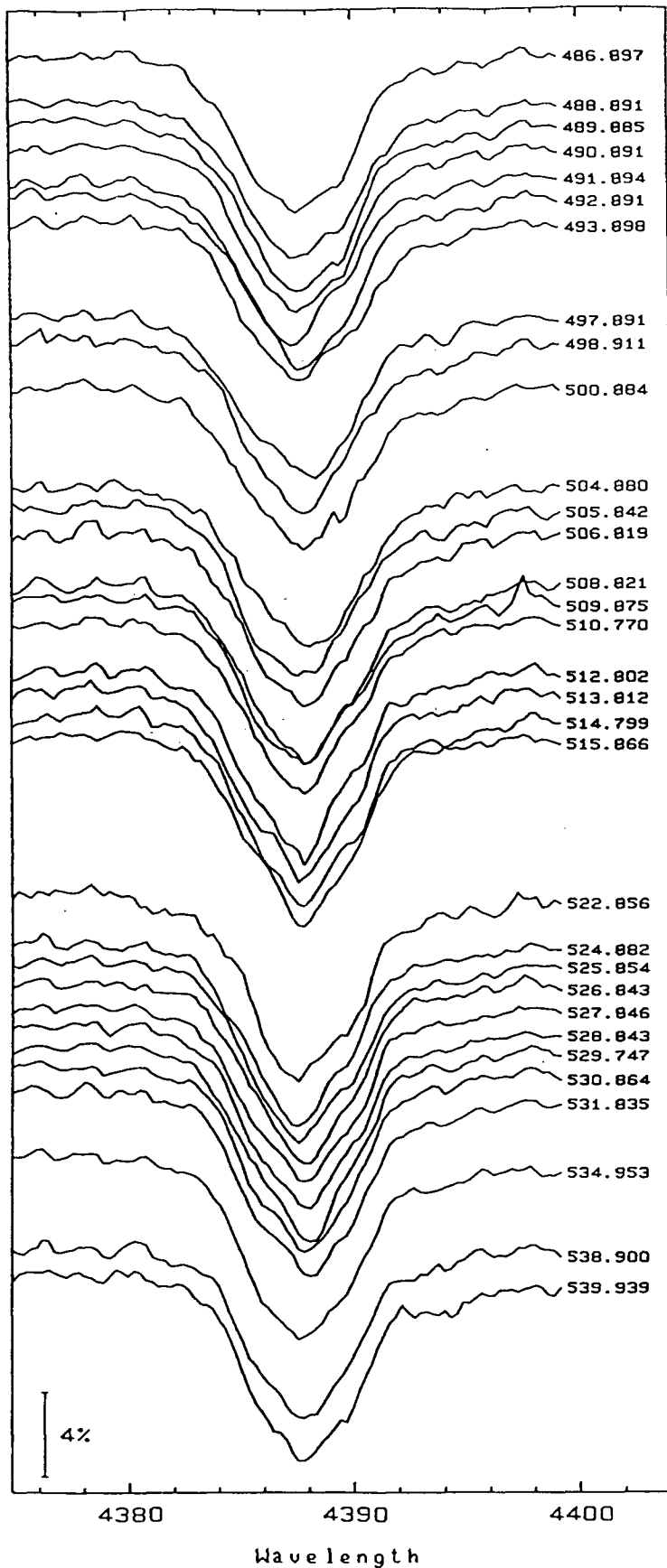
19

The average of all spectra in which the binary lines were coalesced was used to determine the shape of the underlying broad profile. The underlying Mg II profile has a FWHM of about 6.3 Å while the coalesced narrow components have a FWHM of about 1.2 Å. The core of the underlying profile, upon which the coalesced narrow components were superimposed, was approximated by fitting a fourth order polynomial to the underlying profile on either side of the central 2.5 Å. The profile adopted to represent the underlying broad profile was thus the combination of the polynomial in the central 2.5 Å and, on either side, the average spectrum described above. The connections between the two were smoothed. The underlying Mg II profile, thus determined, was subtracted from each observed Mg II line profile prior to measuring the SB2 line positions. The line positions were measured using the weighted mean of the pixels in the line profiles of each of the narrow features with the depth below continuum acting as weights. The average of iron-argon hollow-cathode lamps taken before and after each exposure were used to set the wavelength calibration. The average of the doublet rest wavelengths, 4481.228 Å, was adopted as the rest wavelength. Radial velocities corrected to the solar system barycenter, midexposure times, and phases are presented in Table I. In ten of the spectra the two components are too closely coalesced to yield useful radial velocities. The DAO radial velocities are averages for each night. The standard deviation about the mean of the DAO velocities for each night was typically 5-6 km/sec. A small part of this represents phase smearing but the majority probably arises from variations in the underlying absorption profile. These variations, which seem to have a time scale of about one day, will be discussed in chapter 3.

TABLE I

o Andromedae Radial Velocity Measurements

BJD 2,440,000+	33.01 day binary phase	V_1 km/s	$(O-C)_1$ km/s	V_2 km/s	$(O-C)_2$ km/s
UBC 0.42m 1986					
6582.992	0.631	— —	— —	— —	— —
6583.925	0.660	— —	— —	— —	— —
6584.921	0.694	−21.1	+4.1	+7.8	+7.8
DAO 1.83m 1986					
6669.891	0.267	+26.8	−3.1	−61.4	+10.6
6671.777	0.324	+22.3	−8.8	−81.4	−7.8
6673.869	0.388	+20.4	−7.7	−64.8	+4.8
6674.833	0.417	+23.0	−2.5	−64.9	+1.4
6720.824	0.809	−54.6	+2.9	+39.9	−2.2
6722.950	0.874	−72.0	+1.1	+60.7	−1.9
6723.768	0.899	−74.9	+2.0	+68.6	+1.1
UBC 0.42m 1987					
6922.965	0.931	−68.8	+9.4	+75.0	+5.8
6923.951	0.961	−76.8	−2.3	+50.1	−14.4
6932.942	0.233	+24.5	−2.5	−67.5	+0.7
6935.929	0.323	+25.3	−5.8	−73.0	+0.6
6936.919	0.353	+25.8	−4.3	−72.9	−0.6
6937.919	0.384	+23.9	−4.4	−72.2	−2.4
6938.916	0.414	+27.1	+1.5	−72.8	−6.6
6939.912	0.444	+25.8	+3.5	−62.2	−0.1
6940.916	0.474	15.3	−3.1	−52.8	+4.1
6948.897	0.716	−37.8	−6.0	+17.8	+9.2
6949.901	0.746	−42.3	−2.1	+18.2	−1.4
6950.896	0.777	−55.6	−6.9	+30.2	−0.5
6952.890	0.837	−73.0	−7.7	+55.2	+2.8
6953.901	0.867	−73.9	−1.6	+52.3	−9.2
6954.890	0.897	−82.7	−5.8	+69.8	+2.2
6960.882	0.078	— —	— —	— —	— —
6962.882	0.139	+0.9	−4.3	−46.7	−7.0
6963.856	0.169	+12.0	−2.6	−51.3	+0.7
6964.889	0.200	+18.8	−3.1	−58.0	+3.6
6965.873	0.230	+30.5	+3.8	−69.8	−2.1
6966.877	0.260	+26.7	−2.9	−73.3	−1.7
6969.877	0.351	+30.5	+0.3	−65.7	+6.7
6970.880	0.382	+29.3	+0.9	−71.4	−1.4
6971.883	0.412	+20.9	−4.9	−68.7	−2.1
6972.886	0.442	+17.5	−5.0	−66.8	−4.6
6973.888	0.473	+18.5	−0.1	−61.0	−3.9
6974.888	0.503	+13.6	−0.5	−59.4	−8.1
6975.885	0.533	+8.7	−0.4	−46.9	−2.1
6976.890	0.564	−2.8	−6.3	−44.1	−6.6
6977.887	0.593	— —	— —	— —	— —

TABLE I cont.

BJD 2,440,000+	33.01 day binary phase	V_1 km/s	$(O-C)_1$ km/s	V_2 km/s	$(O-C)_2$ km/s
6978.886	0.623	––	––	––	––
6986.897	0.867	−66.9	+5.2	+62.0	+0.7
6988.892	0.927	−80.8	−2.5	+75.4	+6.1
6989.886	0.957	−77.7	−2.6	+66.1	+0.9
6990.892	0.988	−62.0	+4.7	+62.2	+8.0
6991.894	0.018	−55.9	−2.2	+40.9	+3.6
6992.892	0.048	−32.9	+5.2	+21.8	+5.0
6993.899	0.078	––	––	––	––
6997.892	0.200	+24.3	+2.4	−61.0	+0.5
6998.912	0.231	+24.3	−2.5	−68.5	−0.6
7000.880	0.290	+35.8	+4.8	−73.6	−0.2
7004.841	0.410	+25.4	−0.5	−61.4	+5.4
7004.918	0.412	+25.2	−0.5	−64.8	+1.7
7005.841	0.440	+23.7	+1.0	−60.6	+1.9
7006.823	0.470	+18.7	−0.2	−63.9	−6.3
7008.822	0.531	+16.1	+6.6	−37.7	+7.6
7009.875	0.562	+6.7	+3.0	−40.8	−3.1
7010.771	0.590	+1.8	+3.5	−24.4	+6.3
7012.802	0.650	––	––	––	––
7013.813	0.682	−31.6	−8.7	−1.8	+1.2
7014.800	0.712	−35.8	−5.0	+7.3	+0.0
7015.803	0.742	−42.7	−3.6	+26.2	+8.0
7015.928	0.746	−41.5	−1.3	+17.7	−1.9
7022.857	0.956	−85.0	−9.6	+71.5	+6.0
7024.843	0.016	−65.7	−11.0	+40.6	+2.1
7024.922	0.018	−48.5	+5.0	+41.3	+4.3
7025.793	0.045	−39.5	+0.4	+23.2	+4.0
7025.917	0.048	−37.9	+0.0	+8.7	−7.9
7026.843	0.076	––	––	––	––
7027.785	0.104	––	––	––	––
7027.909	0.108	––	––	––	––
7028.780	0.135	+13.7	+9.9	−39.2	−1.4
7028.906	0.139	+12.3	+7.1	−35.9	+3.8
7029.737	0.164	+16.6	+3.2	−42.2	+8.2
7029.817	0.166	+17.2	+3.1	−43.0	+8.3
7030.865	0.198	+24.1	+2.5	−59.4	+1.7
7031.836	0.228	+23.6	−2.8	−64.5	+2.9
7034.954	0.322	+39.1	+8.0	−79.0	−5.4
7038.900	0.441	+24.3	+1.8	−65.3	−3.0
7039.939	0.473	+14.4	−4.1	−44.9	+12.1

2.3 The Orbit of o And B

We identify the stronger of the two narrow components visible in the the Mg II λ 4481 profile with the primary component of the spectroscopic binary and the weaker with the secondary component of the spectroscopic binary. The radial velocities measured for these features are presented in Table I in the columns headed V_1 and V_2 respectively. Before using a computer program to solve the orbit, the radial velocities were searched for periodicity using the phase dispersion minimization (PDM) technique of Stellingwerf (1978). The primary and secondary velocities were searched separately and a period of 33.02 days was returned for both. For both period searchs, the minimum Θ (a measure of the dispersion) obtained was about 0.10. The smaller this value, the more significant the period. The half width at half minimum of the theta versus possible period plot indicates the degree of uncertainty in the period returned by the search. For both searchs the half width at half minimum was about 1.0 day. The size of this uncertainty results from the fact that the majority of the data was obtained over less than four complete cycles of the 33.0 day period.

The radial velocities were folded back with the 33.02 day period and and the orbit was solved graphically using the method of Lehmann-Filhés. A brief description of how this method works and what orbital parameters it solves for is presented in Appendix A. These values were then used as the starting values for the computer solution. The orbit was solved using the program RVORBIT, kindly supplied by Dr. Graham Hill. The single-line option of RVORBIT was used to solve the orbit of each component separately. The double-line solution was adopted after finding that the

23

single-line solutions agreed with it to within their mutual uncertainties. The velocities presented in Table I were given equal weights when determining the orbital elements of the double-line spectroscopic binary. The solution was obtained with respect to time of periastron passage using the method of Lehmann-Filhés. The observed minus calculated residuals are given in Table I. The orbital elements are presented in Table II. The period found by RVORBIT, 33.01 days agrees with the period of 33.02 days found using the phase dispersion minimization (PDM) technique of Stellingwerf (1978). The fit of the solution to the data is shown in Figure 3.

2.4 Discussion

The multiple nature of o Andromedae leads one to ask, which of the resolved components is the double-lined spectroscopic binary? The parallax for o Andromedae, 0.015 ± 0.008 arcsec (van Altena, private communication), yields a distance of 67 parsecs. At this distance the maximum observed separations of components a and B correspond to 3.9 and 25.1 AU, respectively. The spectroscopic binary must therefore be one of the three, as opposed to two of the three, resolved components. There must be a minimum of four stars present.

Table III presents masses for the spectroscopic binary stars for various values of the inclination. Since component B is 0.5 to 1.0 magnitudes fainter than component A and component a fainter still, (McAlister, private communication), one may determine an approximate lower limit to the inclination. Assuming component B contributes 40 percent of the total flux, the spectral type - M_v calibration of Balona and Crampton (1974) implies that the binary stars are around B8IV-V and differ by about one spectral

<div align="center">

TABLE II

Orbital Elements For The Spectroscopic Binary

</div>

	Primary				Secondary		
Period (days)			+33.01	± 0.02			
T_{per} (2,440,000+)			+6925.3	± 0.2			
V_o (km/sec)			−14.3	± 0.5			
e			+0.24	± 0.01			
ω (degrees)			+226.2	± 2.3			
K (km/sec)	54.8	±	0.8		71.6	±	0.8
asini (AU)	0.161	±	0.003		0.211	±	0.002
$m \sin^3 i$ ($M_\odot$)	3.74	±	0.05		2.86	±	0.05
σ fit (km/sec)	4.6				5.2		

<div align="center">

TABLE III

Masses of Spectroscopic Binary Stars

</div>

inclination (degrees)	M_1 ($M_\odot$)	M_2 ($M_\odot$)
50	8.32	6.36
55	6.80	5.20
60	5.76	4.40
65	5.02	3.84
70	4.51	3.45
75	4.15	3.17
80	3.92	2.99
85	3.78	2.89
90	3.74	2.86
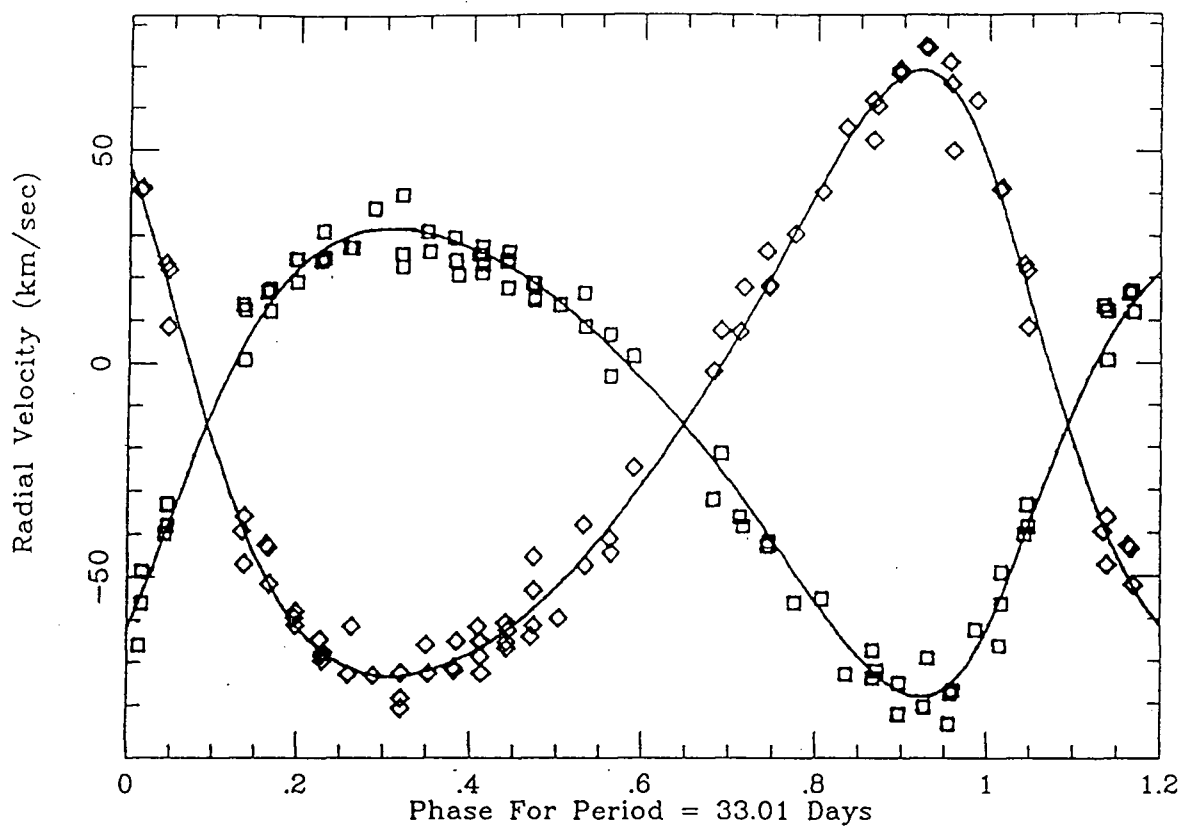
Fig. 3 — Mg II narrow component radial velocities phased to a period of 33.01 days for o Andromedae. The solid line is the calculated curve corresponding to the orbital solution presented in Table II. Squares denote primary radial velocities and diamonds denote secondary radial velocitites.

subclass. Assuming the two stars are B7V and B8V and using the spectral type - mass calibration of Popper (1980) implies $i \geq 65°$. Assigning late B spectral types to the double-lined spectroscopic binary is compatible with the absence of reports of UV or IR excesses. That the lines of the binary are most visible in Mg II and visible but to a lesser degree in He I also agrees with this assignment. No 33 day photometric period arising from eclipses is known so $i < 89°$.

Of the two resolved companions to component A, component B seems the more likely candidate for the double-lined spectroscopic binary. We have detected no trace of component a in our data. Given its faintness this is not surprising. If component a were the binary, one would have to explain the absence of a contribution to the spectrum from the brighter component B. Further, in one year there has been no change in the systemic velocity. Omicron Andromedae would seem to be (at least) a double-binary system. A schematic illustration of the system geometry is presented in Figure 4.

Using a reasonable estimate of the total mass of the system, Kepler's third law, and a separation of 25 AU yields a period for Aa-B of about 30 years. It is interesting to recall that various groups have suggested a 31 year periodicity in shell outbursts and radial velocity periodicities of about 25 years have been reported. However, in ten years of speckle interferometry measurements the AB position angle has only changed by about 10° and the separation has gone from about 0.375 to about 0.266 arc seconds. A much longer period than 30 years is possible if one adopts a smaller value for the parallax or, the orbit is quite eccentric. Encounters at periastron due to an eccentric orbit are one possible mechanism to trigger shell outbursts.

Period (Aa—B) = 30 years ?

a ·

: B

A ●

Sp. Type(A): B5IIIe

Sp. Types: B7—8 IV—V

Period (A—a) = 4 years ?

Period = 33 days
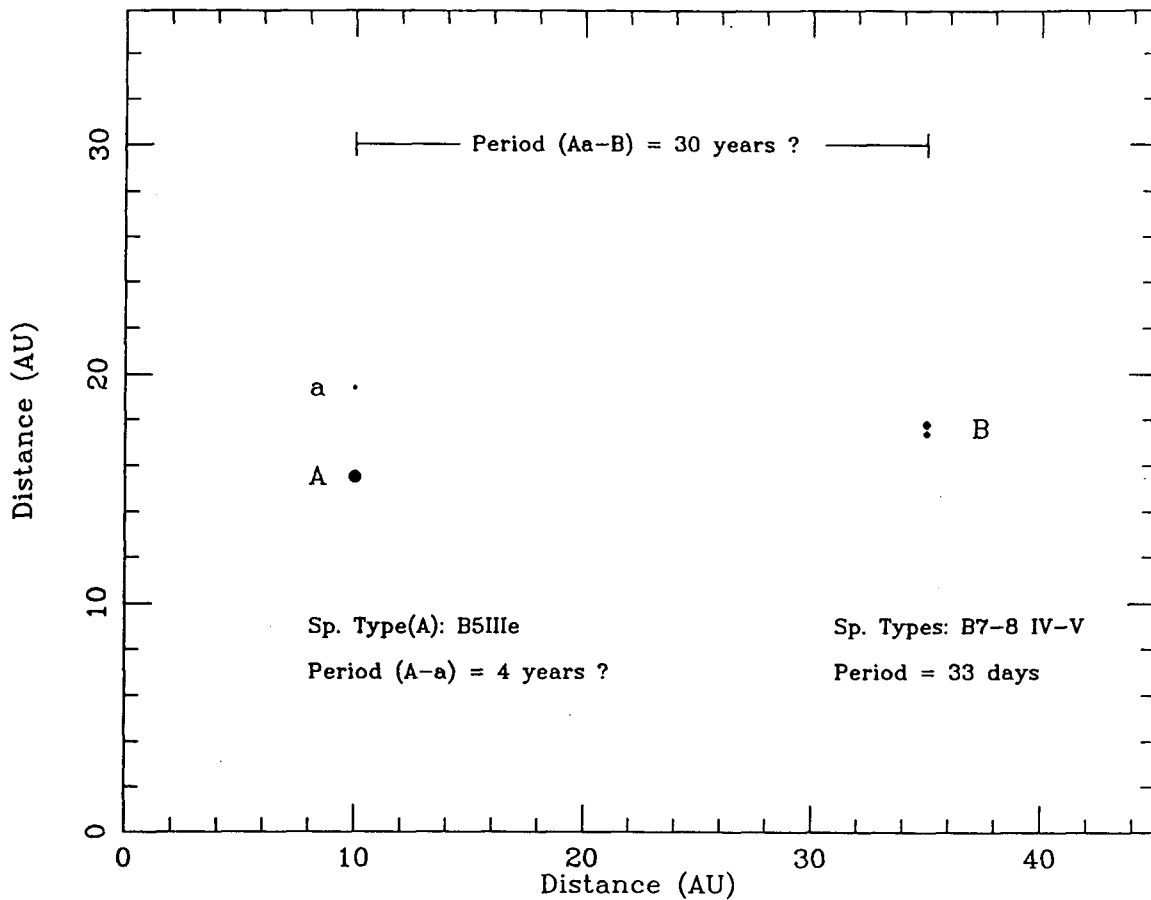
Distance (AU)

Distance (AU)

Fig. 4 — Schematic diagram of o And system. Distances are to scale assuming a parallax of 0.015 arcseconds. The spectral type of o And a is not known. The spectroscopic binary o And B contributes 20 to 40 percent of the total flux from the system.

Only four measurements of separation and position angle exist for Aa. Never-the-less, given the 180° indeterminacy of speckle interferometric position angle measurements one can construct an orbit with a period of 3.7 years. Kepler's third law, a separation of four AU and reasonable mass estimates yield periods in the range three to four years. For a smaller parallax the period would be longer and could be on the order of the 8.5 year period advocated for shell outbursts by Harmanec (1984).

Omicron Andromedae has been an object of considerable attention in recent years and in fact has been included in several photometric and spectroscopic campaigns. It is clear that certain medium-term spectral variations arise from its multiplicity. Some long-term variations may also be a result of this multiplicity. Continued interferometric measurements of the system will hopefully settle some of the questions regarding long-term variations.

Chapter 3. Rapid Line Profile Variations

3.1. Introduction

In the previous chapter it was shown that o And consists of two widely separated binaries. The brightest of the four stars is presumably the source of the 1.57 day photometric variations. In this chapter, a search for spectral changes which might be related to the photometric variations is described. The analysis is based on additional high time resolution time series of spectra. The proper analysis of any rapid line profile variations found requires accurate knowledge of the spectral type and $v \sin i$ of o And A. Since spectral classifications and $v \sin i$ determinations in the past were obtained without regard to the multiplicity of o And, these parameters are re-evalutated.

3.2. Observations

Time series of Reticon spectra with signal-to-noise in the range 600 to 1600 were obtained using the cassegrain spectrograph of the 1.83 m and the coudé spectrograph of the 1.22 m telescopes of the Dominion Astrophysical Observatory. The 1.83 m observations are those already described in section 2.2. Both spectrographs were used in the first order which provided a reciprocal dispersion of about 10 Å/mm. For the detector used, this corresponded to about 0.14 Å per diode and a spectral coverage of about 270 Å.

The spectra presented here were obtained on three observing runs. Two runs were on the 1.83 m in August and October 1986 and one run was on the 1.22 m in September

1987. For all three runs the spectra were centered at approximately 4375 Å. The principle lines present are C II λ4267, Hγ λ4340, He I λλ4388,4471 and Mg II λ4481. The spectra are dominated by the rotationally broadened lines of the primary, o And A. Superimposed upon these are the narrower lines of the double-lined spectroscopic binary (probably o And B) discussed in chapter 2. The mean exposure time, time coverage, mean S/N per diode and number of spectra for each night are presented in Table IV. Iron/Argon comparison spectra were recorded before and after each exposure on the 1.83 m to calibrate wavelength drifts due to spectrograph flexure. For the coudé spectrograph of the 1.22 m this was not necessary and comparison spectra were recorded at the beginning, midpoint, and end of each time series. The FWHM of the instrumental profile was about 2 or 3 diodes (about 0.3 to 0.4 Å).

TABLE IV. The observations

Date (UT)	Exp.(sec)[a]	N[b]	S/N[c]	Time (days)[d]
27/Aug/86	803	20	——	0.299
29/Aug/86	2533	3	——	0.102
31/Aug/86	1560	5	——	0.109
01/Sept/86	1830	6	——	0.228
17/Oct/86	1551	13	1144	0.314
19/Oct/86	1264	14	1497	0.371
20/Oct/86	780	24	1568	0.302
22/Sept/87	2354	13	1106	0.361
23/Sept/87	2650	12	1034	0.363
24/Sept/87	2450	12	915	0.335
25/Sept/87	3120	5	636	0.296

Notes to TABLE IV

[a]Mean exposure time for night
[b]Number of spectra obtained
[c]Mean S/N for night
[d]Length of time series

A description of the procedures used for preprocessing the data to maximize S/N can be found in Walker, Johnson and Yang (1985). The data reduction program RETICENT (Pritchet, Mochnaki, and Yang 1982) was used to reduce the spectra. For each spectrum, the average of a number (about 10 to 15) of dark exposures was subtracted from the data frame. These were taken throughout the course of the night and the ones taken nearest a given spectrum were used. The dark exposures were typically 10 seconds in duration. This subtraction of dark exposures quite effectively removes the baseline associated with the Reticon electronics. A 4-pixel, multiplicative fixed pattern resulting from slight differences in gain between the 4 video lines was removed by division of a flat-field lamp which also removed diode-to-diode variations. These were exposed to a similar mean signal as the spectra. Any remaining 4 or 8 line multiplicative fixed patterns were removed by multiplicative line normalizations. For each night, a mean spectrum was formed and rectified with a fifth order polynomial fit to the continuum. All spectra for a given night were then divided by the rectified mean for that night. A fifth order polynomial was then fitted through 200 evenly space points in each divided spectrum and the polynomial divided through the original spectrum. In this manner the spectra in a given time series were rectified in a consistent manner. The algorithms of Stumpff (1980) were used to derive barycentric Julian days for the midexposure times and barycentric radial velocties with which to correct the dispersion relations for the motion of the earth.

3.3. Spectral Type and V$\sin i$

Spectra of o And have been studied for nearly a century, beginning with the first

classification in 1890. At that time two HD numbers were assigned when the presence of a strong shell spectrum caused the star to be erroneously classified as a B5 + A2 binary (Wilson 1950). By 1894 the shell spectrum had disappeared (Vogel and Wilsing 1899). The next 50 years saw the shell reappearing several times but it was not until 1952 that Slettebak classified o And as a Be shell star based on Hα plates taken by Hansen and Morgan in 1946, and on plates of his own obtained in 1949-1951. Slettebak (1982) has recently classified o And as B6IIIe.

Most of these classifications have been performed without the knowledge that a significant fraction of the equivalent width of the Mg II λ4481 line may arise from o And B. He I λ4471 is also affected by contamination from o And B but not so strongly. We have measured the line strength ratio (R) of He I λ4471 to Mg II λ4481 on the average of spectra obtained on September 1987. On this night the narrow lines from o And B were coalesced so that it was possible to interpolate across the central 2.5 Å of the He I λ4471 and Mg II λ4481 line profiles. The equivalent widths of the two lines were measured with a digital planimeter after compensating for the presence of the spectrum of o And B in this manner and R was found to be about 2.2 $\pm$ 0.1. From Collins (1974) this value implies that o And A is at least as early as B5. For slowly rotating stars, R varies from 3.8 at spectral type B3 to 1.2 and B7. As stars rotate faster the value of R for a given spectral type decreases. Since o And A has a rotational velocity of the order of half its critical velocity the results of Collins (1974) imply that o And A may be earlier than B5. As we have already noted in chapter 2, the presence of C II λ4267 implies a spectral type earlier than B6.

We have measured the equivalent width of Hγ and used the value (5.5 Å) with the M$_v$-W(Hγ) calibration of Millward and Walker (1985) to obtain M$_v$ = −2.3. This absolute magnitude is compatible with a MK class B4IV or B4.5III according to the spectral type M$_v$ calibration of Balona and Crampton (1974). There is no evidence of emission in Hγ in our spectra. Since the stars which constitute o And B are less luminous than o And A and probably (as shown in chapter 2) of later spectral type they will tend to make our measurement of W(Hγ) too large, and thus o And A may be more luminous than M$_v$ = −2.3. Unless a significant amount of emission is present in Hγ our value of M$_v$ is not too unrealistic. As such it would appear that o And A is at least one spectral subclass earlier than B6III. A spectral type of B5IIIe will thus be adopted for our analysis.

A large range of v sin$i$ values has been determined for o And A. The value most commonly quoted is the one found in the Bright Star Catalogue, which at 330 km s^{-1} is also the largest. The source of the Bright Star Catalogue estimate is probably the catalogue of v sin$i$ determinations by Uesugi and Fukuda (1970). The Uesugi and Fekuda determination was most likely made using the old scale of Slettebak, now acknowledged to be too high (Slettebak et al., 1975) and thus should be rejected. Slettebak (1982) measured v sin$i$ = 260 km s^{-1} on his new scale. Stoeckly and Buscombe (1987) give 212 km s^{-1} with i = 48. The most recent estimate of v sin$i$ is also the lowest, 195 km s^{-1} (Harmanec 1988, private communication). Any determination of projected rotational velocity is model dependent, which may account for the large range of values. Additionally, as with past spectral classifications, some of these determinations may have

been affected by the presence of a contribution to the spectrum by o And B. We have formed the mean of all spectra obtained with the 1.22 m telescope and measured the FWHM of He I λ4471 and Mg II λ4481 compensating for the presence of the spectrum of o And B in the manner described above. Using the scale of Slettebak et al. (1975) we obtained $v \sin i = 213$ km s^{-1} using He I λ4471 and $v \sin i = 250$ km s^{-1} using Mg II λ4481. The differences may be due to the effects of differential rotation. For the work presented here we shall adopt the straight average of the values found in the literature and our measurements, 225 ± 25 km s^{-1} .

3.4. The Line Profile Variations

The detection and measurement of line profile variations in the spectrum of o And A was complicated by the presence of a contribution to the spectrum from o And B. During the October 1986 run the double-line spectroscopic binary o And B (P=33 days) was at such a phase that the SB2 lines were near their maximum velocity excursion and so during the course of one night they were not moving rapidly across the underlying broad profile of o And A. The detection of the line-profile variations is enhanced by forming a mean profile for a given time series and subtracting this average profile from each spectrum in the time series. In this way, time varying residuals between individual spectra and the mean spectrum are emphasized. Being nearly stationary in the spectrum allowed the sharp components to be removed by forming a mean spectrum for a night and subtracting it from individual spectra. During the September 1987 run however, the SB2 stars were near their gamma velocity (the velocity of their center of mass) and thus over the course of a time series moved a noticable amount. This resulted

in incomplete subtraction when forming the residuals so that an s-shaped distortion was created by each SB2 line in the residuals. The SB2 lines were clearly visible in Mg II λ4481 and present, but not so obviously, in the other lines in our spectra.

Since the presentation of all our spectra would occupy considerable space we only present selected examples in this chapter and include all spectra in Appendix B. Figures 5 and 6 present the time series of He I λ4471 and Mg II λ4481 line-profiles from October 17 1986 (UT) and September 24 1987 (UT) respectively. The spectra have been smoothed with a Gaussian transfer function having a σ value of 0.8 diodes (about 0.1 Å). Variations in the line-profiles can be seen in the 1987 data but are not so obvious in the 1986 spectra. Due to a problem with the flat field lamps the August 1986 data was of not quite high enough S/N to detect rapid line profile variations. During the August 1986 run, the beam from the flat field lamp was much larger in diameter than the beam from the telescope. The result was that the image-slicer entrance was overfilled and the Reticon chip was not illuminated by the lamp in the same way as by the light from the star. It was thus not possible to properly divide out the diode-to-diode variations.

Figures 7 and 8 show the residuals, formed in the manner described above, of the spectra presented in Figures 5 and 6 respectively. As can be seen from Figures 7 and 8, the variations are at quite a low level (about 0.4 percent on September 24 1987 and about 0.2 percent on October 17 1986). At such a low level, accurate measurement of the variations is very difficult. In order to better detect and measure the variations, four of the lines present in our spectra were transformed into velocity space and added together. The rest wavelengths used were C II λ4267.160, He I λ4387.928, He I
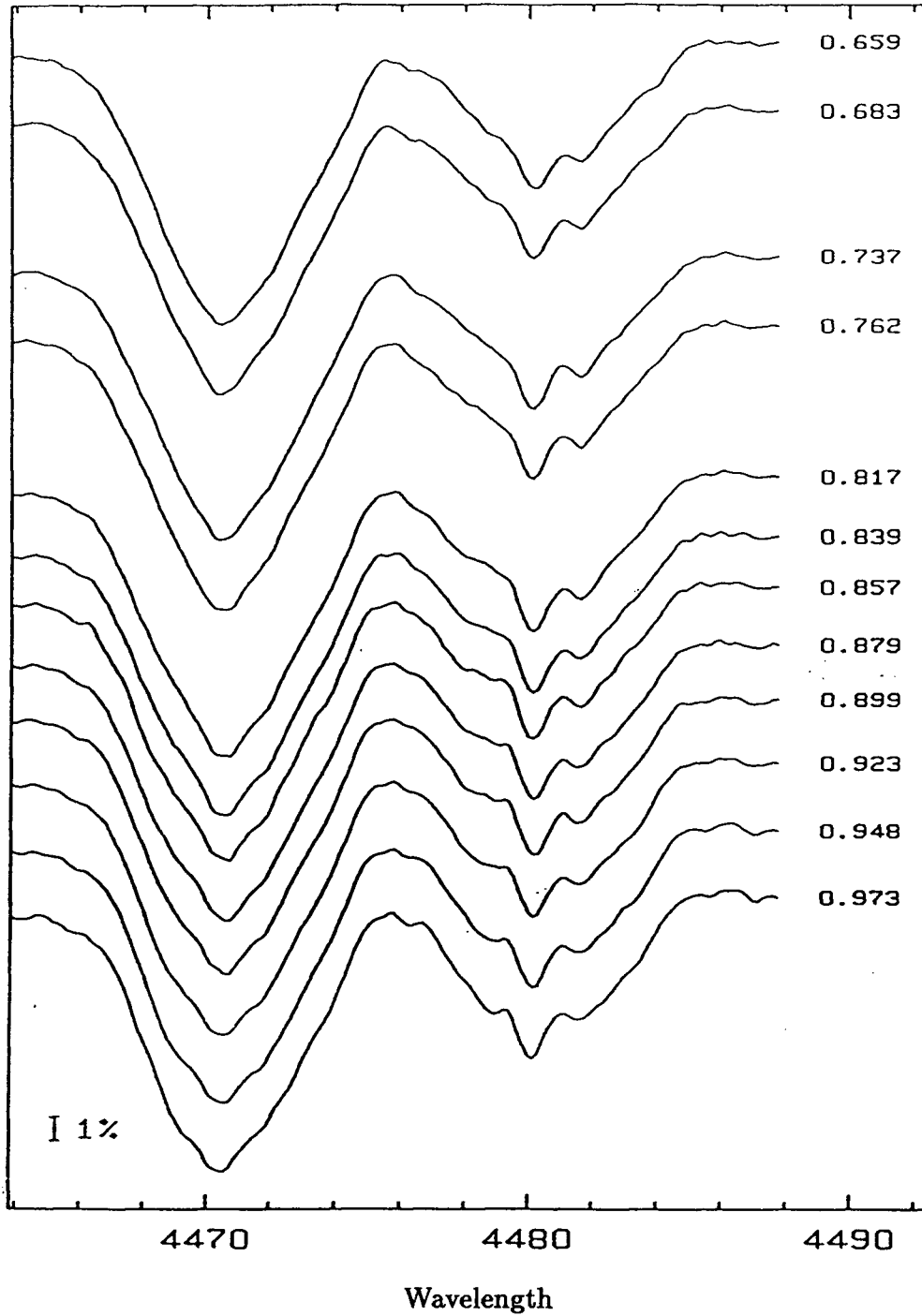
Fig. 5 — Time series of spectra showing He I λ 4471 and Mg II λ 4481 line profiles obtained on 17 October 1986 (UT). The number at the right of each spectrum is the corresponding mid-exposure time in fractions of a day from BJD 2446720.
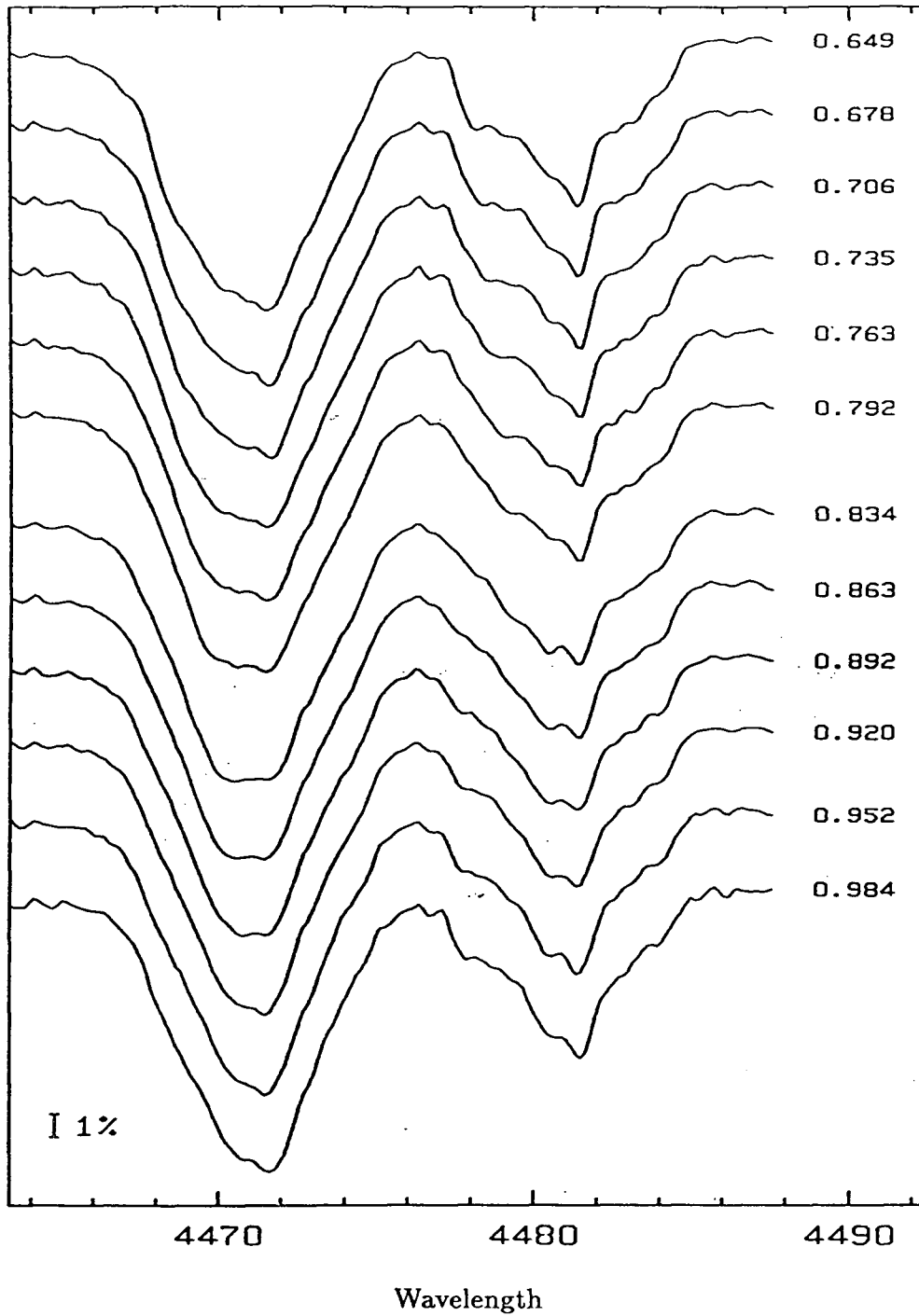
Fig. 6 — Time series of spectra showing He I λ 4471 and Mg II λ 4481 line profiles obtained on 24 September 1987 (UT). The number at the right of each spectrum is the corresponding mid-exposure time in fractions of a day from BJD 2447062.
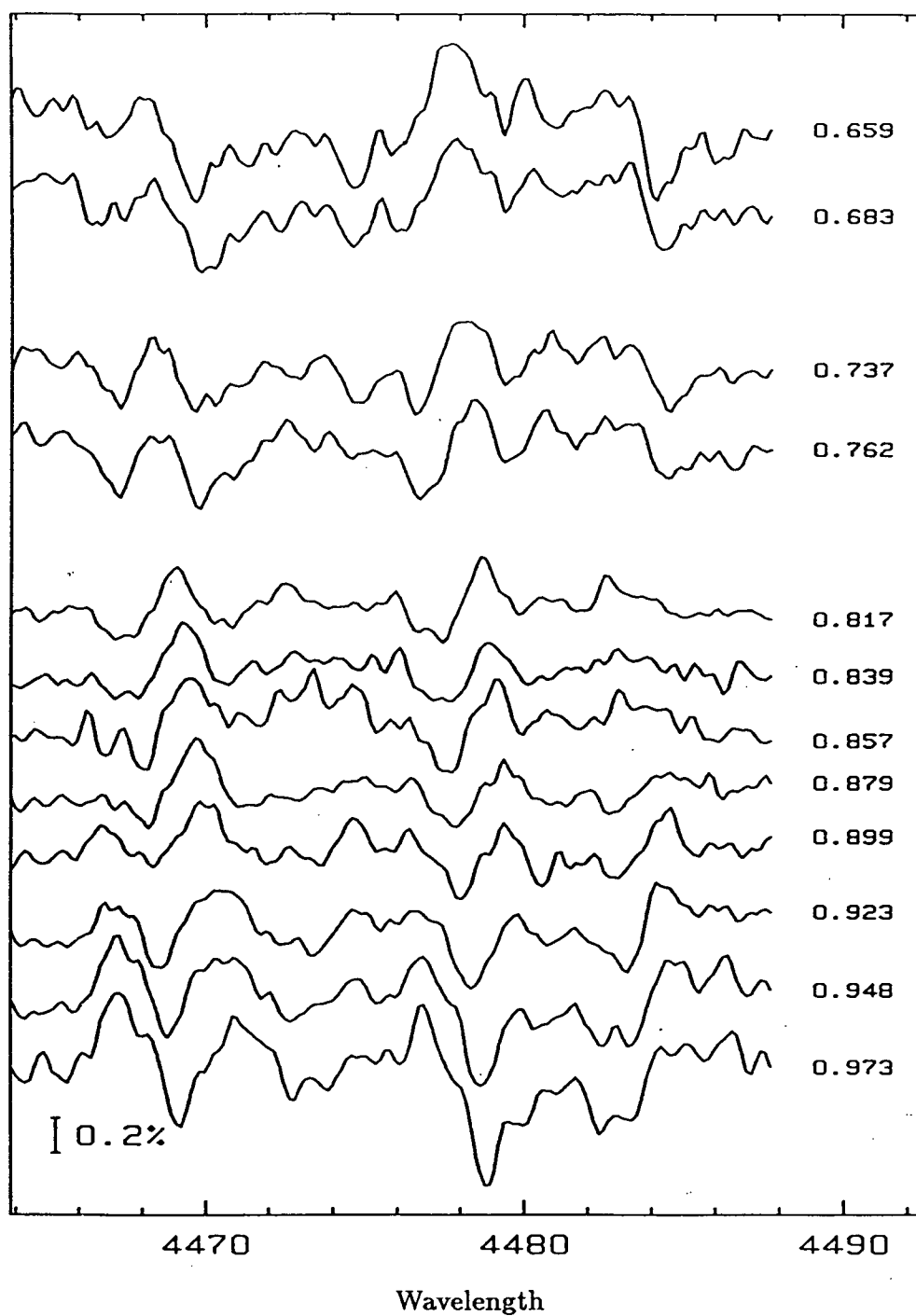
Fig. 7 — The residuals formed by subtracting the mean of the spectra presented in Figure 5 from the individual spectra.
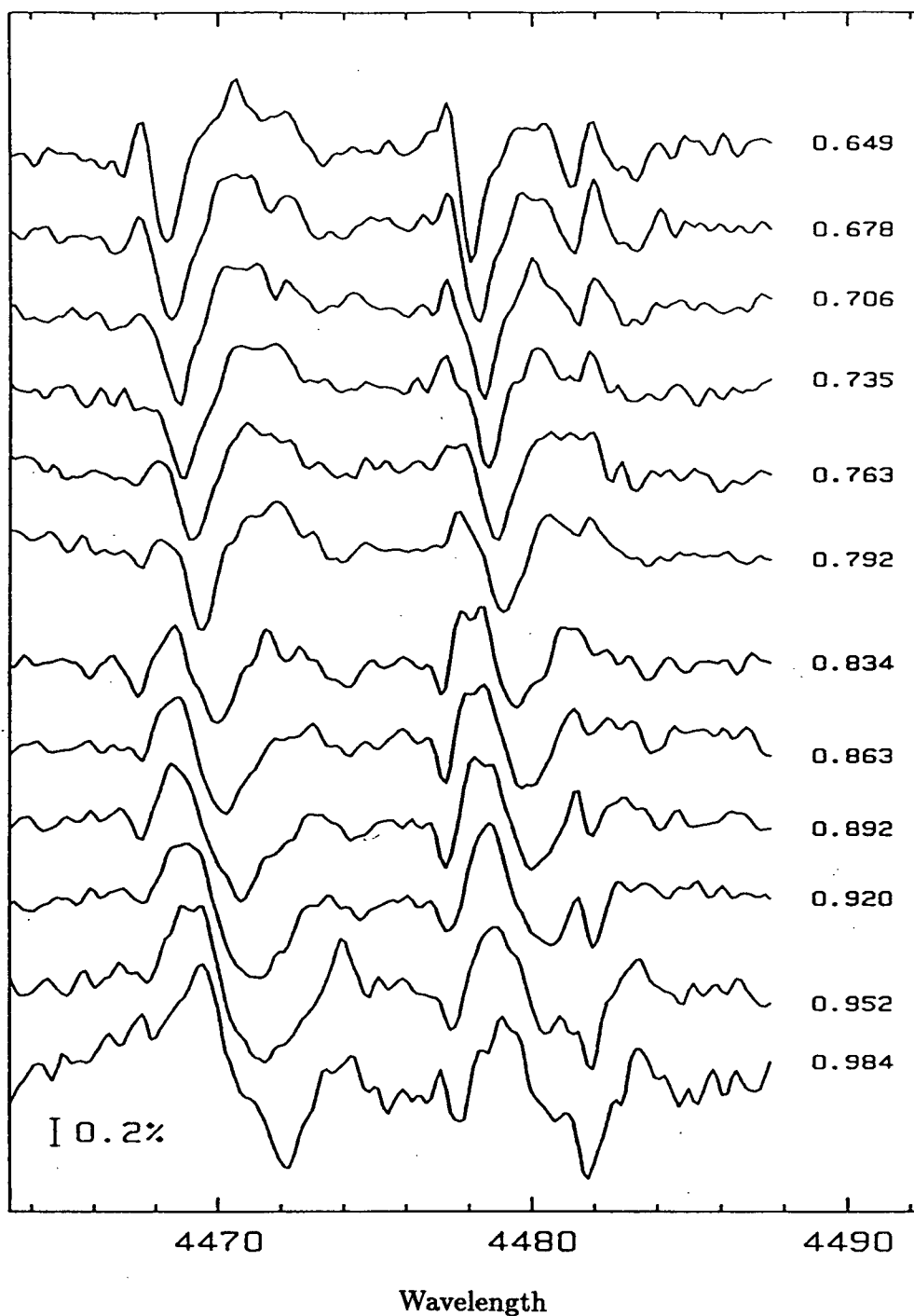
Fig. 8 — The residuals formed by subtracting the mean of the spectra presented in Figure 6 from the individual spectra.

$\lambda 4471.507$, and Mg II $\lambda 4481.228$. In adding the lines together the two He I lines were given unit weight and the C II and Mg II lines were given half weight due to their weakness and the strong presence of the lines of o And B in the Mg II line-profile. Hγ was not included in the analysis due to its wide intrinsic profile. The forming of the weighted mean of four lines of different physical character was not done without some trepidation. Before adding the lines together in velocity space, the residuals from all four lines were examined in wavelength space to ensure that they all exhibited variations and that those variations were of the same nature and in phase. On all nights where variations were visible this was the case.

After performing the transformation to velocity space for the six time series, the residuals were formed from the co-added lines. In the case of October 20 1986 the 24 spectra were binned into 12 bins to further improve the S/N. The co-added lines in velocity space are presented in the Appendix B. Figures 9 to 12 present the residuals thus formed for the October 17, 19 and 20 1986 and September 24 1987 respectively. As can be seen, during the October run the amplitude of the line profile variations remained at about 0.2 to 0.3 percent. On September 22 and 23 1987 the residuals were dominated by the s−shaped distortions caused by motion of the narrow-line contributions from o And B. There may have been line-profile variations present in the broad profile of o And A on these two nights but they were not obvious. On September 24 however, a single strong feature moved through the line from blue to red. This (comparatively) large amplitude feature was preceded by a weak feature just barely visible if one views Figure 12 from a shallow angle. The strong feature was also followed by a

41
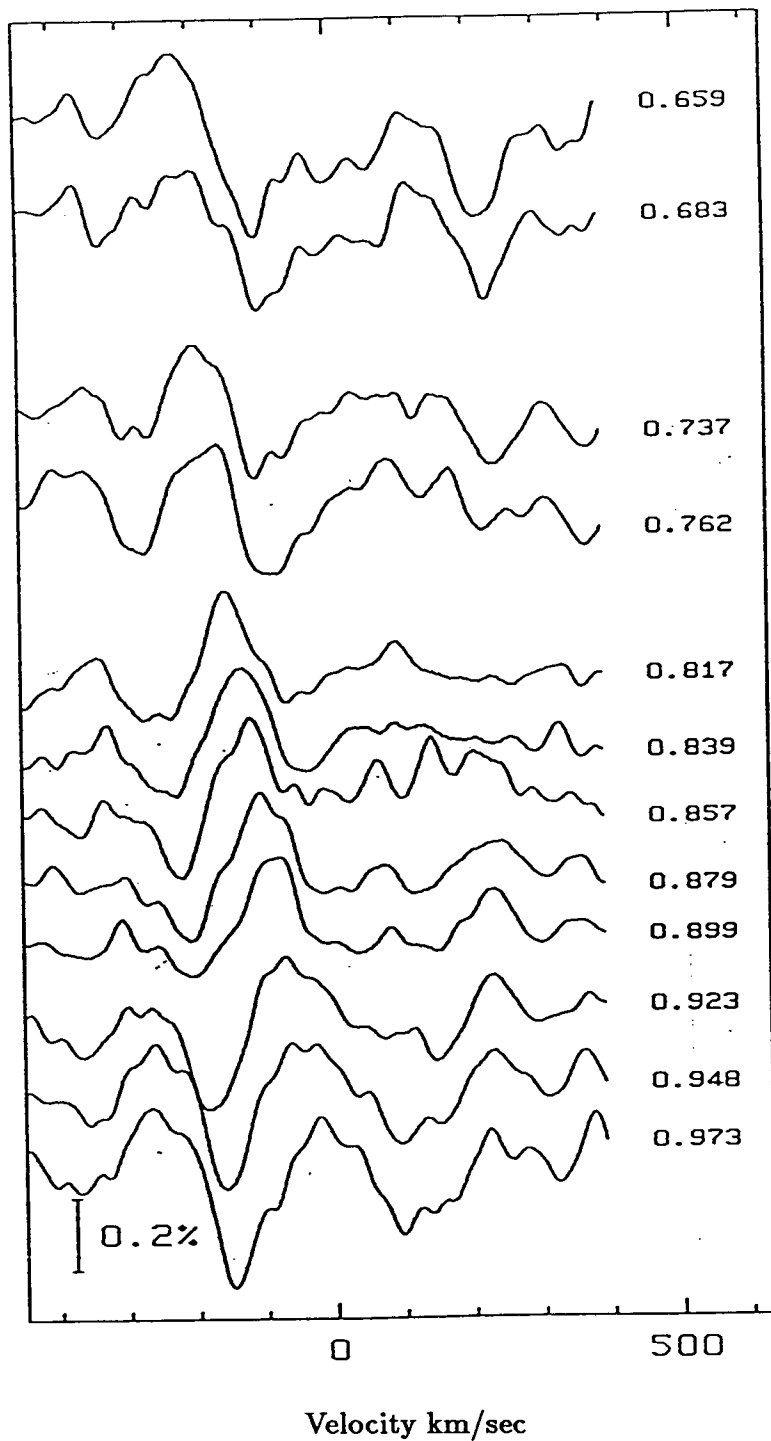
Fig. 9 — 17 October 1986 (UT) residuals formed in the same manner as in Figure 7 but using the weighted mean of C II λ 4267, He I λ λ 4388,4471 and Mg II λ 4481 transformed to velocity space.

0.593
0.609
0.620

0.731
0.747
0.766

0.806
0.825
0.843
0.865

0.894
0.921
0.943
0.964

0.2%

0   500

Velocity km/sec
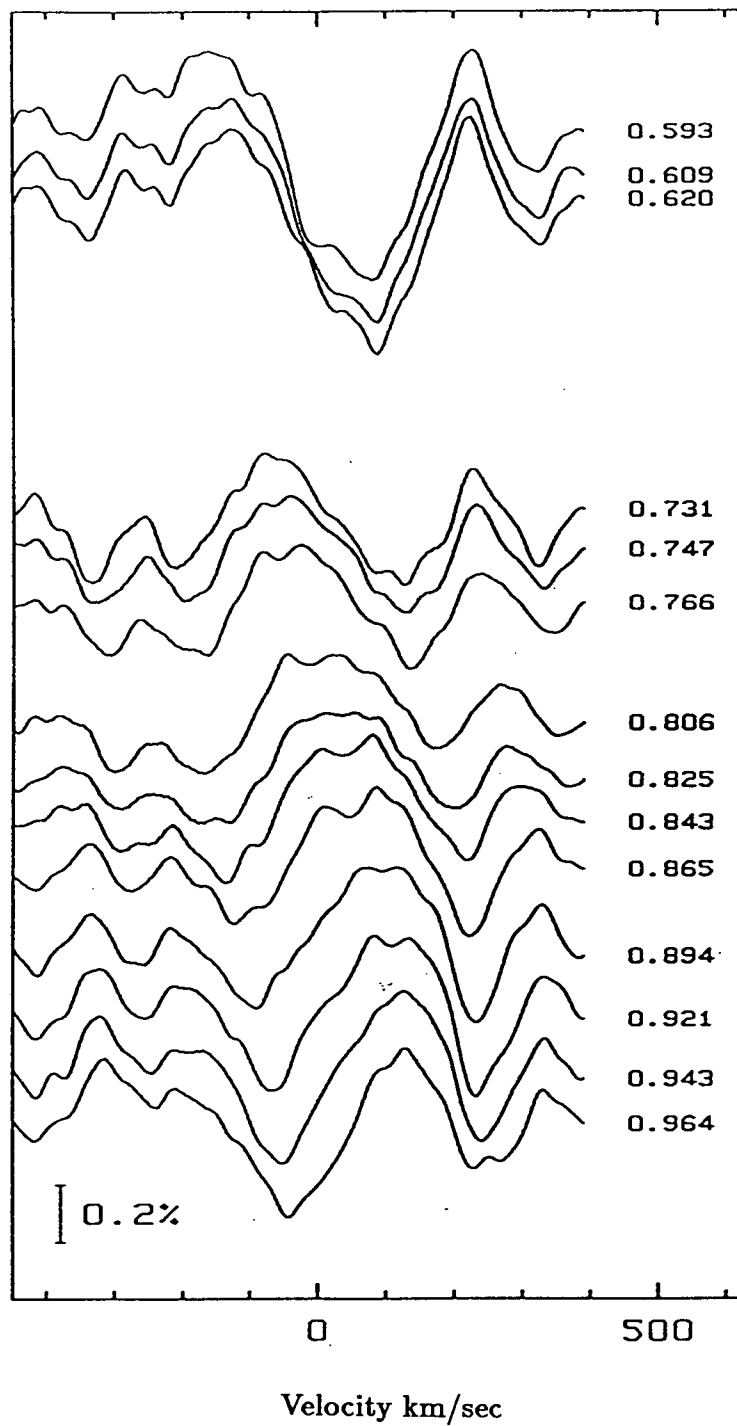
Fig. 10 — As for Figure 9 but for 19 October 1986 (UT)

43

0.629
0.644
0.653
0.666
0.673
0.684
0.693

0.722
0.729

0.743
0.753

0.768
0.779

0.793
0.802

0.821
0.830
0.844

0.852

0.867
0.878

0.892
0.904

0.931

0.2%

0

500

Velocity km/sec
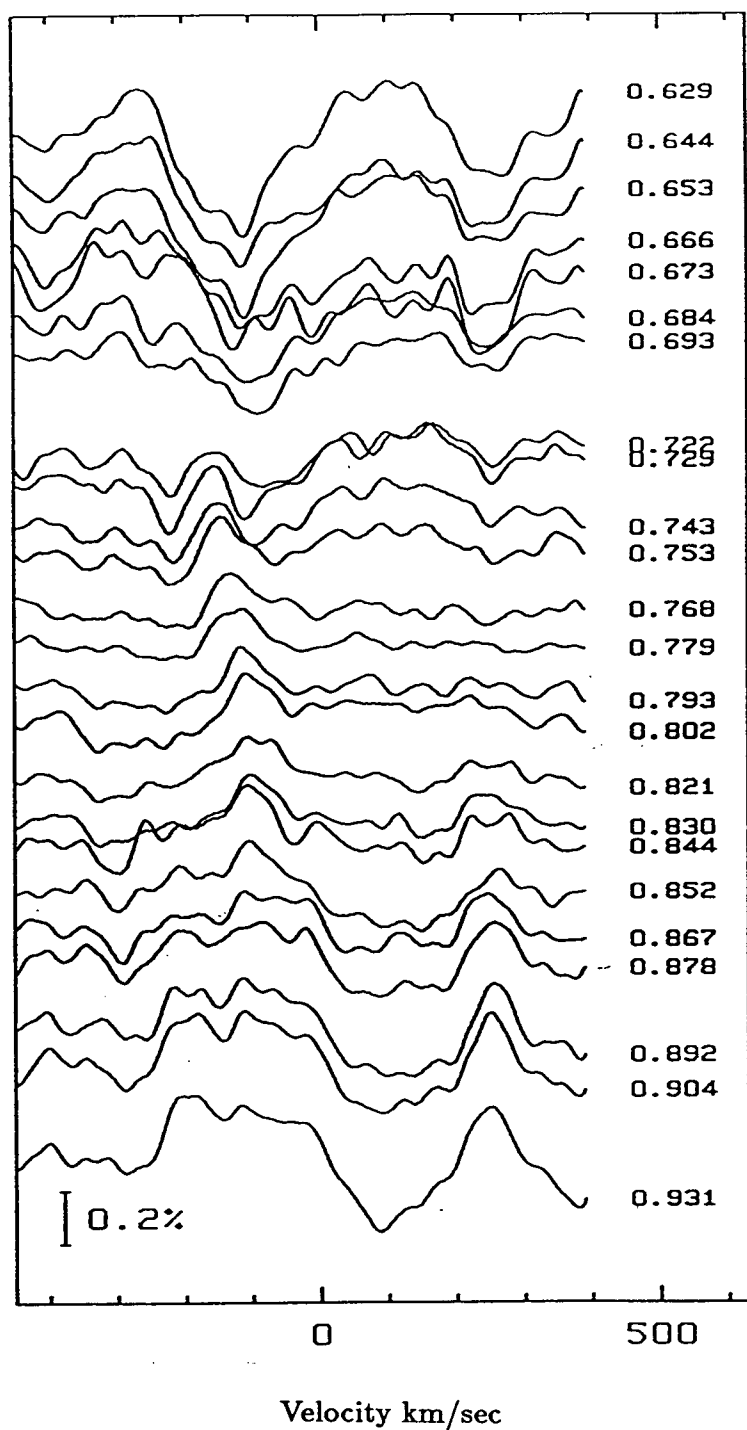
Fig. 11 — As for Figure 9 but for 20 October 1986 (UT)

44
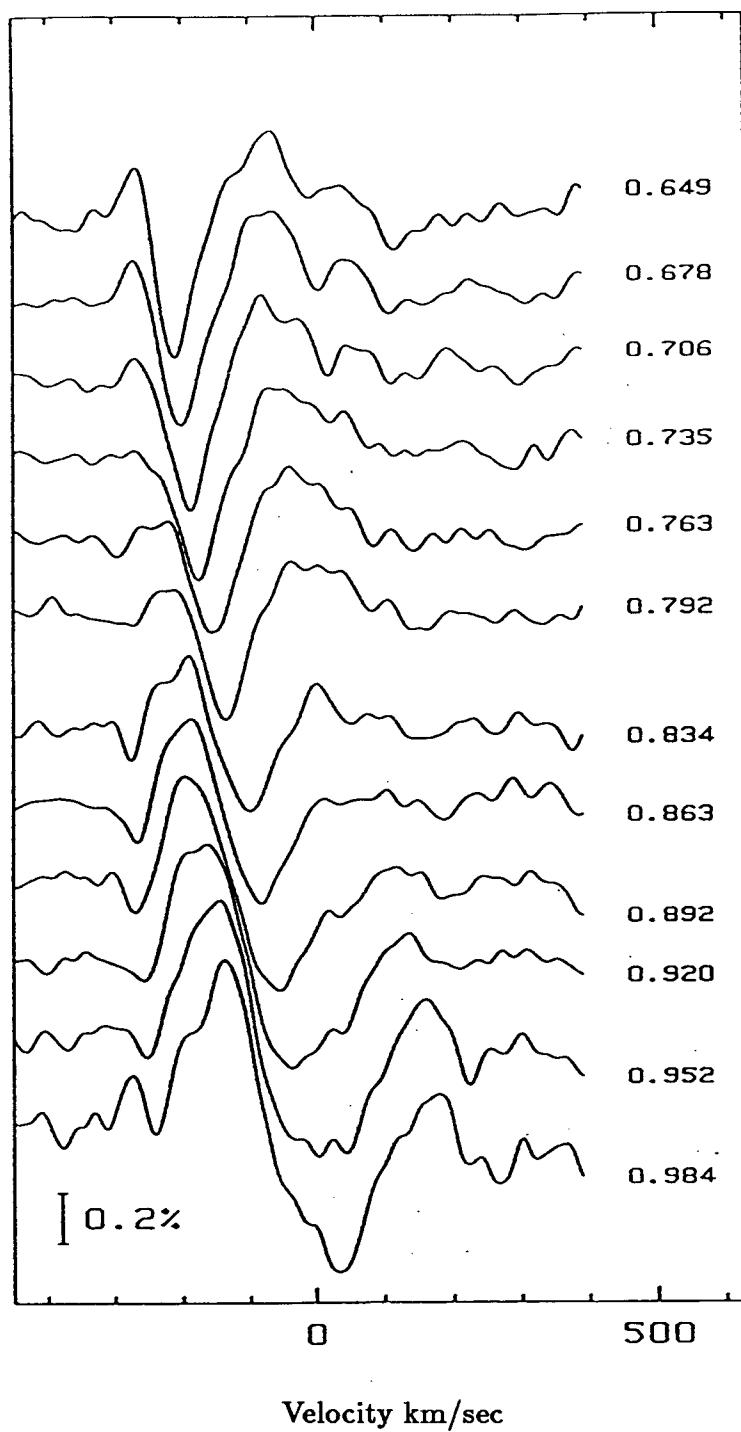
Fig. 12 — As for Figure 9 but for 24 September 1987 (UT)

weaker feature which enters the line-profile part way through the time series. For the four nights where moving absorption sub-features were visible we have measured their velocity as a function of time. These velocities are presented in Figures 13 to 16 with linear fits to the variation of each sub-feature.

In addition to the rapid variations discussed above we have detected line-width variations with a period of about 0.79 days. The full width of the four lines added together in velocity space was measured at 3 and 4 percent below the continuum and averaged. It was hoped that the effect of narrow moving sub-features on the line-width measurements would thus be reduced. The separation in velocity space of points on the line profile at 3 and 4 percent below the continuum was slightly more than the width of a moving sub-feature. The line-widths thus measured were searched for periodicity using the phase dispersion minimization (PDM) technique of Stellingwerf (1978). A period of 0.7924 days was found, with $\Theta_{min} = 0.53$. The half width at half minimum of the Θ transform was 0.0004 days. Due to the fact our data is clumped in three observing runs significant side lobes exist. The variations found were large enough to be accurately measured on the August 1986 data so that all three data sets were included in the period search. It is unlikely that the period found (0.7924 days) is an alias of a shorter period since the 0.79 day variations are visible in real time and most of our data consists of continuous strings (10 to 20 spectra) with string lengths of about 0.4 days. Figure 17 shows all the data phased to the 0.7924 day period and Figure 18 presents the same data binned into P/10 bins.

Previous spectroscopic investigations of o And have searched not only for line
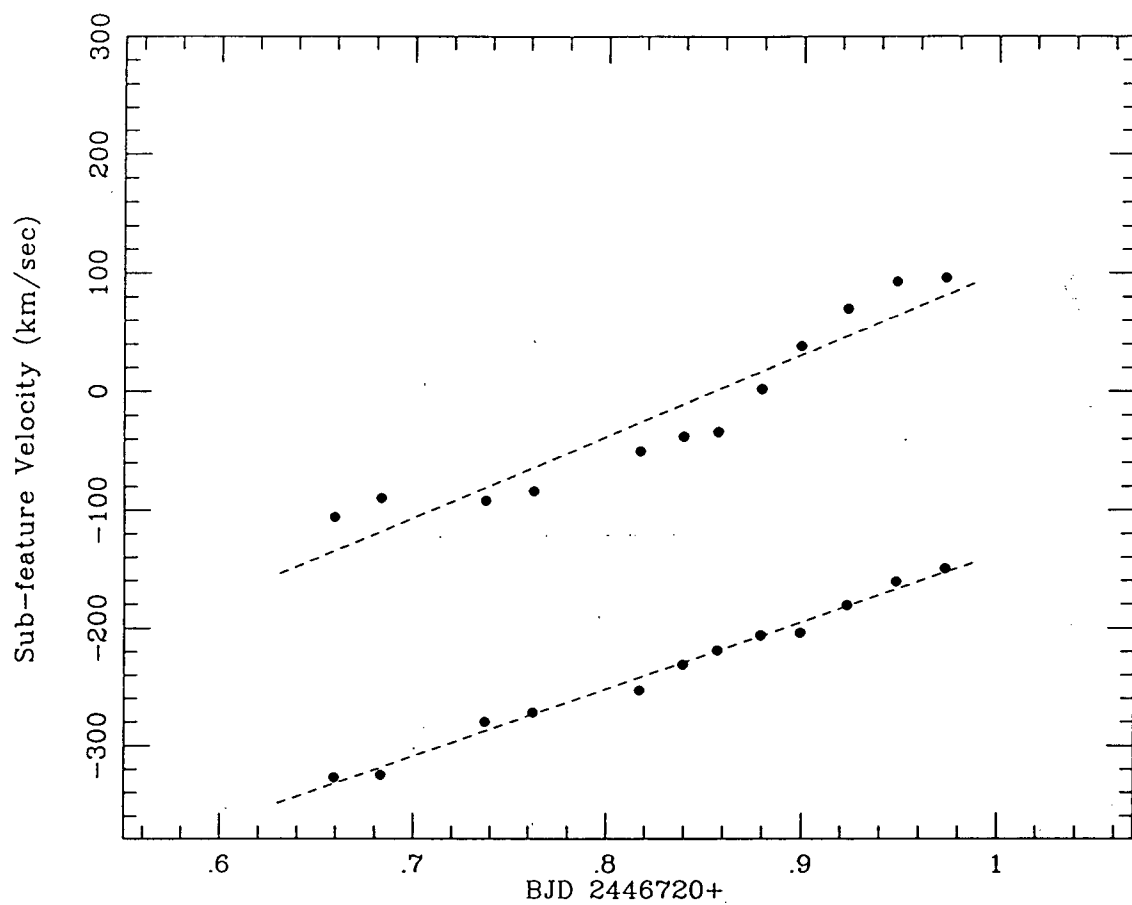
Fig. 13 — Acceleration of the moving sub-features measured on the time series residuals presented in Figure 9.
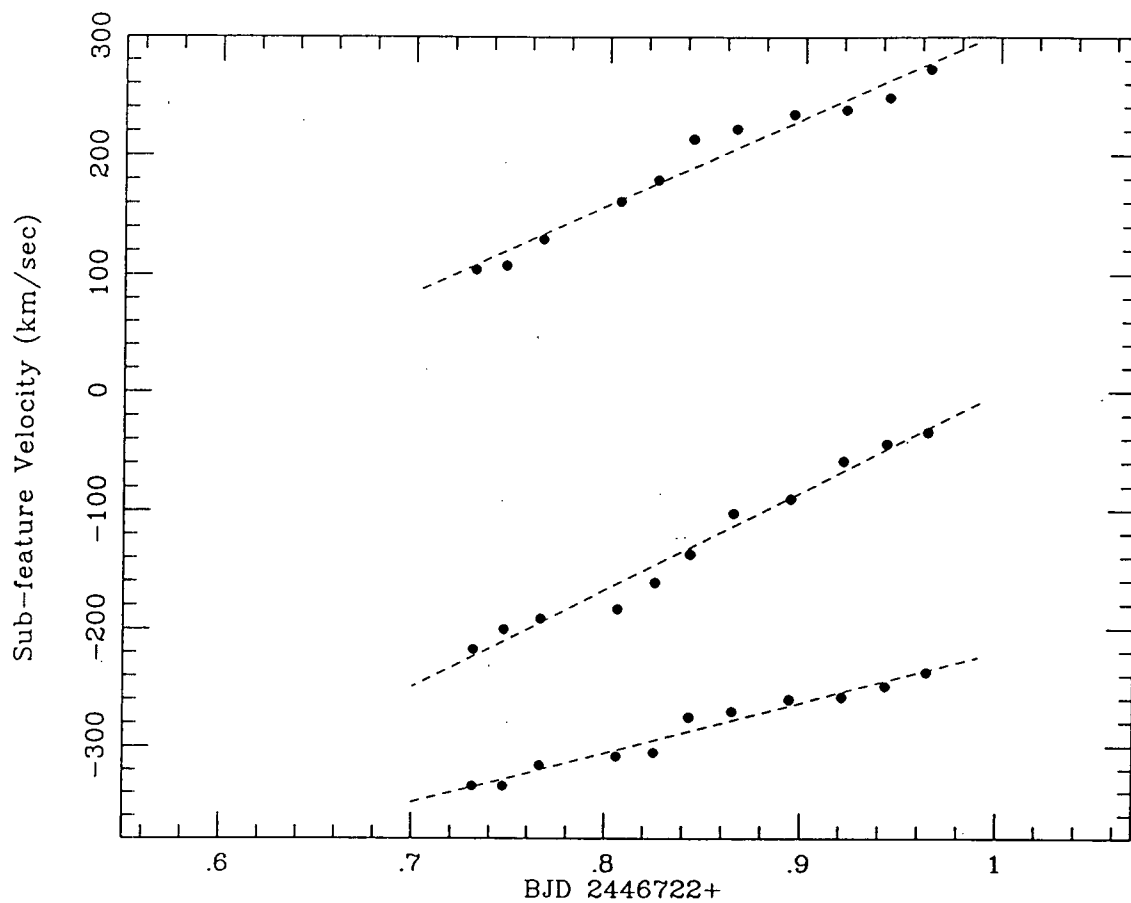
Fig. 14 — Acceleration of the moving sub-features measured on the time series residuals presented in Figure 10.
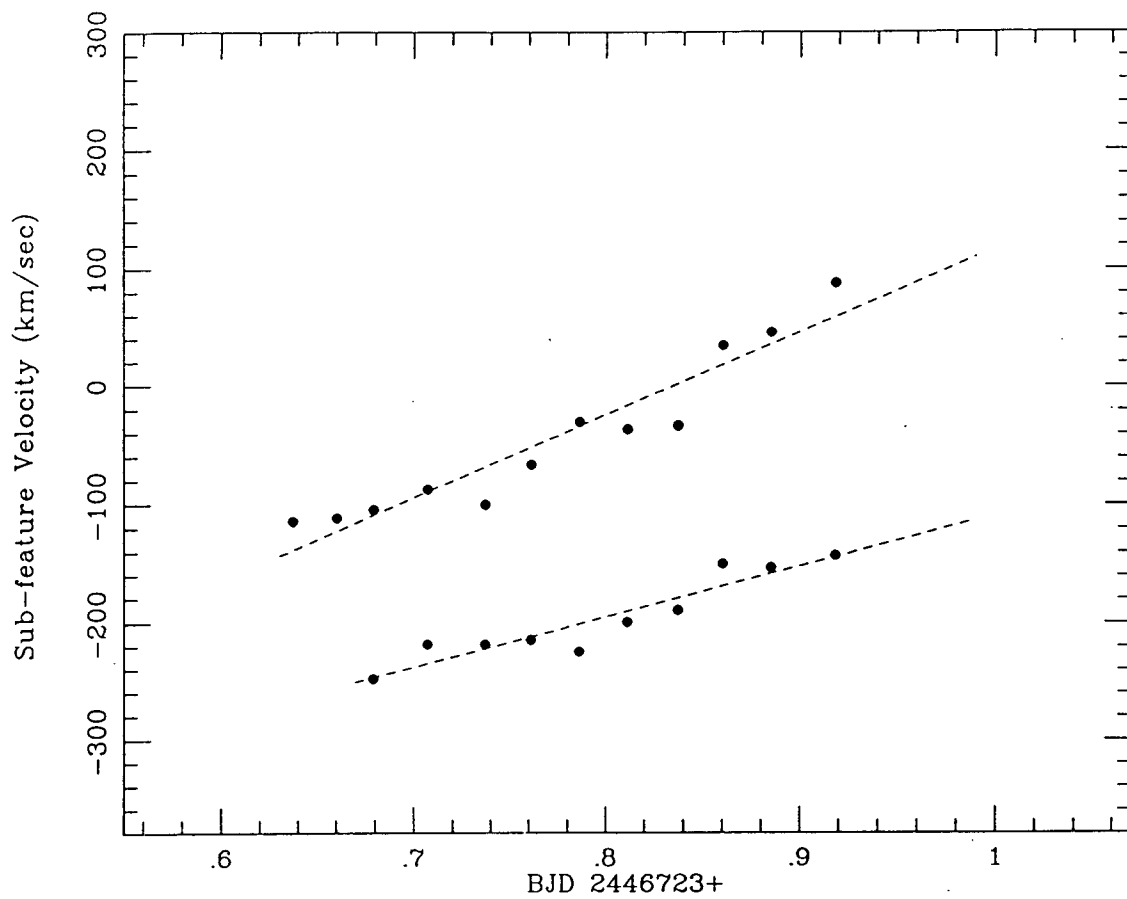
Fig. 15 — Acceleration of the moving sub-features measured on the time series residuals presented in Figure 11.
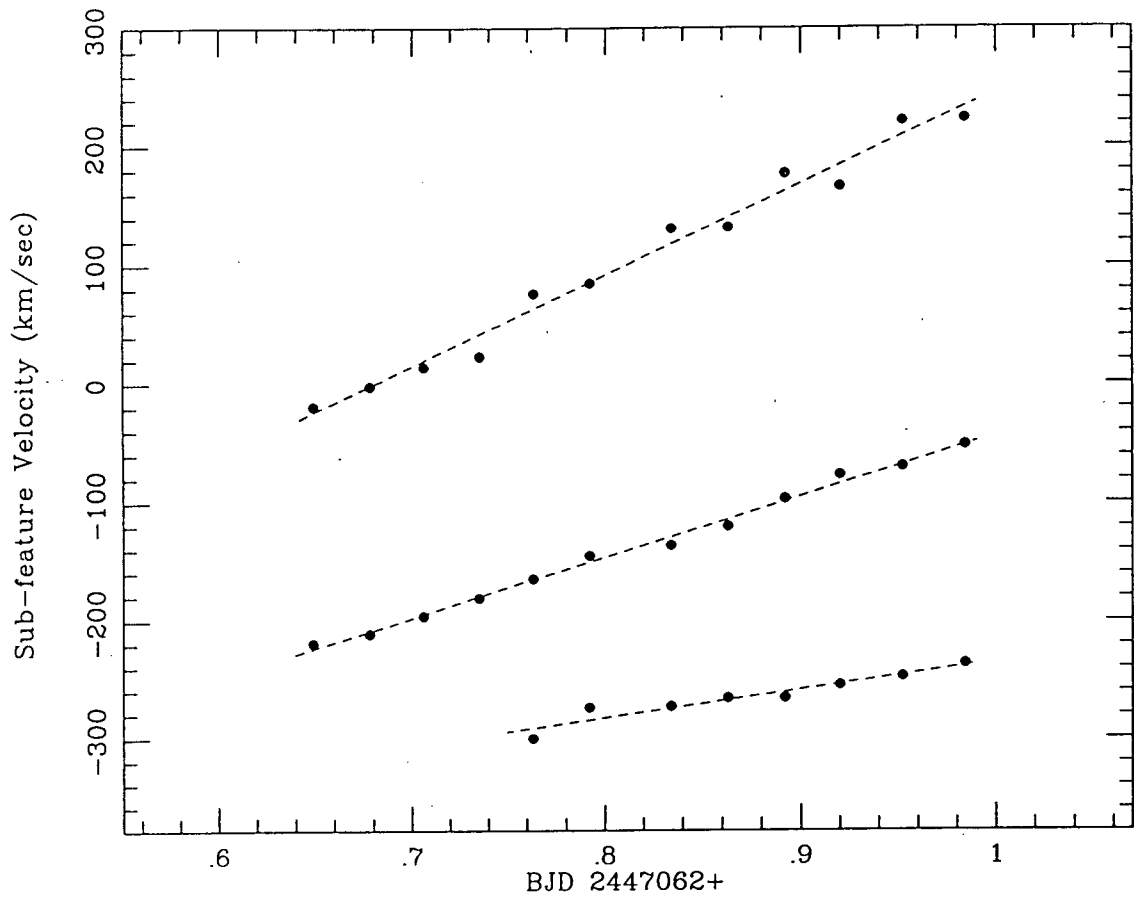
Fig. 16 — Acceleration of the moving sub-features measured on the time series residuals presented in Figure 12.
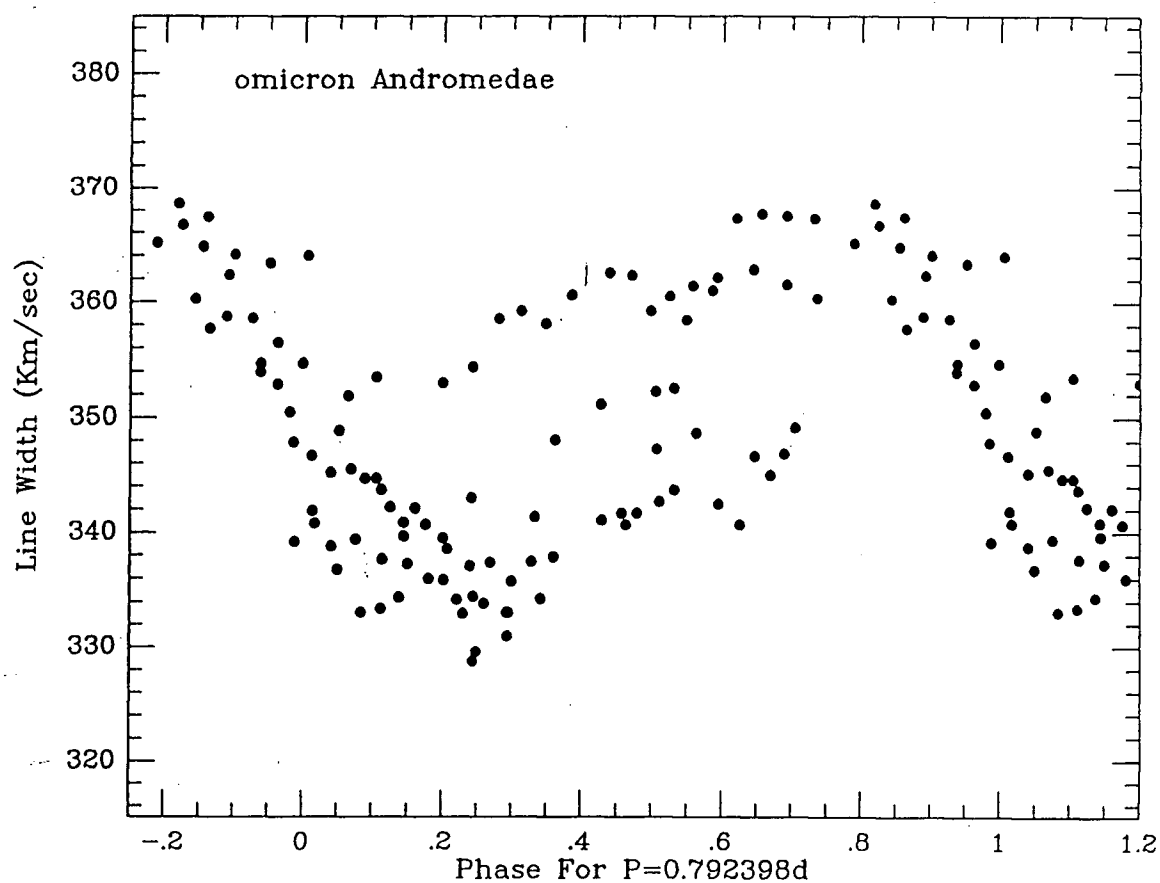
Fig. 17 — Line width variations measured from weighted mean of C II λ 4267, He I λ λ 4388,4471 and Mg II λ 4481 transformed to velocity space. The measurements were made at 3 and 4 percent below the continuum and averaged.
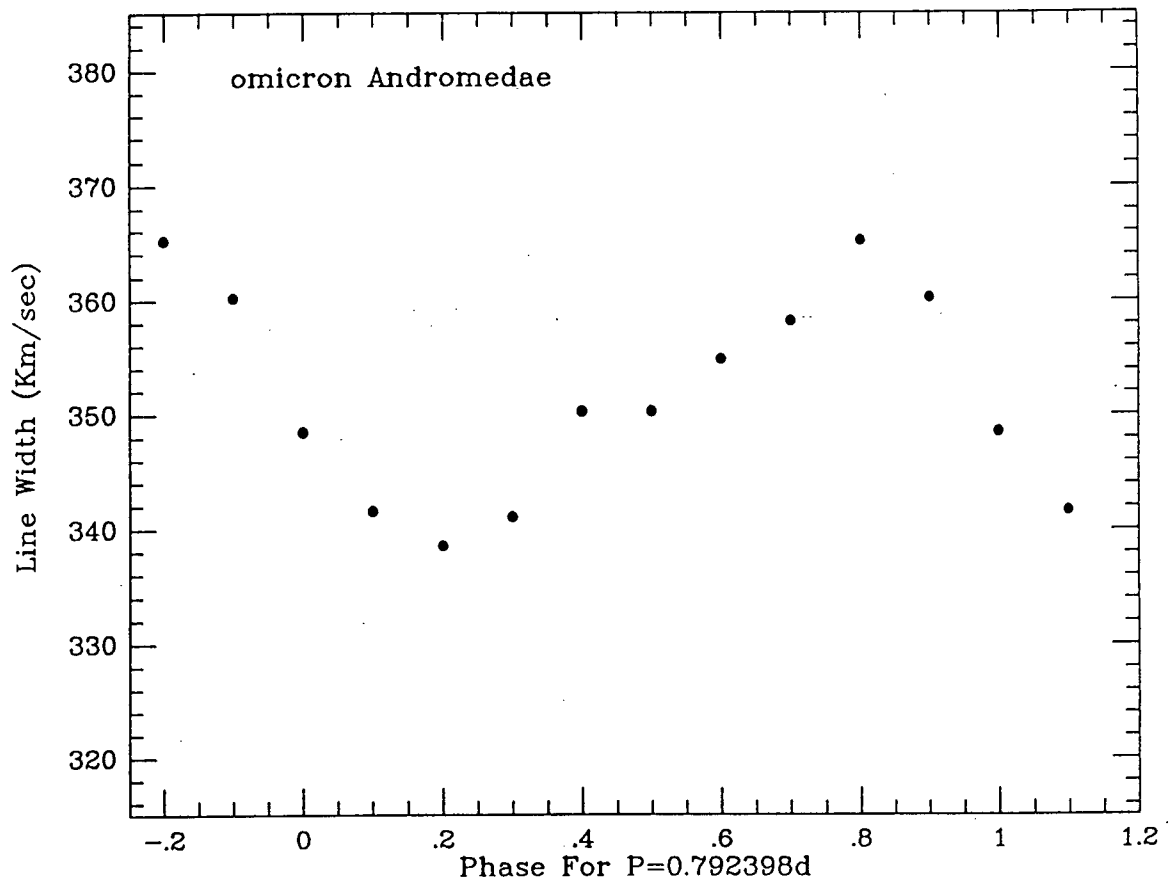
Fig. 18 — As for Figure 17 but binned into P/10 bins.

profile variations but radial velocity variations. The search for radial velocity variations is unfortunately confined to the line wings since the contribution to the spectrum of o And B precludes measuring the line cores. Additionally, one can confidently measure the radial velocity from the line wings only when the velocities of the two stars which constitute o And B are near their systemic values. At these times the narrow lines which originate in the double-line spectroscopic binary o And B are blended and very close to the line center of the underlying broad profile. These restrictions arise, in part, from the requirement that the radial velocity measurements be made using the entire line wings so that the effects of the moving sub-features are minimized.

Only our September 1987 spectra were searched for radial velocity variations since the narrow lines of o And B were at their maximum excursion in the line wings during both runs in 1986. All the spectra from the run were used to form an average. The technique of Fahlman and Glaspey (1973) was used to measure wavelength shifts of individual spectra with respect to the average spectrum. The wavelength shifts found were those which minimized, in a least squares sense, the sum over the line wings of the residuals between the average spectrum and the individual spectra. Each of C II $\lambda 4267$, He I $\lambda\lambda 4388,4471$ and Mg II $\lambda 4481$ was measured. All were found to exhibit low amplitude ($2K \approx 10$ km s^{-1}) variations. Despite the low amplitude it was apparent the variations from all lines were in phase. A weighted mean of the velocities was formed with the He I velocities given unit weight and those from C II and Mg II given half weight. The PDM technique of Stellingwerf (1978) was used to search for periodicity in these velocities. The best period found was 1.45 days ($\Theta_{min} = 0.23$) although,
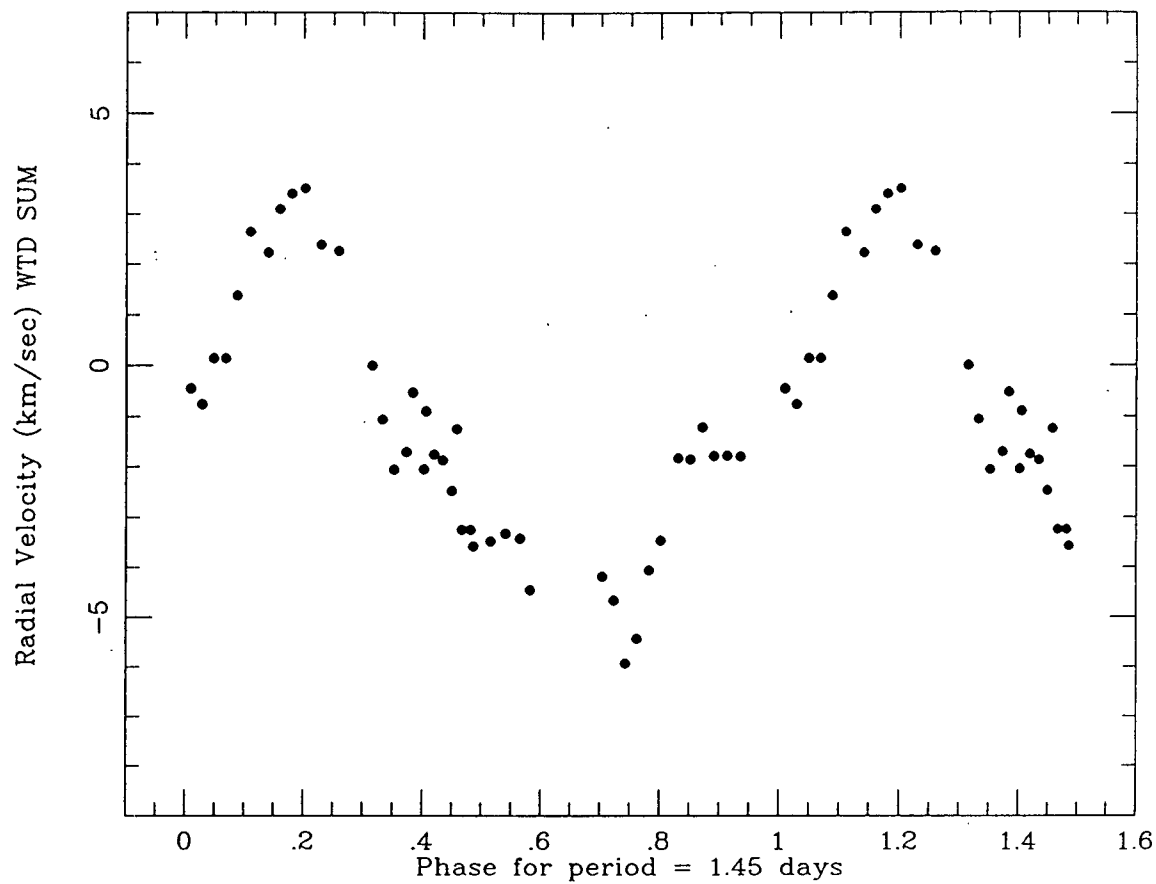
Fig. 19 — Weighted mean of radial velocity variations measured from the wings of C II λ 4267, He I λ λ 4388,4471 and Mg II λ 4481.

given the short length of the data set this number is quit uncertain. The half width at half minimum of the Θ transform was about 0.25 days. The radial velocities phased to a 1.45 day period are presented in Figure 19.

3.5 Discussion

The line profile variations evident in the residuals from the spectra are typical of those found in rapidly rotating early type nonradial pulsators. The presence of a dip or a trough in a residual indicates the presence of greater absorption than the mean for the time series at that location in the line profile. The blue to red movement across the line profiles of these narrow absorption features is typical of the moving distortions present in time series of model line profiles produced for rapidly rotating nonradially pulsating stars (Fahlman et al. 1988). As such, the assumption that NRP gives rise to the observed line profile variations is not unreasonable.

For a star undergoing sectorial mode NRP ($l = |m|$), there will be m waves around the equator of the star (Cox 1984). Likewise, around the equator of the star will be m sections that have a net outward velocity alternating with m sections that have a net inward velocity. It is these $2m$ inward moving and outward moving sections that are carried across the line of sight of the observer by the stellar rotation plus the azimuthal velocity of the waves and which combine to form the blue to red moving absorption features. The wavecrests propagate with angular velocity

$$\omega = \sigma/\mathrm{m} \tag{1}$$

55

where σ is the wave frequency. The observed wave frequency σ_o is σ plus the fequency of waves brought across the line of sight by stellar rotation (Cox 1984):

$$\sigma_o \quad = \quad \sigma + m\phi(1-C_{kl}) \tag{2}$$

where the convention that $m > 0$ indicates prograde motion has been adopted. $\phi = 1/P_{rot}$ is the stellar rotation frequency and C_{kl} is a first order correction for the effects of Coriolis forces. The quantity C_{kl} is a dimensionless number depending on the stellar structure. We use here the approximation of Smith (1985) for C_{kl} :

$$C_{kl} \quad = \quad (l(l+1))^{-1} \tag{3}$$

For high degree pulsations and for rapid rotation $\sigma_o >> \sigma$ and $C_{kl} << 1$ so that

$$\sigma_o \quad \approx \quad m\phi \tag{4}$$

Since $\phi = 1/P_{rot}$ and $\sigma_o = 1/\Delta t$ (Δt is the time between successive sub-features crossing the line centre) one may show (Fahlman et al. 1988) that:

$$|m| \quad \approx \quad \frac{2\pi(V_e \pm V_\phi)\sin i}{a_o \Delta t} \tag{5}$$

where a_o is the acceleration of the absorption sub-feature as it crosses the line center. V_e is the equatorial rotational velocity of the star and V_ϕ is the velocity of the wave in the azimuthal direction. The plus or minus corresponds to prograde or retrograde motion respectively.

The values of a_o and Δt were found from the velocities presented in Figures 13-16. Sub-features measured too far from the line center yield values of a_o that are too low (Fahlman et al. 1988) so one sub-feature that entered the line profile part way through the time series on September 24 1987 was excluded from the analysis. The measured a_o and Δt values are presented in Table V with the number of sub-features used to form the mean for a given night. In forming the mean for a given night, different weights were attached to the measured a_o and Δt depending on whether the sub-feature in question crossed the line center. For a_o, if the sub-feature crossed the line center the measured a_o was given double weight, otherwise it was given unit weight. For Δt, if both sub-features used, crossed the line center, double weight was assigned, otherwise it was given unit weight. Using our adopted $v \sin i$ of 225 km s^{-1} and the mean values of a_o and Δt presented in Table V in equation (5) yields $|m| = 6.4$ for $V_\phi = 0$. The uncertainties associated with $(V_e + V_\phi) \sin i$, a_o and Δt imply an uncertainty of about 25 percent in this value. The largest contribution to the uncertainty comes from the $(V_e + V_\phi) \sin i$ term. The atmospheric sound speed limits V_ϕ to ~ 10 km/sec.

TABLE V. Sub-feature accelerations and time separations

Date (UT)	a_o (km s^{-1} d^{-1})	Δt (d)	n
17/Oct/86	648	0.357	2
19/Oct/86	702	0.342	3
20/Oct/86	611	0.293	2
24/Sept/87	700	0.316	2
wtd mean	669	0.329	

At this point it should be noted (as pointed out by Myron Smith) that in order to properly determine the values of l and $|m|$, comparison with model line profiles is also desirable. Unfortunately, for o And A the presence in the spectrum of a contribution from o And B makes this virtually impossible. If $l = |m|$, as is usually found to be the case (Baade 1987), and l values are constrained to be even integers, then $|m| = 6$ would appear to be the most likely value for $|m|$, although $|m| = 8$ cannot be ruled out.

The value of $|m|$ may be further constrained by examining the rotational periods implied by various $|m|$ values. One can use equation (4) to find the rotational period for the star. Since $\sigma_o = 1/\Delta t$ and $\phi = 1/P_{rot}$

$$P_{rot} \quad = \quad |m|\Delta t \qquad\qquad (6)$$

Equation (6) yields rotational periods of 1.3, 2.0 and 2.6 days for $|m| = 4$, 6 and 8 respectively with uncertainties of about 15 or 20 percent. For vsin$i$ equal to 225 km/sec, a rotational period of 2.6 days implies an Rsin$i$ of about 12 $R_\odot$. Typical radii for B5 or B6 giants are about 5 $R_\odot$ (Underhill and Doazan, 1982). This would seem to favour concluding $|m| \leq 6$. At this point we recall that there exists a photometric period of 1.57 days. If this is also the rotational period of the star then $|m| = 8$ would again appear unlikely.

The 0.79 day periodicity in line width variations is remarkably close to exactly one half the 1.57 day period for the photometric variations. The 1.57 day light curve is in the form of a double wave with two unequal minima. The depth of the minima, the shape of the light curve and the comparative depth of the two minima seems to change

on a time scale of about 11-15 days (see Harmanec et al. 1987). Since we measured these line width variations on the velocity space added spectra which are dominated by the two He I lines and the C II line, all of which strengthen with increasing temperature for late B stars it was natural to wonder whether the line width variations reflected temperature variations. For late B stars the Mg II line strengthens with decreasing temperature so we measured the line width variations of the Mg II line alone. The variations measured were in phase with those of the co-added lines. It would appear the line width variations do not represent temperature variations.

A rapidly rotating star that possesses an $l = 2$ NRP mode produces line width variations with a period about half the rotational period (Unno et al, 1979). The existence of a higher degree mode does not preclude the existence of an $l = 2$ mode. Among rapidly rotating Be stars the presence of both an $l = 2$ mode and a higher degree mode is believed to be fairly common, (Smith, 1986). Since an $l = 2$ mode represents in a sense an ellipsoidal variable, one would expect to also observe a single wave light curve with the same period as the line width variations. High degree NRP modes commonly exhibit cycle to cycle variations in amplitude and sub-feature spacing, whereas the $l = 2$ modes are much more stable (Smith, 1986). The superposition (and interference) of an intermediate or high degree mode with some irregularity and a low order mode could produce a double wave light curve with a period equal to the rotational period of the star. If the azimuthal velocities of the two modes are not the same and/or if the higher degree mode irregularities change with time then the shape of the light curve may vary as the interference between the two modes varies. This could also explain the

very strong sub-feature observed on September 24 1987 as a superposition of an $l = 2$ mode and a higher degree mode.

The radial velocity variations exhibited by the wings of the lines represent formal measurements. It is difficult to say just to what degree the measurements reflect the profile variations as opposed to true radial velocity changes in the star. This ambiguity is further emphasized by the fact that an $l = 2$ mode can mimic binarity and the presence of a companion star can tidally drive an $l = 2$ mode. The underlying assumption of our measurement technique, or for that matter any cross-correlation type measurement, is that the profile is unchanging. This is certainly not the case. If the radial velocity variations presented in Figure 19 are due to binarity with $2K = 8$ km s^{-1} and assuming a circular orbit one obtains $a_1 \sin i = 8 \times 10^4$ km. The mass function would be 0.1 M$_\odot$ so that for a mass of 5 M$_\odot$ for o And A, $M_2 \sin i = 0.06$ M$_\odot$. The mass ratio would thus be about 0.01 and the two stars would be separated by about 10 R$_\odot$. Since o And A is observed to have a high projected rotational velocity, the $\sin i$ term is not likely to be too small since the rotational angular momentum vector of o And A would presumably be aligned with any orbital angular mometum vector that may exist.

A close companion star to o And A, if it exists, would be very small, only just barely able to burn hydrogen if at all. Since the 10 R$_\odot$ separation represents near-contact, photometric variations due to eclipsing should be observed unless the orbit is pole-on or nearly so. To be nearly pole-on would require the orbital angular momentum vector and the rotational angular momentum vector of o And A to be at large angles to each other. A stable single-wave light curve would be expected if one interprets the radial

velocity variations as due to binarity. The light curve for o And is a variable double wave. Additionally, if a small opaque companion were passing in front of o And A one should observe a single quasi-emission feature move across the line profile from blue to red. The term quasi-emission is used since the feature would actually be a lack of absorption as opposed to a true emission feature. The strong feature observed moving across the line profiles on September 24 1987 was in absorption not in emission. Since a stable single-wave light curve and moving quasi-emission features are not observed it seems more likely that the variable radial velocity measurements are due to line profile variability than to binarity.

Chapter 4. Conclusions

In chapter 2 it has been shown that o And is a quadruple system consisting of two widely separated binaries. The narrow absorption features superimposed on the rotationally broadened Mg II λ 4481 line are from o And B which has been shown to be a double-lined spectroscopic binary with a period of 33 days. The brightest member of the system, o And A (a Be/shell star), and the faintest o And a, form a resolved binary while o And B is unresolved. The two stars which make up o And B are probably late B stars on or just off the main sequence. If one accepts the parallax of 0.015 arcseconds, the binary pair is separated by about 25 AU and the two resolved binary stars (A-a) are separated by about 4 AU. The solution of the orbit of the (unresolved) spectroscopic binary o And B yields a separation of about 0.4 AU.

Assigning reasonable mass estimates for their spectral types, the periods of A-a and Aa-B are on the order of four and thirty years respectively. For a smaller parallax the periods would be longer. The small change in the Aa-B position angle over the past 10 years implies either an eccentric orbit or a much longer period.

In chapter 3, based on the ratio of the strength of He I λ 4471 to Mg II λ 4481, the equivalent width of Hγ and the presence of C II λ 4267, it has been shown that o And A is at least one spectral subclass earlier than the commonly quoted classification B6IIIe. Past determinations of spectral class and v sin$i$ were performed without the knowledge of the multiple nature of o And. The unresolved binary, o And B, may contribute up to 40 percent of the total flux from the system which has resulted in a misclassification of o And A toward a later spectral type. A new determination of

v sin$i$ is presented where the presence in the spectrum of a contribution from o And B is compensated for.

Rapid line profile variations, typical of sectorial nonradial pulsations, have been detected for o And A. Both the moving absorption subfeatures, which suggest an intermediate or high degree mode, and line width variations typical of an $l = 2$ mode, have been detected. The line width variations do not arise from temperature variations. Radial velocity variations measured from the line wings are probably not due to a fifth star, but rather are a result of the underlying profile variations. If the radial velocity variations are interpreted as arising from binarity, the resulting (very small) fifth star in the system would be in near contact with o And A and a stable light curve would be expected due to eclipses. The light curve is variable and double.

The intermediate mode is most likely $l = 6$. A larger value ($l = 8$) implies a stellar radius inconsistent with a mid-B giant. A smaller value ($l = 4$) is beyond our estimated uncertainty. The 1.57 day photometric variations are interpreted as resulting from the $l = 2$ NRP mode. The variable shape and amplitude of the double-wave light curve is explained as resulting from varying interference between the $l = 2$ and the $l = 6$ modes. Some of the longer term photometric and spectroscopic variations may result from the multiplicity of the system. Since o And A is nonradially pulsating and is a member of a multiple system it may represent an excellent opportunity to test two of the many theorems advanced to explain the Be phenomenon, namely the binary model and the NRP model.

Bibliography

Baade, D., 1982a, *Astr.Ap.*, **105**, 65.

Baade, D., 1982b, *Astr.Ap.*, **110**, L15.

Baade, D., 1983, *Astr.Ap.*, **124**, 283.

Baade, D., 1984a, *Astr.Ap.*, **134**, 105.

Baade, D., 1984b, *Astr.Ap.*, **135**, 101.

Baade, D. 1987, in *Physics of Be Stars*, Proc. IAU Col. 92, eds. A. Slettebak and

T. P. Snow, (Cambridge: Cambridge University Press), p. 361.

Baade, D., Pollok, H., Schumann, J. D., and Duerbeck, H. W., 1982, *I.A.U. Inf. Bull.*

Var. Stars. No. 2125.

Balona, L. A., and Crampton, D., 1974, *Mon. Not. Roy. Astr. Soc.*, **166**, 203.

Barker, P. K., 1982, *Ap.J. Suppl.*, **49**,89.

Barker, P. K., 1983, *Pub. A.S.P.*, **95**, 996.

Blazit, A., Bonneau, D., Koechlin, L., and Labeyrie, A. 1977, *Ap.J.*, **214**, L79.

Bolton, C. T., 1982, in *Be Stars*, Proc. IAU Symp. 98, ed. M. Jaschek and H. G.

Groth, (Dordrecht: Reidel Publishing Company), p. 181.

Bonneau, D., Balega, Y., Blazit, A., Foy, R., Vakili, F., and Vidal, J. L., 1986,

Astr. and Ap. Suppl., **65**, 27

Bossi, M., Guerrero, G., Mantegazza, L., and Scardia, M., 1982, *I.A.U. Inf. Bull. Var.*

Stars., No. 2082.

Collins, G. W. II, 1974, *Ap.J.*, **191**, 157.

Cox, A. N., 1984, *Pub.A.S.P.*, **96**, 577.

Dachs, J., 1987, in *Physics of Be Stars*, Proc. IAU Col. 92, eds. A. Slettebak and

   T. P. Snow, (Cambridge: Cambridge University Press), p. 149.

Dachs, J., Eichendorf, W., Schleicher, H., Schmidt-Kaler, Th., Stift, M., and

   Tug, H., 1981, *Astron. Astrophys. Suppl.*, **43**, 427.

Dachs, J., Hanuschik, R., Kaiser, D., Ballereau, D.,Bouchet, P., Keiling, R., Kozok, J.,

   Rudolph, R., and Schlosser, W., 1986, *Astron. Astrophys. Suppl.*, **63**, 87.

Doazan, V. 1973, *Astron. Astrophys.*, **27**, 395.

Doazan, V., Harmanec, P., Koubsky, P., Krpata, J., and Zdarsky, F., 1982, *Astron.

   Astrophys. Suppl.*, **115**, 138.

Doazan, V. 1987, in *Physics of Be Stars*, Proc. IAU Col. 92, eds. A. Slettebak and

   T. P. Snow, (Cambridge: Cambridge University Press), p. 384.

Ebbets, D., 1981, *Pub. A.S.P.*, **93**, 119.

Fahlman, G. G., Francis, D., Fraser, G., Grieve, G., Thibault, D., Walker, G. A. H.,

   and Yang, S., 1988, preprint, submitted to *Ap.J.*.

Fahlman, G. G., and Glaspey, J. W., 1973, in *Astronomical Observations With

   Television − Type Sensors*, ed.J. W. Glaspey and G. A. H. Walker,

   (Vancouver: University of British Columbia), p. 347.

Fracassini, M., and Pasinetti, L. E., 1975, *I.A.U. Inf. Bull. Var. Stars.* No. 1044.

Fracassini, M., and Pasinetti, L. E., 1977, *I.A.U. Inf. Bull. Var. Stars.* No. 1341.

Fracassini, M., Pasinetti, L. E., and Pastori, L., 1977, *Ap. and Space Sci.* **49**, 145.

Gehrz, R. D., Hackwell, J. A., and Jones, T. W., 1974, *Ap.J.*, **191**, 675.

Gulliver, A. F., 1977, *Ap.J. Suppl.* **35**, 441.

Gulliver, A. F., and Bolton, C. T., 1978, *Pub. A.S.P.*, **86**, 732.

Gulliver, A. F., Bolton, C. T., and Poeckert, R., 1980, *Pub. A.S.P.*, **92**774.

Harmanec, P., 1982, in *Be Stars*, Proc. IAU Symp. 98, ed. M. Jaschek and H. G.

    Groth, (Dordrecht: Reidel Publishing Company), p. 413.

Harmanec, P., 1983, *HvarObs.Bull.*, **7**, 55.

Harmanec, P., 1984, *I.A.U. Inf. Bull. Var. Stars.* No. 2506.

Harmanec, P., 1987, in *Physics of Be Stars*, Proc. IAU Col. 92, ed. A. Slettebak

    and T. P. Snow, (Cambridge: Cambridge University Press), p. 339.

Harmanec, P., and Kriz, S., 1976, in *Be and Shell Stars*, Proc. IAU

    Symp. 70, ed A. Slettebak, (Dordrecht: Reidel Publishing Company), p.385.

Harmanec, P., Olah, K., Bozic H., Hadrava, P., Horn, J., Koubsky P., Kriz S.,

    Minikunov, N. H., Muminovic M., Percy, J. R., Skcherbakov A. G., Stupar M.,

    and Tarasov A. E., 1987, in *Physics of Be Stars*, Proc. IAU Col. 92,

    ed. A. Slettebak and T. P. Snow, (Cambridge: Cambridge University Press),

    p. 456.

Heintz, W. D., 1978, *Ap.J. Suppl.*, **37**, 343.

Horn, J., Koubsky, P., Arsenijevic, J., Grygar, J., Harmanec, P., Krpata, J., Kriz, S.,

    and Pavlovski, K., 1982, *I.A.U. Symp.* **98**, 315.

Hubert-Delplace, A. M., and Hubert, H., 1981, *Astron. Astrophys. Suppl.*, **44**, 109.

Jaschek, M., and Groth, H. G., eds., 1982, *Be Stars*, Proc. IAU Symp. 98,

    (Dordrecht: Reidel Publishing Company).

Koubsky, P., 1984, *I.A.U. Inf. Bull. Var. Stars.* No. 2584.

Kogure, T., and Hirata, R., 1982, *Bull. Astr. Soc. India*, **10**, 281.

Kriz, S., and Harmanec, P., 1975, *Bull. Astron. Inst. Czech.*, **26**, 65.

Marlborough, J. M., 1987, in *Physics of Be Stars*, Proc. IAU Col. 92, eds.

> A. Slettebak and T. P. Snow, (Cambridge: Cambridge University Press), p. 316.

Marlborough, J. M., and Snow, T. P., 1976, in *Be and Shell Stars*, Proc. IAU Symp.

> 70, ed. A. Slettebak, (Dordrecht: Reidel Publishing Company), p. 179.

McAlister, H. A., 1979, *Ap.J.*, **230**, 497

McAlister, H. A., and Hartkopf, W. I., 1984, *Catalog of Interferometric*

> *Measurements of Binary Stars*, Chara Contr. No. 1, Atlanta, USA.

McAlister, H. A., Hartkopf, W. I., Hutter, D. J., and Franz, O. G., 1987, *A.J.*, **93**, 688.

Millward, C. G., and Walker, G. A. H., 1985, *Ap.J.Suppl.*, **57**, 63.

Osaki, Y., 1986, *Pub.A.S.P.* **98**, 30.

Pasinetti, L. E., 1967, *Atti XI Riunone Soc. Astr. It.*, Padova, 7-9 Oct.

Pasinetti, L. E., 1968, *Mem. Soc. Astron. It.*, **39**, 73.

Penrod, G. D., 1986, *Pub.A.S.P.* **98**, 35.

Penrod, G. D. 1987, in *Physics of Be Stars*, Proc. IAU Col. 92, eds. A. Slettebak

> and T. P. Snow, (Cambridge: Cambridge University Press), p. 463.

Penrod, G. D., and Smith, M., 1985, in *The Origin of Nonradiative*

> *Heating/Momentum in Hot Stars*, eds. A. B. Underhill and A. G. Michalitsianos,

> NASA CP-2358, (Washington: US Government Printing Office), p.53.

Percy, J. R., 1986, in *Highlights of Astronomy*, ed. J. P. Swings, (Dordrecht: Reidel

> Publishing Company), p.265.

Percy. J. R. 1987, in *Physics of Be Stars*, Proc. IAU Col. 92, eds. A. Slettebak and

T. P. Snow, (Cambridge: Cambridge University Press), p. 49.

Peters, G. J., 1986, *Ap.J. Lett.*, **301**, L61.

Poeckert, R., 1980, *Pub. Dom. Astrophys. Obs.*, **15**, 357.

Popper, D. M., 1980, *Ann. Rev. Astron. Astrophys.*, **18**, 115.

Pritchet, C. J., Mochnacki, S., and Yang, S., 1982, *Pub.A.S.P.*, **94**, 733.

Schmidt, H., 1959, *Zeitschrift f. Astrophys.*, **48**, 249.

Singh, M., 1982, *I.A.U. Inf. Bull. Var. Stars.* No. 2188.

Slettebak, A., 1982a, in *Be Stars*, Proc. IAU Symp. 98, ed. M. Jaschek and H. G.

Groth, (Dordrecht: Reidel Publishing Company), p. 109.

Slettebak, A., 1982b, *Ap.J.Suppl.*, **50**, 55.

Slettebak, A., Collins, G. W., Boyce, P. B., White, N. M., and Parkinson, T. D., 1975,

Ap.J. Suppl., **29**, 137.

Slettebak, A., and Snow, T. P., eds. 1987, *Physics of Be Stars*, Proc. IAU Col. 92,

(Cambridge: Cambridge University Press).

Smith, M., 1985, *Ap.J.*, **297**, 206.

Smith, M., 1986, in Proc. Unno Retirement Conf., ed. Y. Osaki,

(Tokyo: University of Tokyo Press).

Smith, M., Gies, D. R., and Penrod, G. D., 1987, in *Physics of Be Stars*, Proc. IAU

Col. 92, ed. A. Slettebak and T. P. Snow, (Cambridge: Cambridge University

Press), p. 464.

Snow, T. P., and Marlborough, J. M., 1976, *Ap.J. Lett.*, **203**, L87.

Snow, T. P., and Morton, D. C., 1976, *Ap.J. Suppl.*, **32**, 429.

Stagg, C. R., 1987, in *Physics of Be Stars*, Proc. IAU Col. 92, ed. A. Slettebak and

    T. P. Snow, (Cambridge: Cambridge University Press), p. 90.

Stagg, C. R., Bozic, H., Fullerton, A., Gao, W. S., Guo Z. H., Harmanec, P.,

    Horn, J., Huang L., Koubsky, P., Pavlovski, K., Percy J. R., Schmidt F., and

    Stefl S., 1985, *J.R.A.S.C.*, **79**, 243.

Stellingwerf, R. F., 1978, *Ap.J.*, **224**, 953.

Stoeckley, T. R., and Buscombe, W., 1987, *M.N.R.A.S.*, **227**, 801.

Struve, O., 1931, *Ap.J.*, **73**, 94.

Stumpff, P., 1980, *Astron. Astrophys. Suppl.*, **41**, 1.

Tokovinin, A. A., 1983, *Pisma Astr. Zhu.*, **9**, 559.

Tokovinin, A. A., 1985, *Astr. and Ap. Suppl.*, **61**, 483.

Uesugi, A., and Fukuda, I., 1970, *Contr. Inst. Astrophys. Kwasan Obs. Univ. Kyoto*,

    No. 189.

Underhill, A. B., 1987, in *Physics of Be Stars*, Proc. IAU Col. 92, eds. A. Slettebak

    and T. P. Snow, (Cambridge: Cambridge University Press), p. 411.

Underhill, A. B., and Doazan, V., 1982, *B Stars With and Without*

    Emission Lines. Washington: NASA SP-471.

Vogel, H. C., and Wilsing J., 1899, *Pub. Astrophys. Obs.*, Potsdam, No. 39.

Vogt, S. S., and Penrod, G. D., 1983, *Ap.J.*, **275**, 661.

Walker, G. A. H., Johnson, R., and Yang, S., 1985, in *Proceedings of the*

    8th Symposium on Photoelectronic Image Devices, ed. B. L. M.

8th Symposium on Photoelectronic Image Devices, ed. B. L. M.
Morgan, published in *Advances in Electronics and Electron Physics*
(London: Academic Press), **64a**, 213.

Walker, G. A. H., Yang, S., and Fahlman, G. G., 1979, *Ap.J.*, **233**, 199.

Willson, L. A., 1986, *Pub.A.S.P.* **98**, 37.

Wilson, R. H., 1950, *A.J.*, **55**, 153.

Woolf, N. J., Stein, W. A., and Strittmatter, P. A., 1970, *Astron. Astrophys.*, **9**, 252.

Yang, S., Ninkov, Z., and Walker, G. A. H. 1988, *Pub.A.S.P.*, **100**, page 233

Appendix A: Binary Orbit Solution by the Method of Lehmann-Filhés

To solve the orbit of a spectroscopic binary is to determine the values of the elements of its orbit. The observed radial velocity V_r is given by

$$V_r = V_o + K(\cos(\omega + v) + e \cos \omega) \qquad (7)$$

where K, the amplitude is

$$K = 2\pi \, a\sin i \, (P(1 - e^2))^{-1} \qquad (8)$$

The logical starting point is to find the period (P). If one is solving the orbit graphically one should at least have some period-finding program at ones disposal. Having found the period the next step is to fold the radial velocities back so that one has a plot of radial velocity versus phase. The next element to be determined is the velocity of the center of mass of the binary system, V_o. The method of finding V_o and the rest of the orbital elements is illustrated in Figure 20. A line of constant velocity is drawn so that the area between the line and each radial velocity curve is equal on either side of the line. This velocity is V_o. For a double-line spectroscopic binary this is also the velocity at which the two radial velocity curves cross. The areas to be equalized for the primary are denoted by A and B in Figure 20. The primary in a double-line spectroscopic binary is the star exhibiting the smaller amplitude radial velocity curve.

The procedure to find the rest of the orbital elements is illustrated for the radial velocity curve of the secondary. The first step is to find the points of maximum velocity

and draw lines of constant phase connecting these points with the line of $V = V_o$. These lines are to be drawn such that areas a and b are equal and areas c and d are equal. If we define V_{bd} as the length of the line separating areas b and d and V_{ac} as the length of
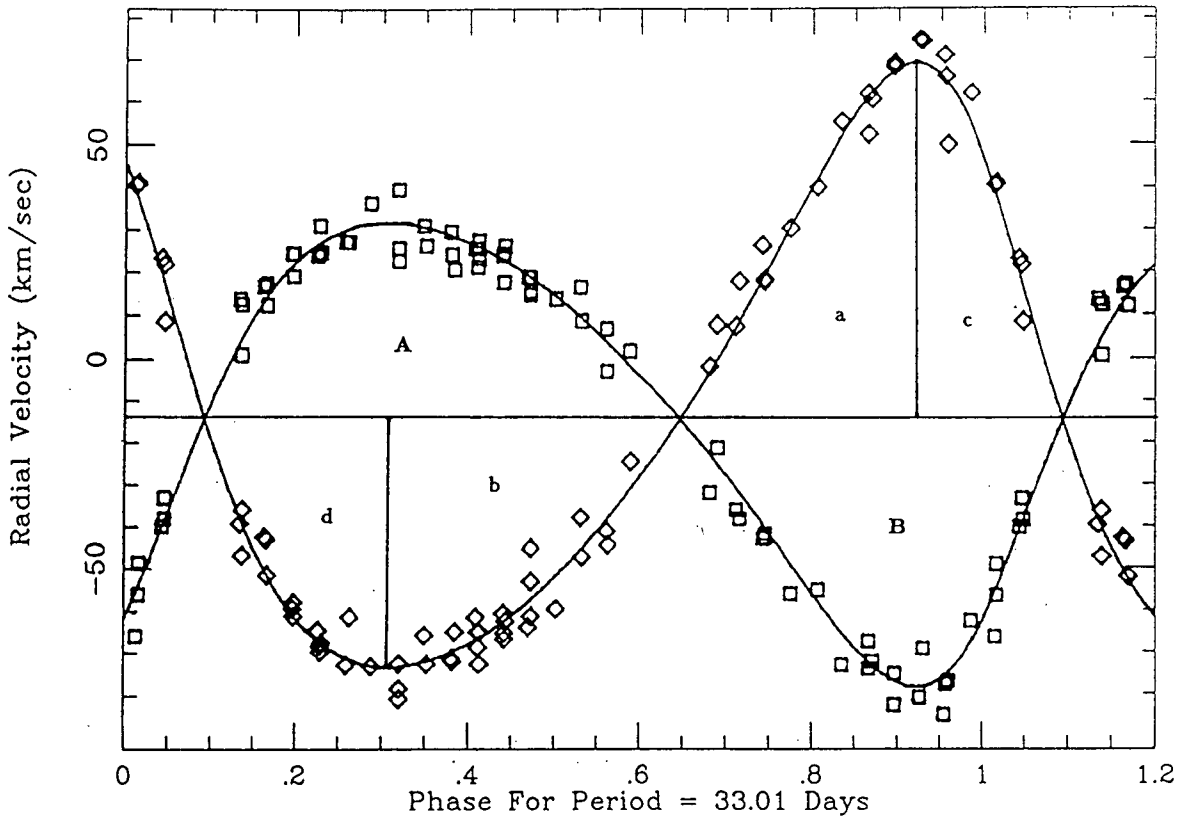
Fig. 20 — Graphical determination of a binary orbit using the method of Lehmann-Filhés. Velocities shown are the same as Figure 3.

the line separating areas a and c it can be shown that

$$e \cos\omega \quad = \quad (V_{ac} - V_{bd})(V_{ac} + V_{bd})^{-1} \qquad (9)$$

and

$$e \sin\omega \quad = \quad 2(V_{ac}\, V_{bd}\,)^{1/2}\, (b{-}c)((V_{ac} + V_{bd})(b{+}c))^{-1} \qquad (10)$$

where e is the eccentricity of the orbit and ω is the longitude of periastron passage with respect to a node.

Equations (9) and (10) can be solved to obtain e and ω. The amplitue K is given by equation (8), but also by K $= (V_{ac} + V_{bd})/2$. So far, four elements have been found; P, K, e, and ω. The first three of these together with equation (8) yield a $\sin i$ where a is the semi-major axis of the orbit and i is the inclination of the orbital plane. Finally we need to find the epoch of periastron passage, T_{per}. By equation (7) the radial velocity curve has a maximum when v the true anomaly equals $-\omega$. At the epoch of periastron passage $v = 0$, so that $V_r - V_o = K(1 + e)\cos \omega$. These two conditions are sufficient to find an epoch of periastron passage.

Appendix B: Spectra and Associated Residuals

Stack plots of time series of spectra are presented. All spectra of o And obtained in October 1986 and September 1987 are presented. Residuals from the time series are presented. Residuals from September 25 1987 are not formed since only five spectra were obtained that night. Details regarding the data are presented in chapter 3.
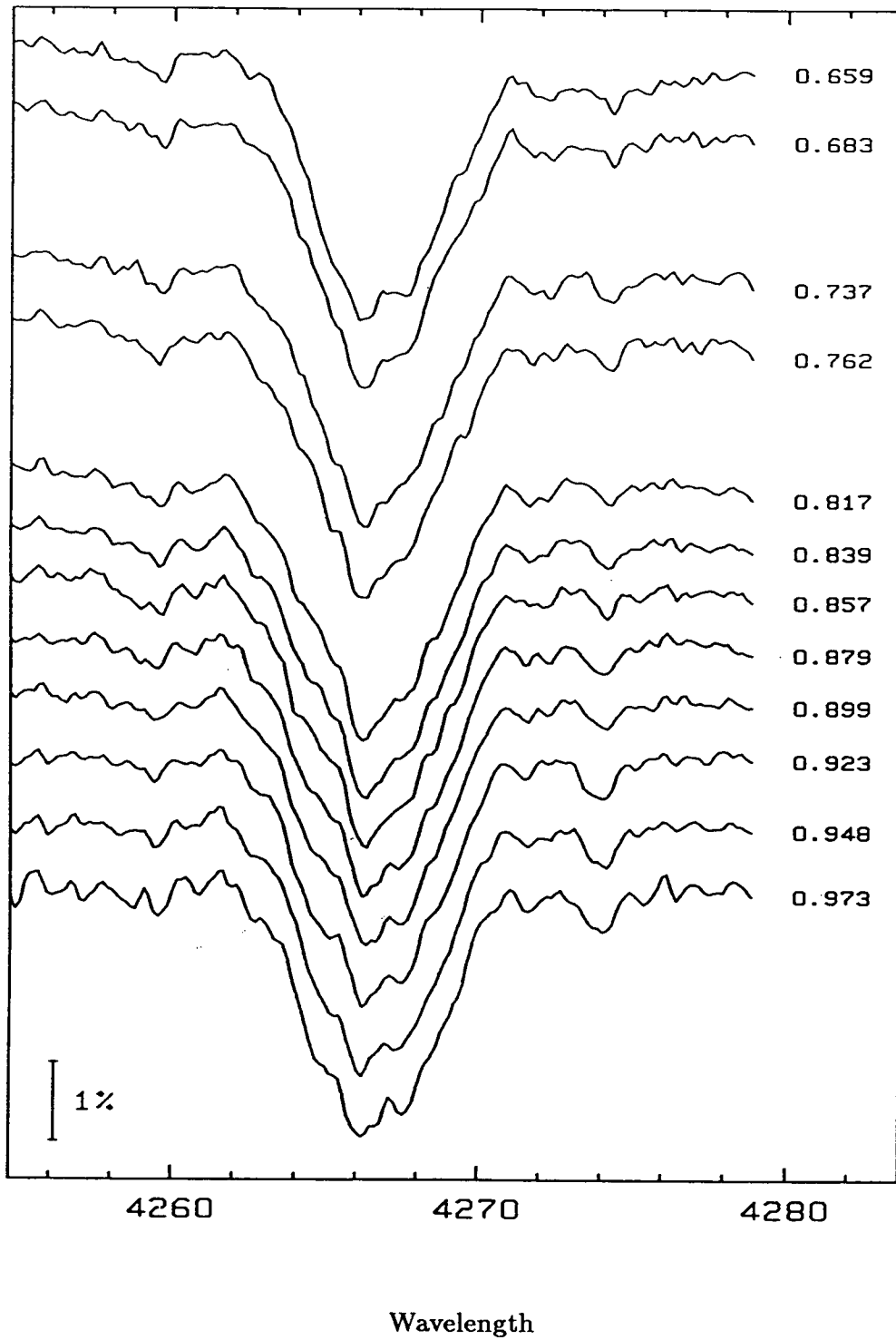
Fig. 21 — Time series of spectra showing C II λ 4267 line profiles obtained on 17 October 1986 (UT). The number at the right of each spectrum is the corresponding mid-exposure time in fractions of a day from BJD 2446720.
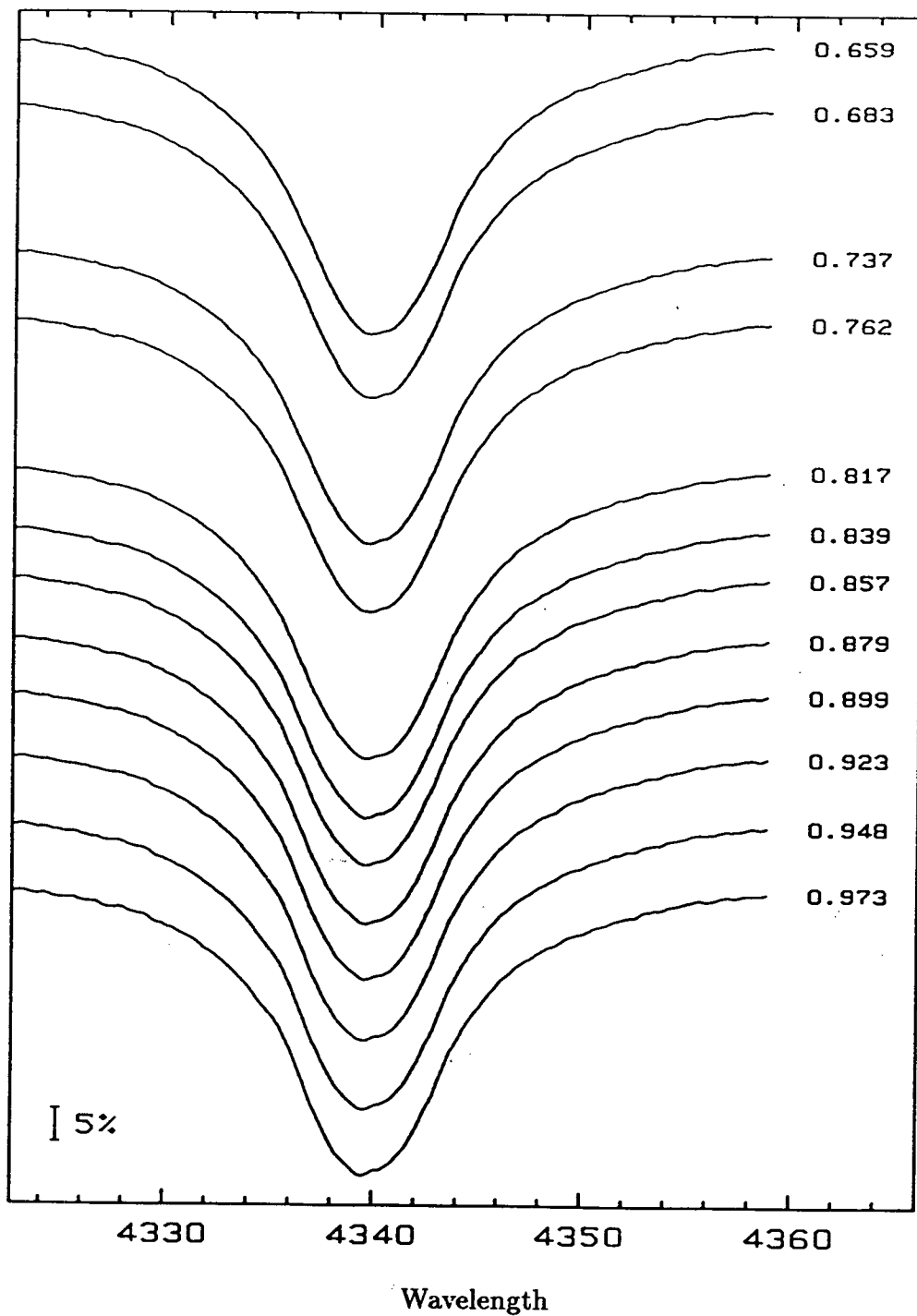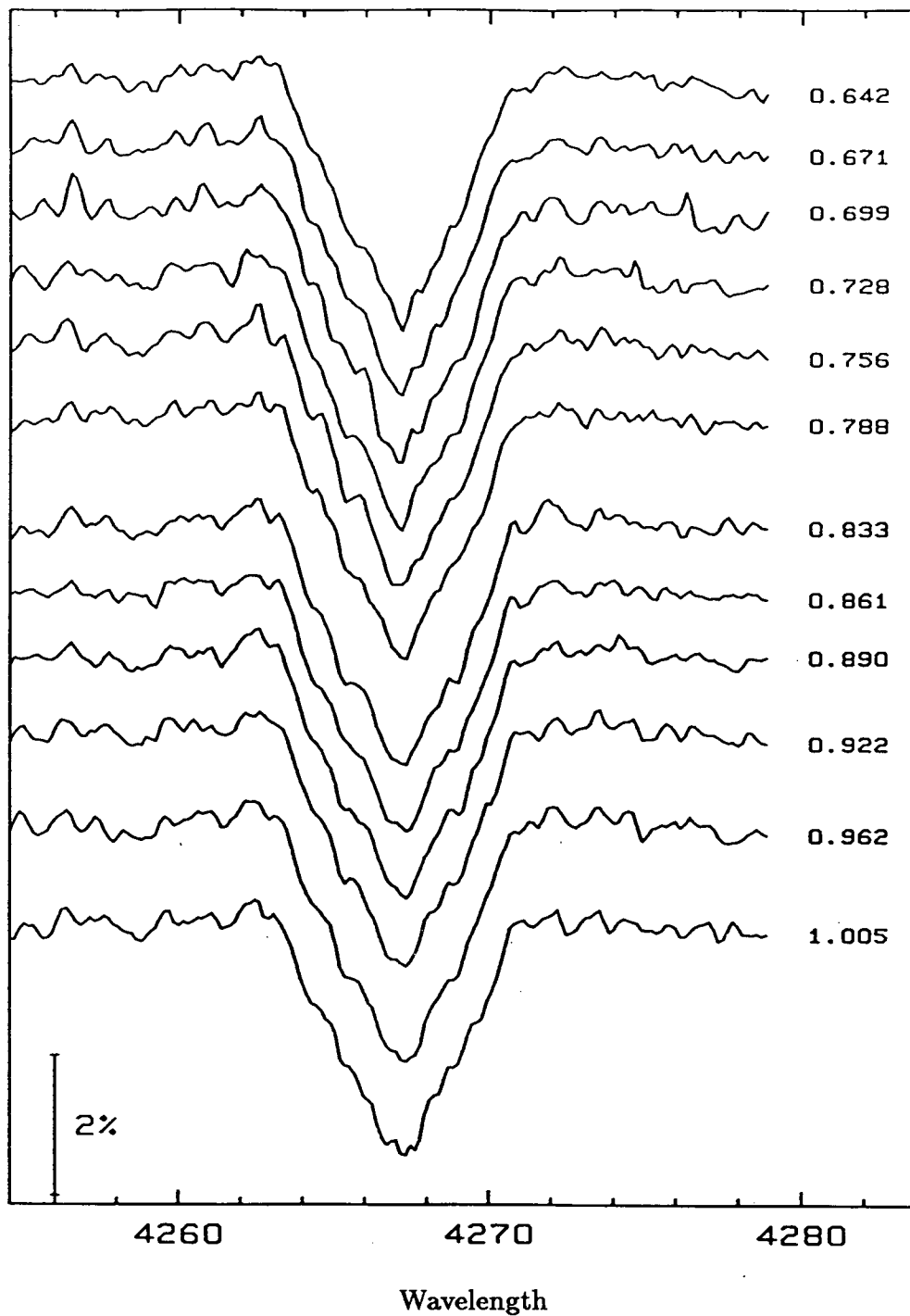
Fig. 22 — Time series of spectra showing Hγ line profiles obtained on 17 October 1986 (UT). The number at the right of each spectrum is the corresponding mid-exposure time in fractions of a day from BJD 2446720.
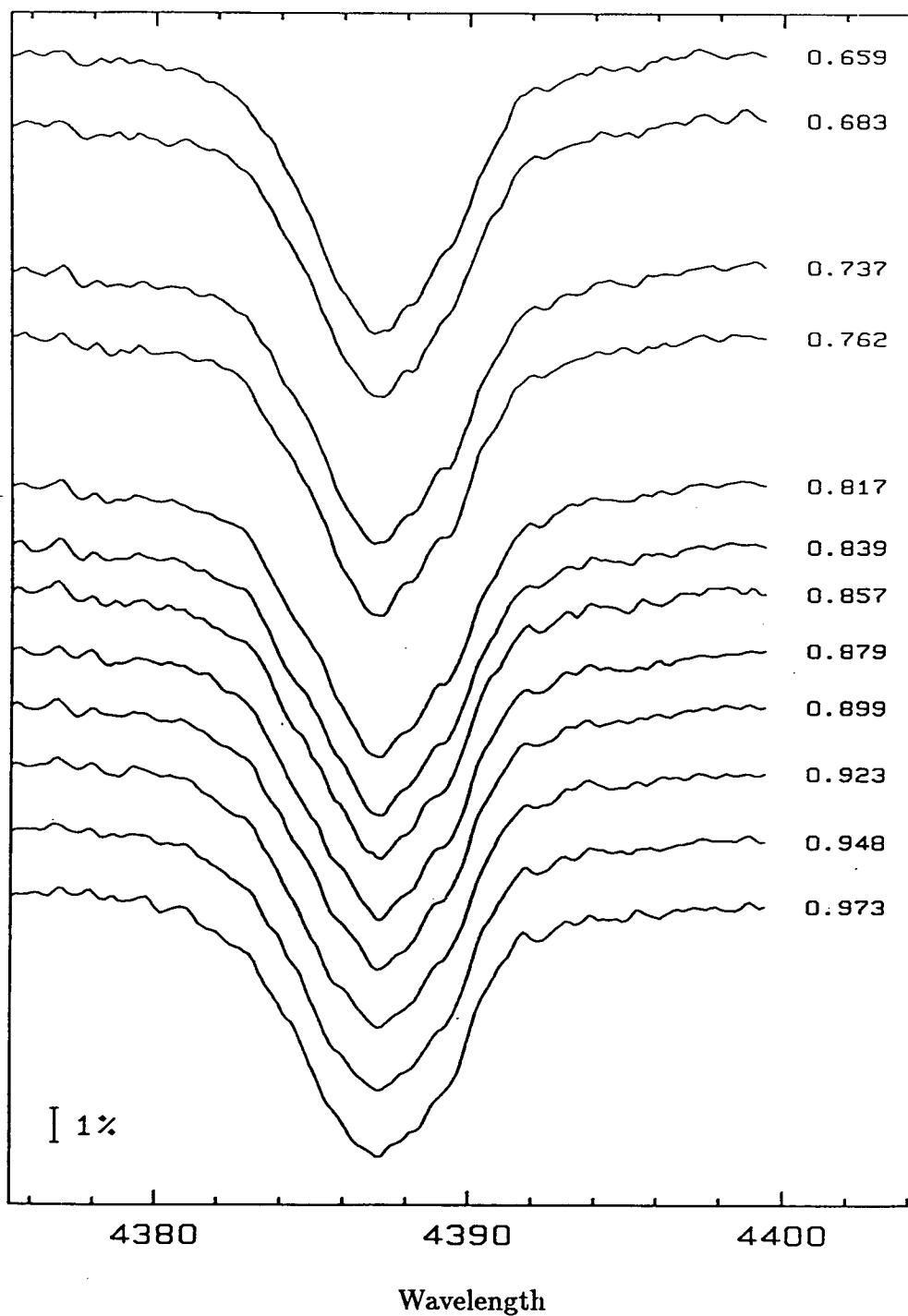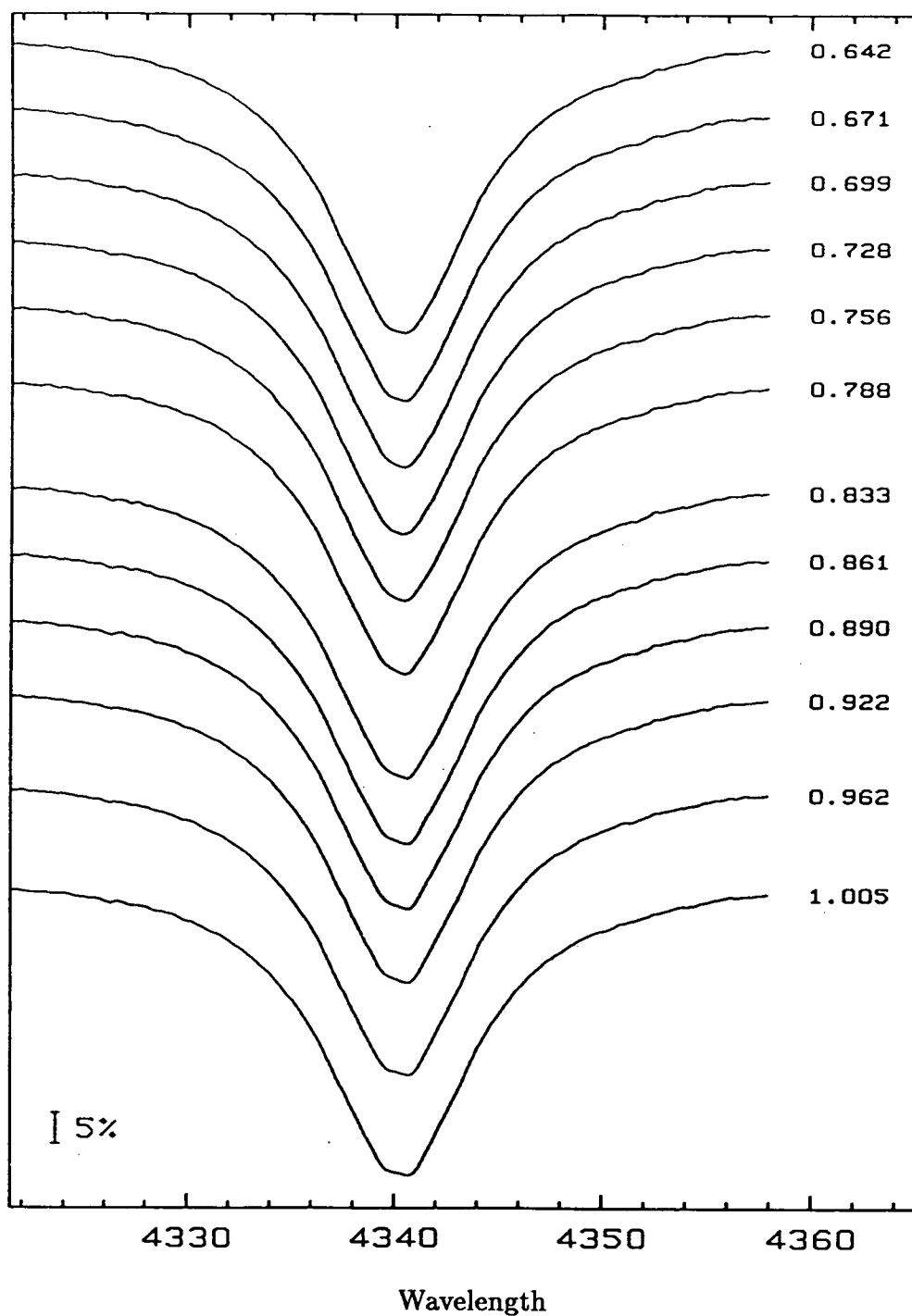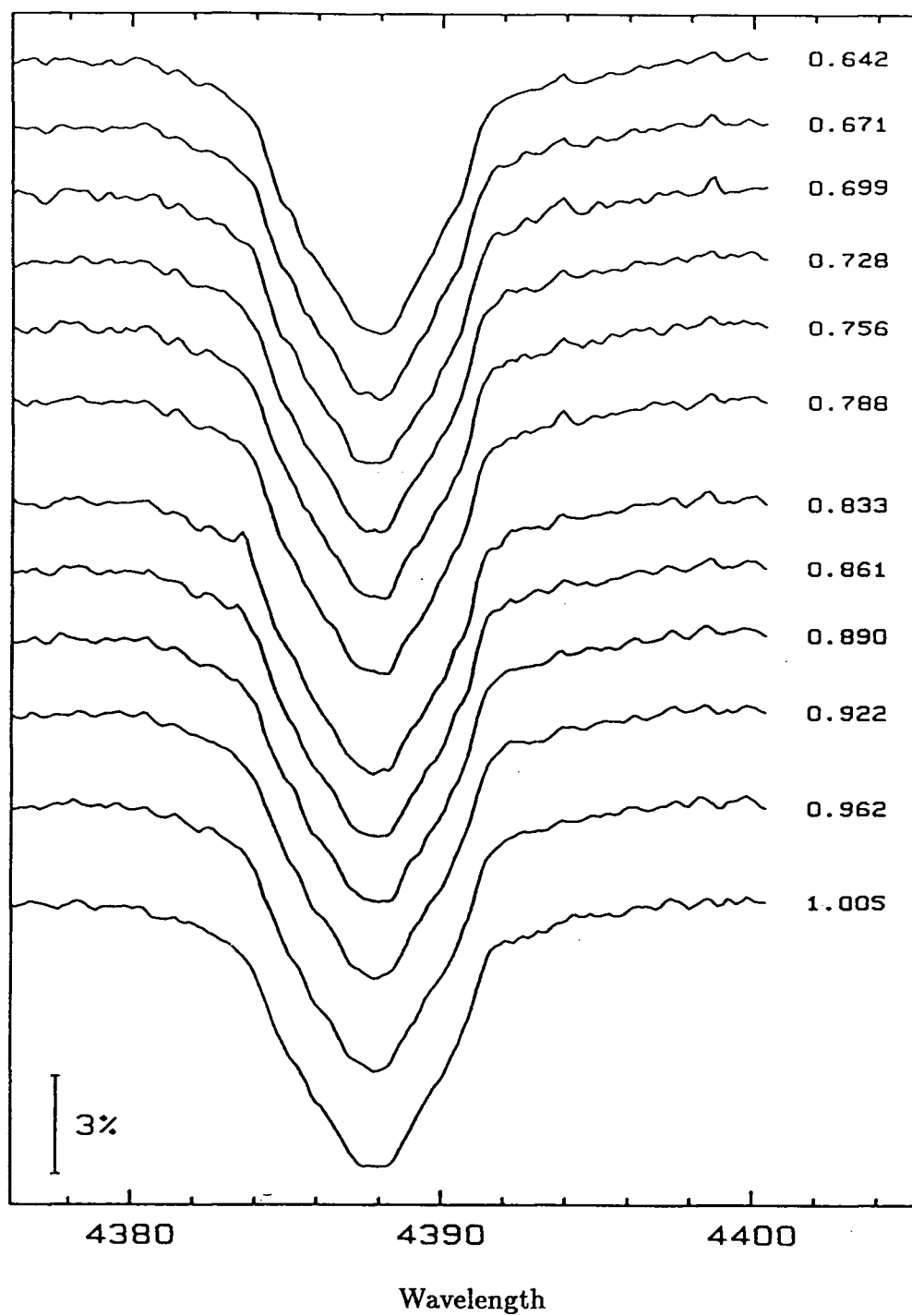
Fig. 23 — Time series of spectra showing He I λ 4388 line profiles obtained on 17 October 1986 (UT). The number at the right of each spectrum is the corresponding mid-exposure time in fractions of a day from BJD 2446720.
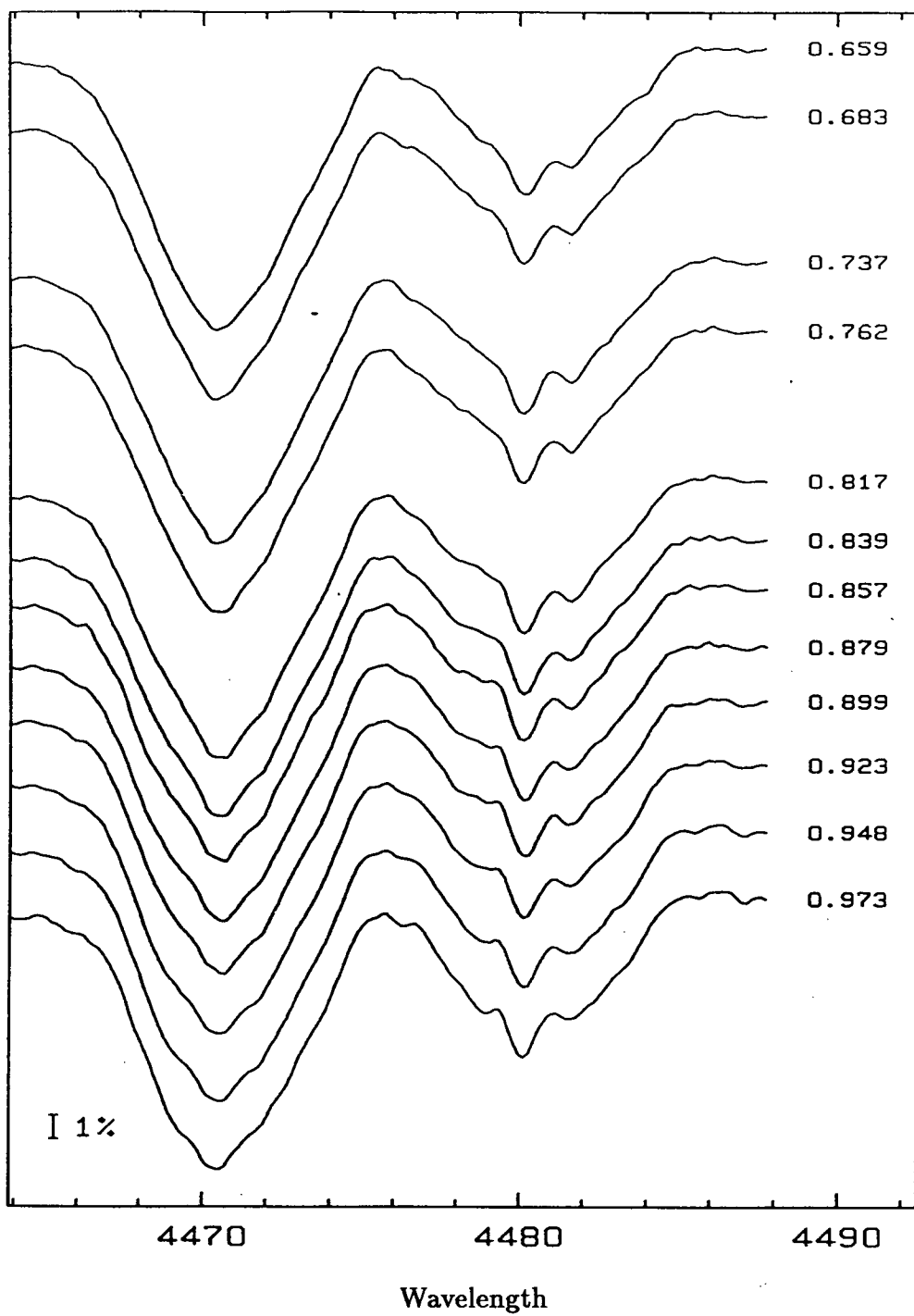
Fig. 24 — Time series of spectra showing He I λ 44471 and Mg IIλ 4481 line profiles obtained on 17 October 1986 (UT). The number at the right of each spectrum is the corresponding mid-exposure time in fractions of a day from BJD 2446720.
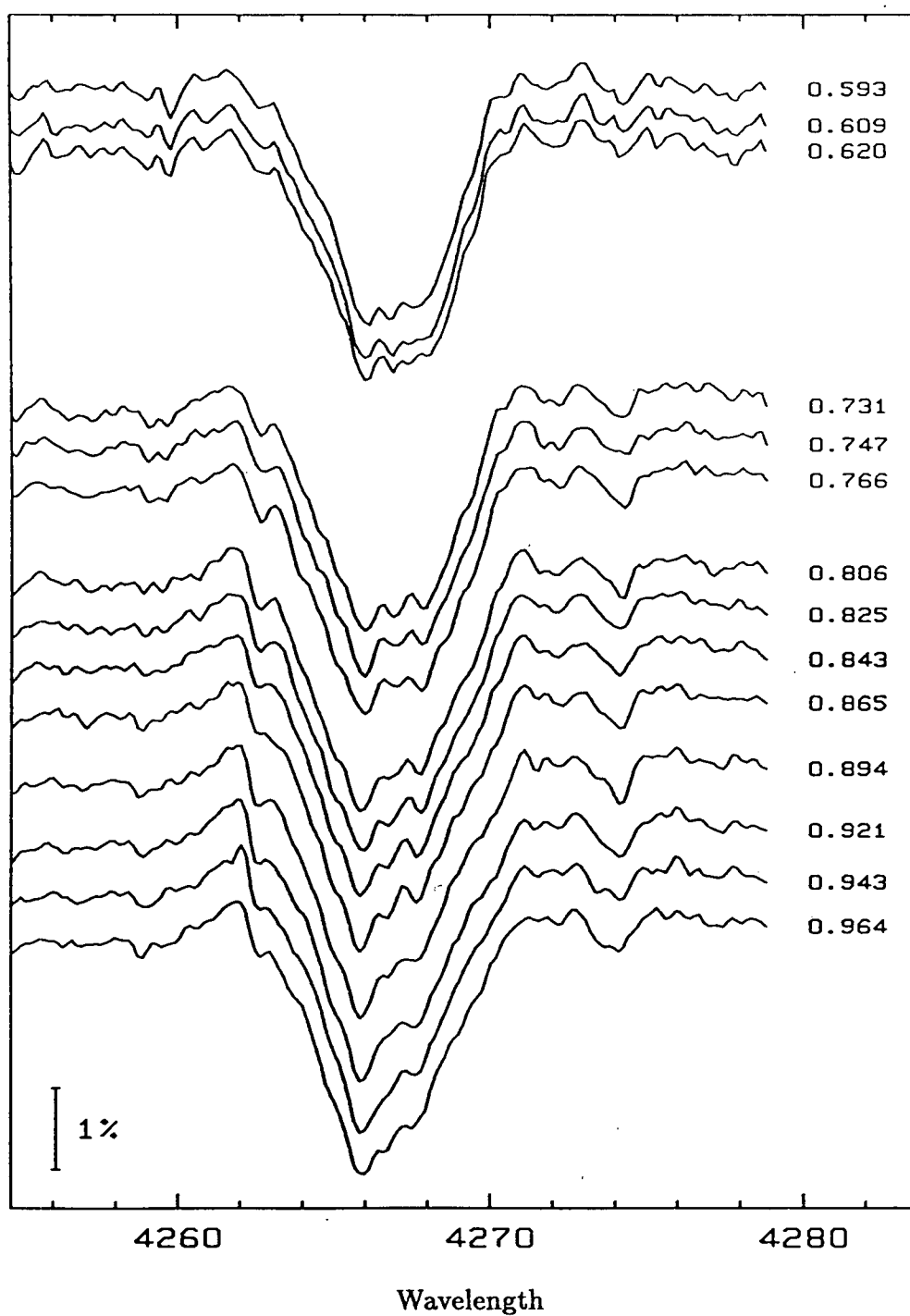
Fig. 25 — Time series of spectra showing C II λ 4267 line profiles obtained on 19 October 1986 (UT). The number at the right of each spectrum is the corresponding mid-exposure time in fractions of a day from BJD 2446722.
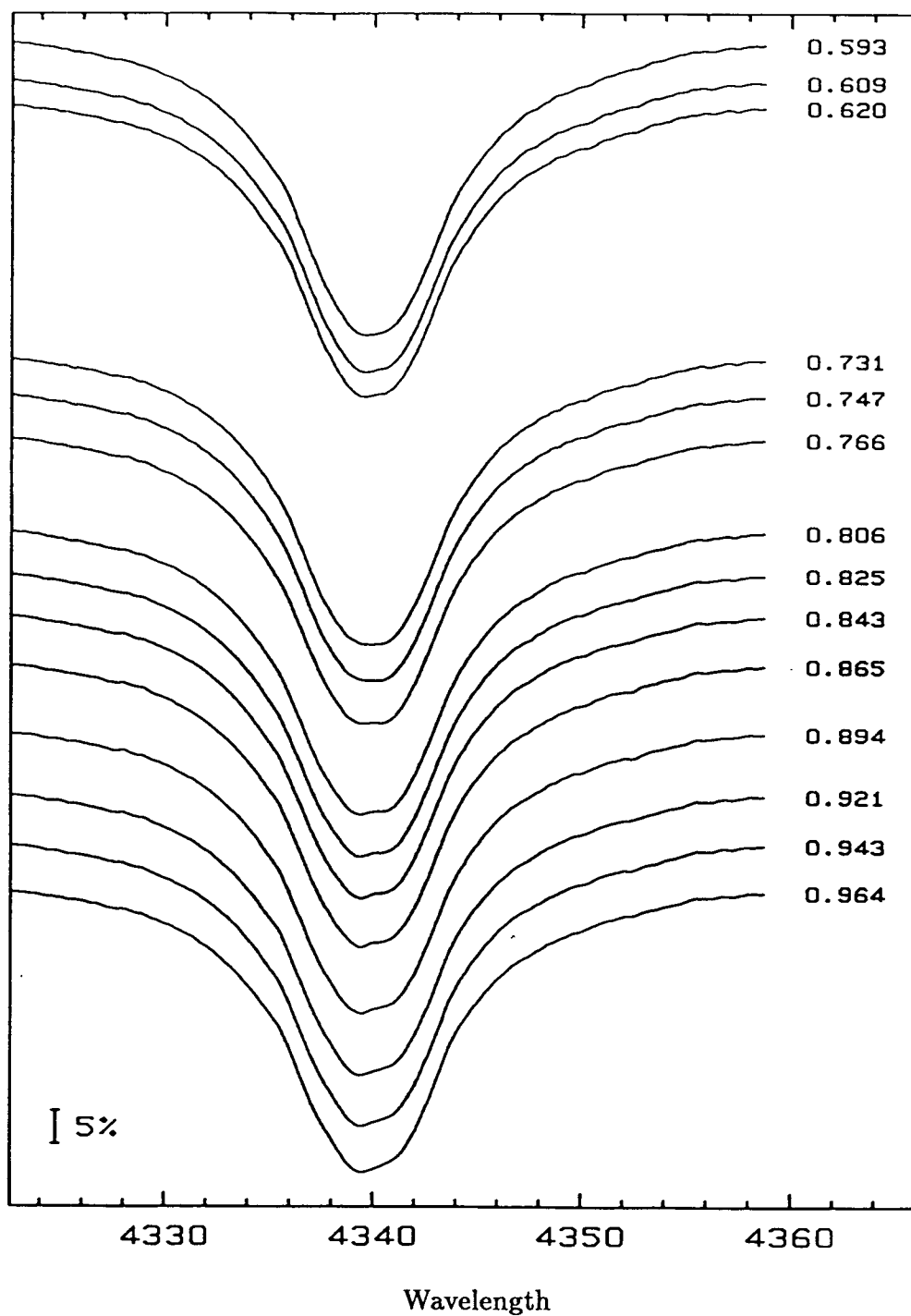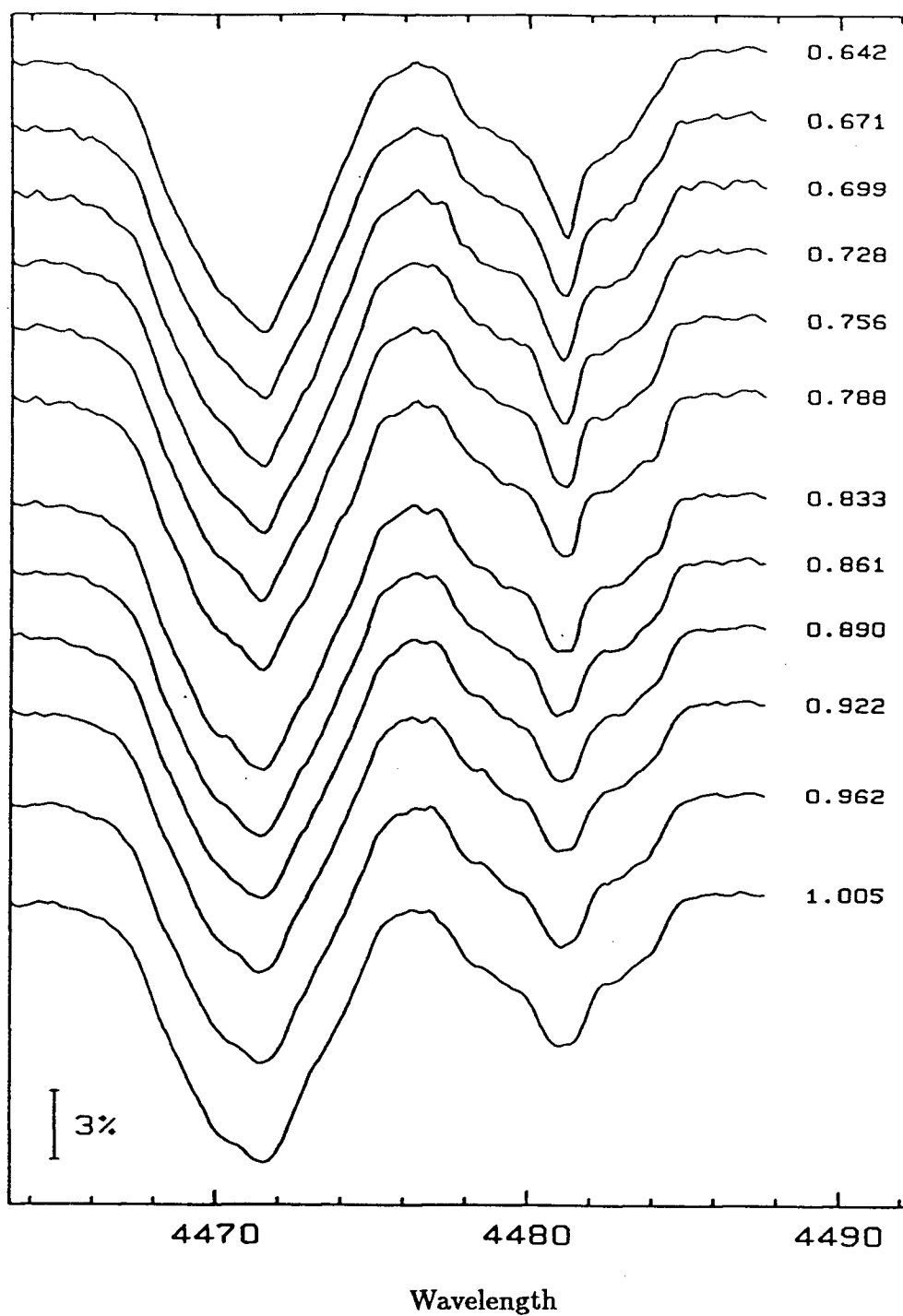
Fig. 26 — Time series of spectra showing Hγ line profiles obtained on 19 October 1986 (UT). The number at the right of each spectrum is the corresponding mid-exposure time in fractions of a day from BJD 2446722.
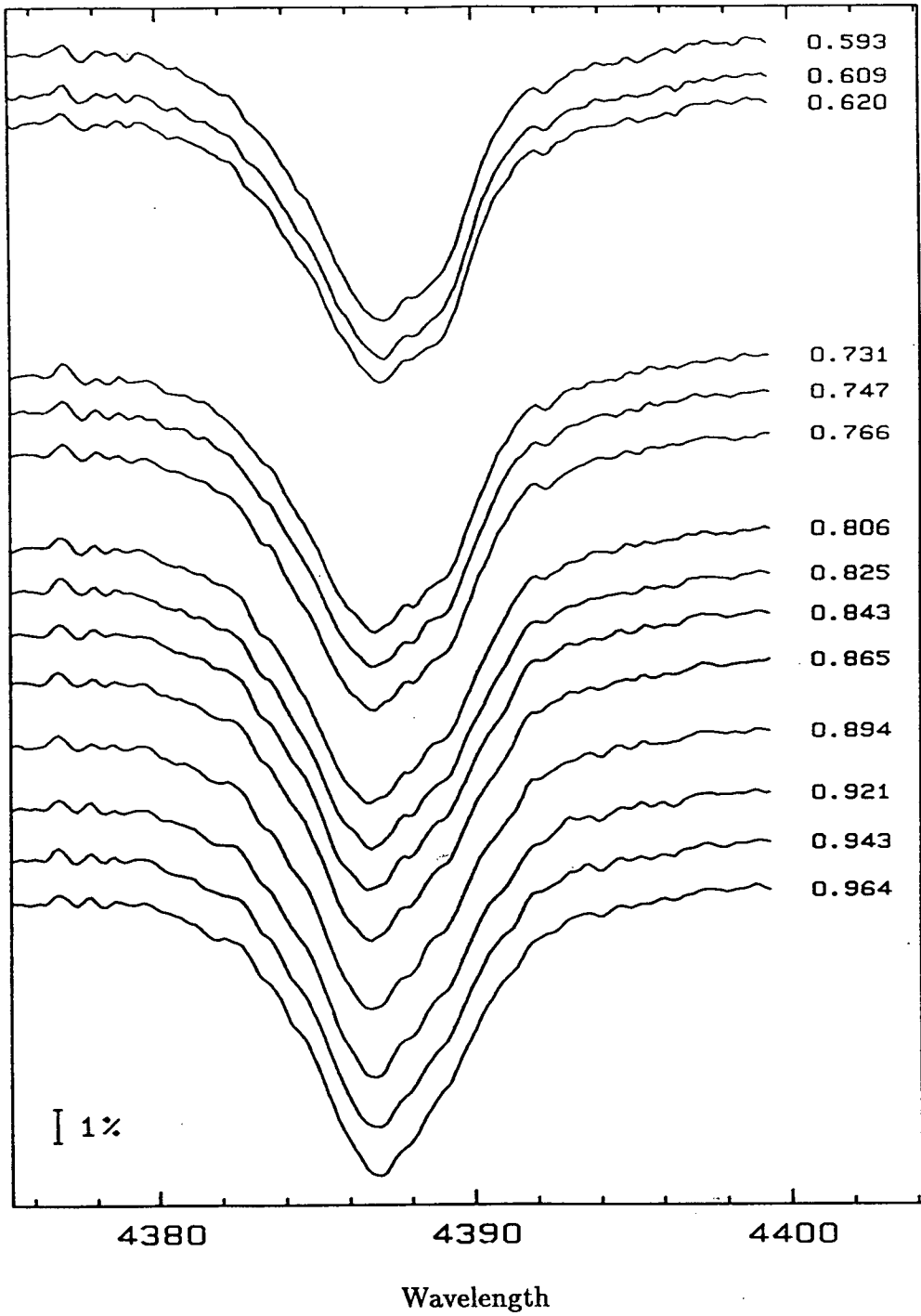
Fig. 27 — Time series of spectra showing He I λ 4388 line profiles obtained on 19 October 1986 (UT). The number at the right of each spectrum is the corresponding mid-exposure time in fractions of a day from BJD 2446722.
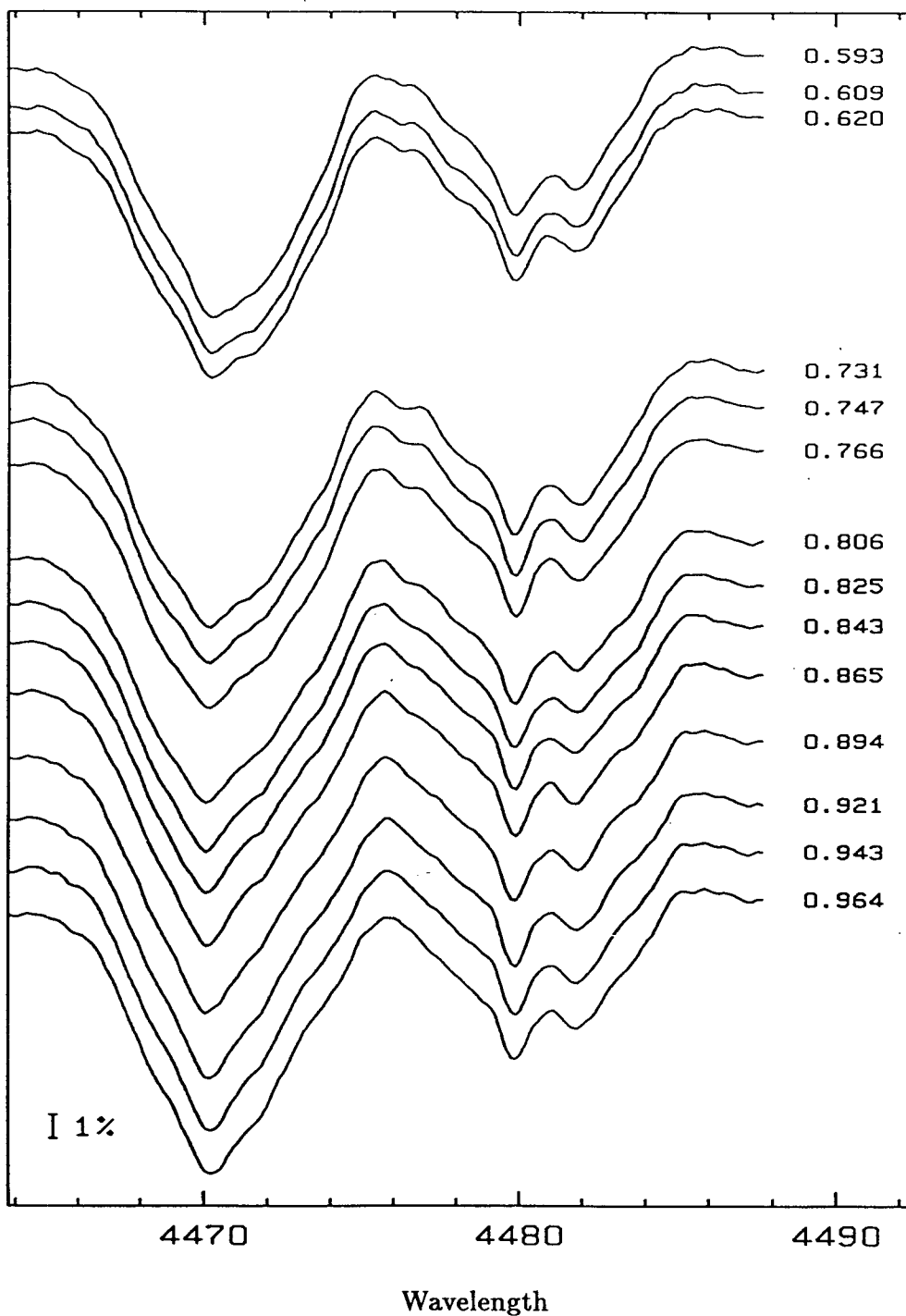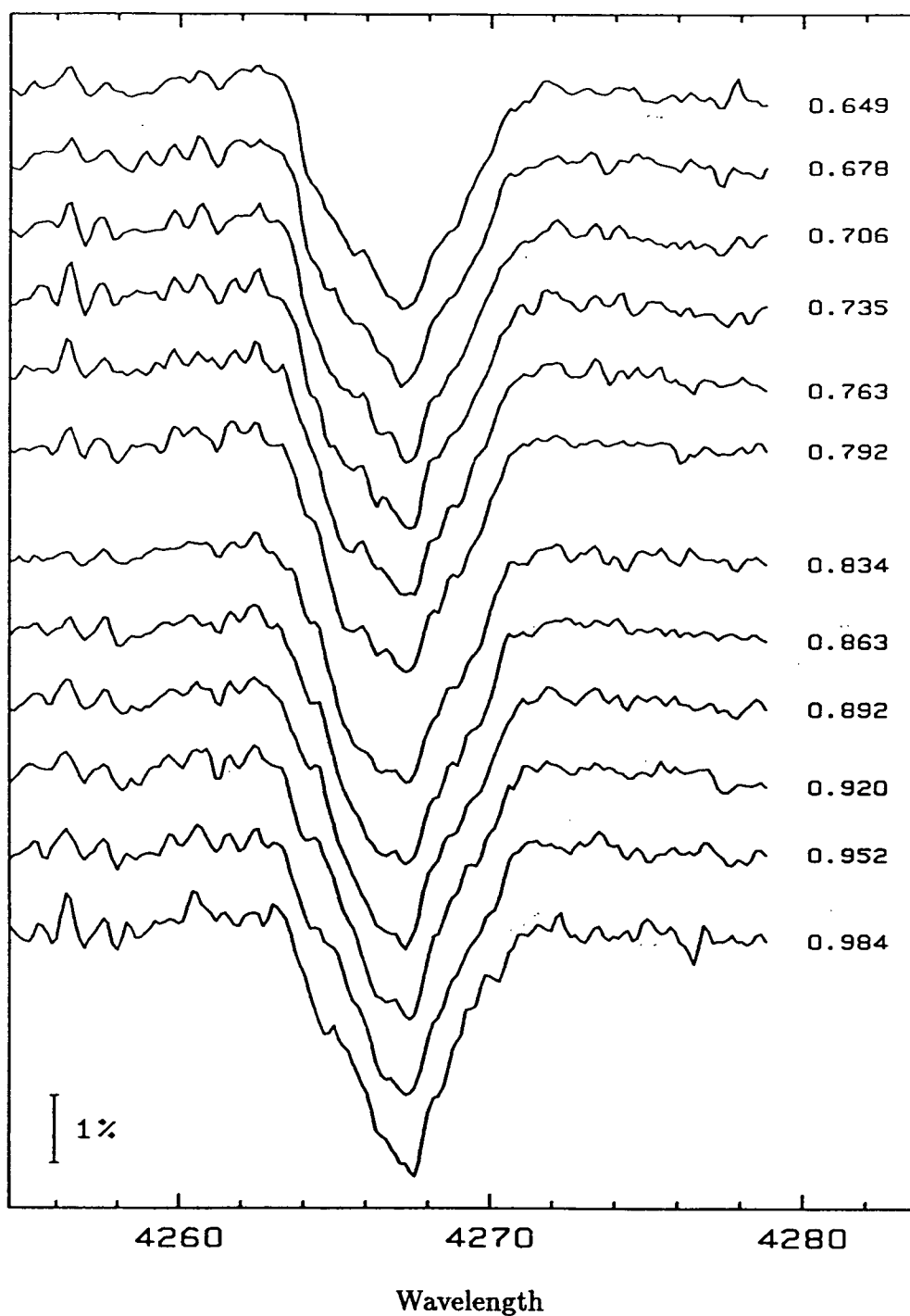
Fig. 28 — Time series of spectra showing He I λ 4471 and Mg II λ 4481 line profiles obtained on 19 October 1986 (UT). The number at the right of each spectrum is the corresponding mid-exposure time in fractions of a day from BJD 2446722.
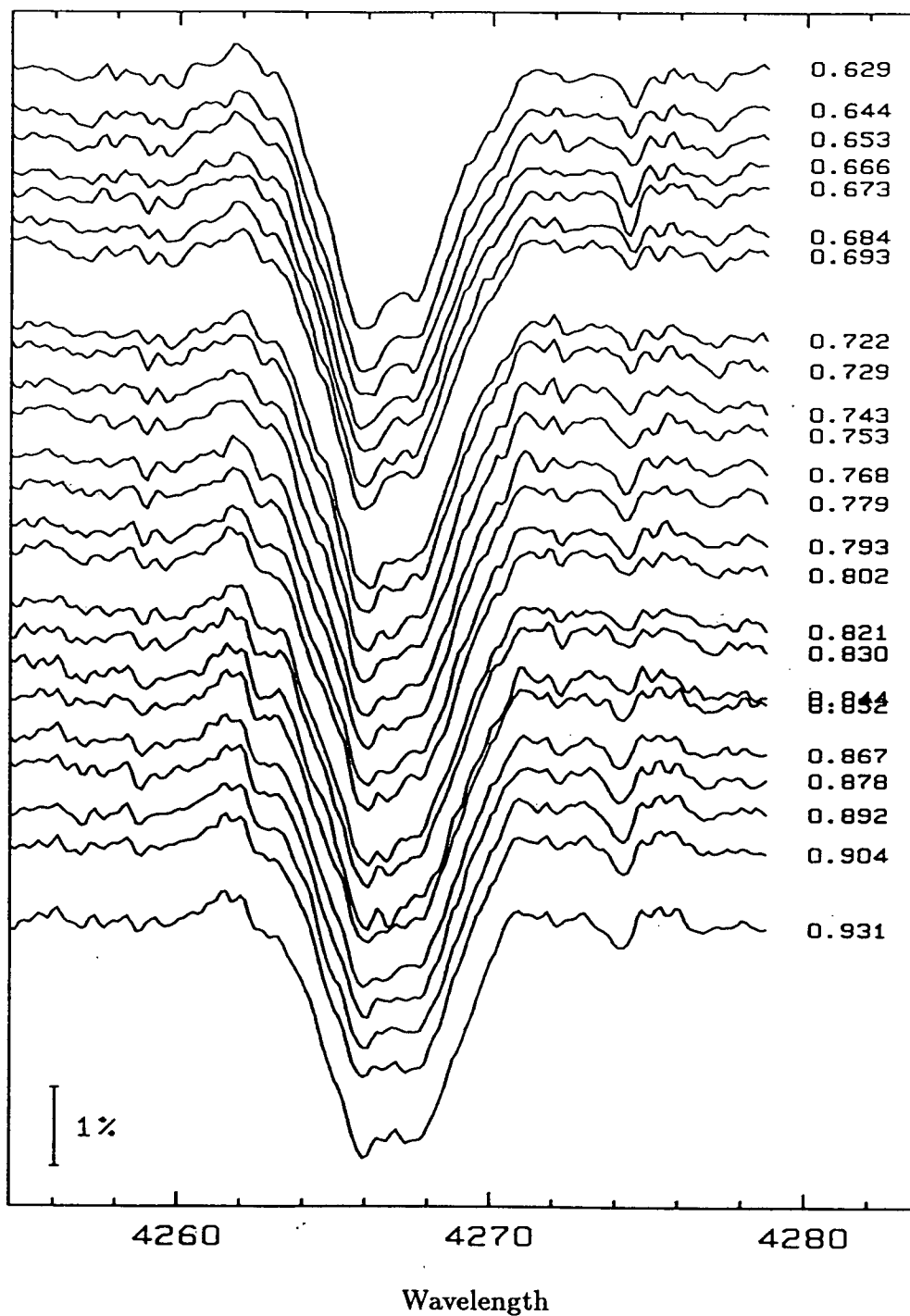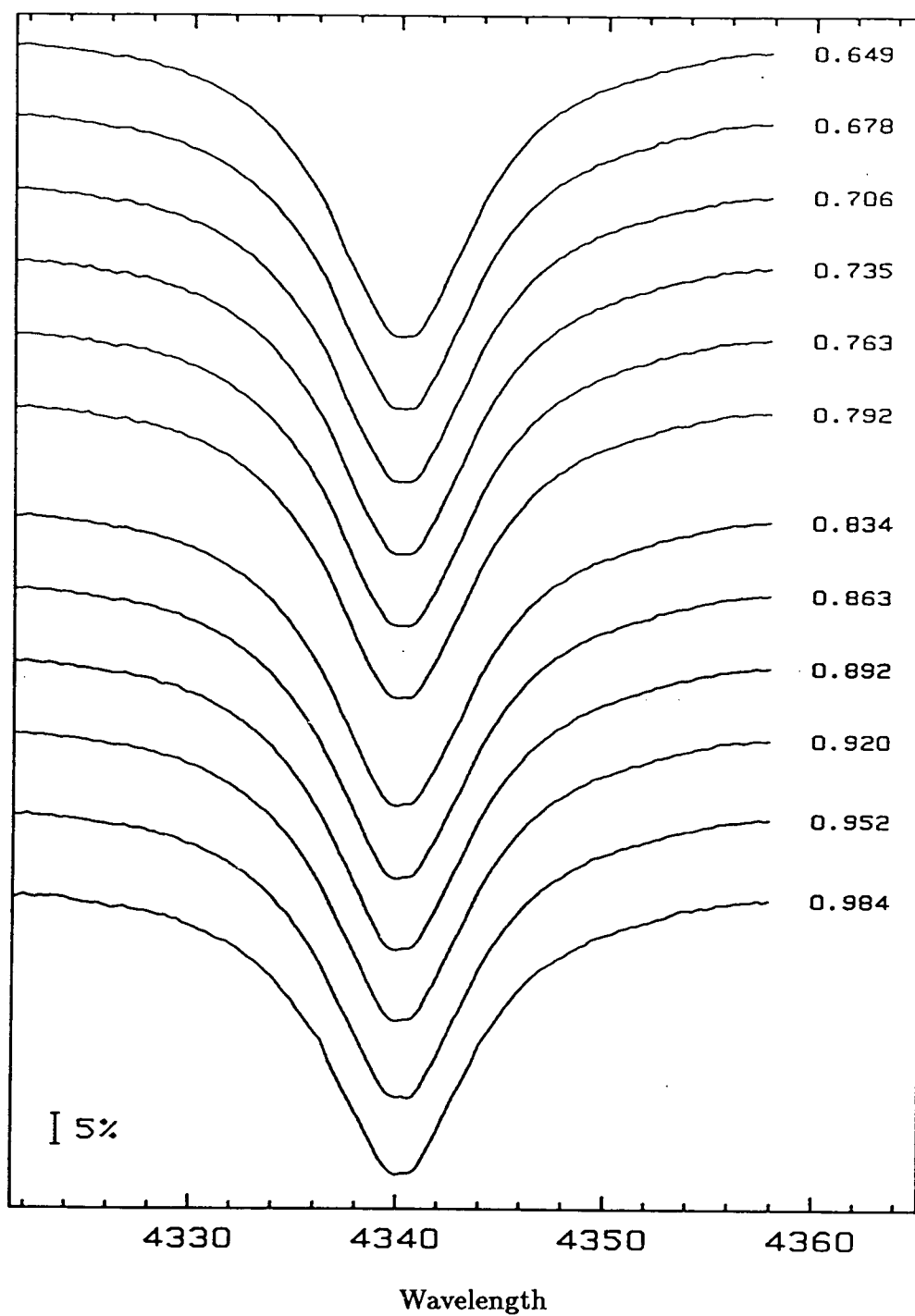
Fig. 29 — Time series of spectra showing C II λ 4267 line profiles obtained on 20 October 1986 (UT). The number at the right of each spectrum is the corresponding mid-exposure time in fractions of a day from BJD 2446723.
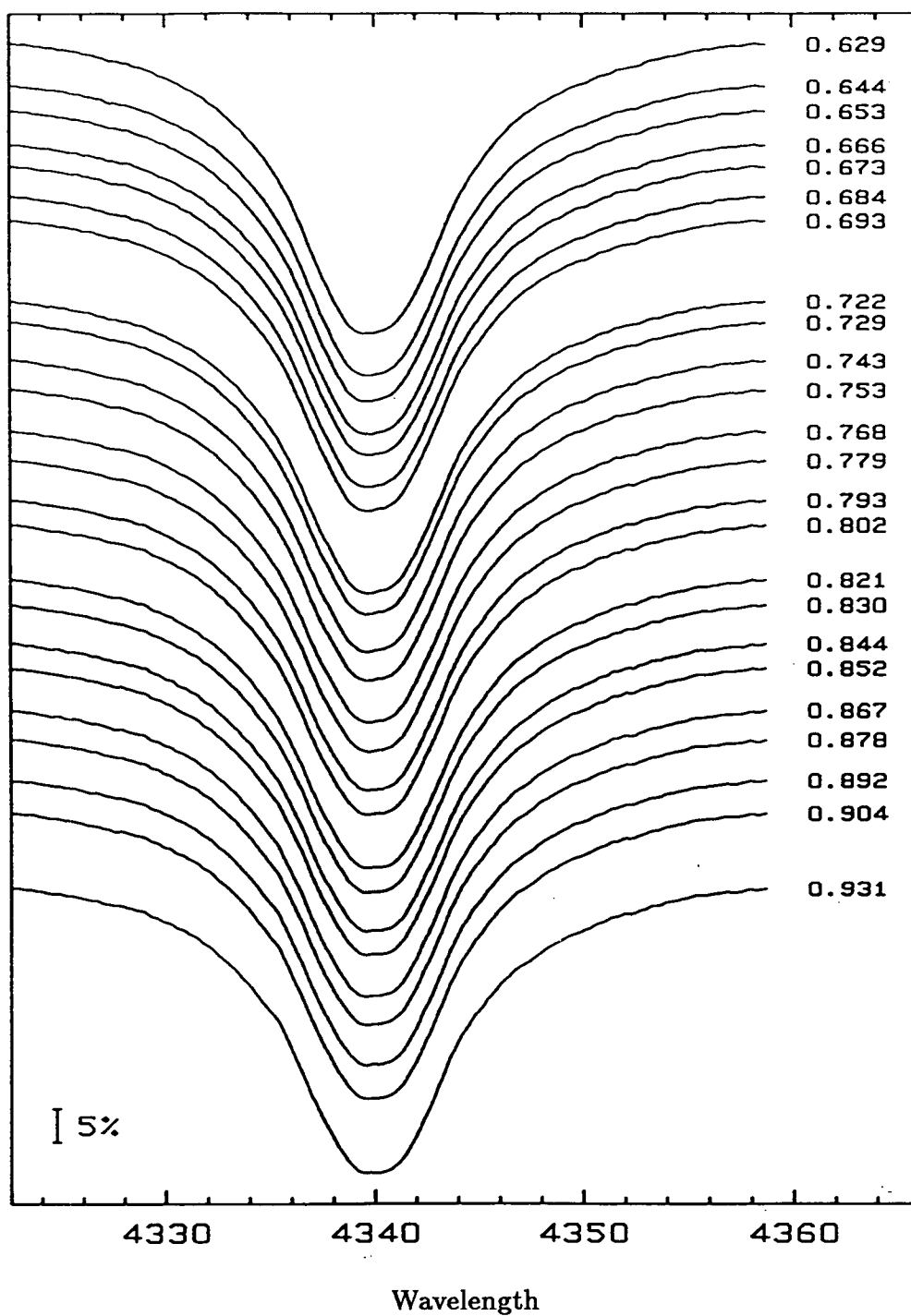
Fig. 30 — Time series of spectra showing Hγ line profiles obtained on 20 October 1986 (UT). The number at the right of each spectrum is the corresponding mid-exposure time in fractions of a day from BJD 2446723.
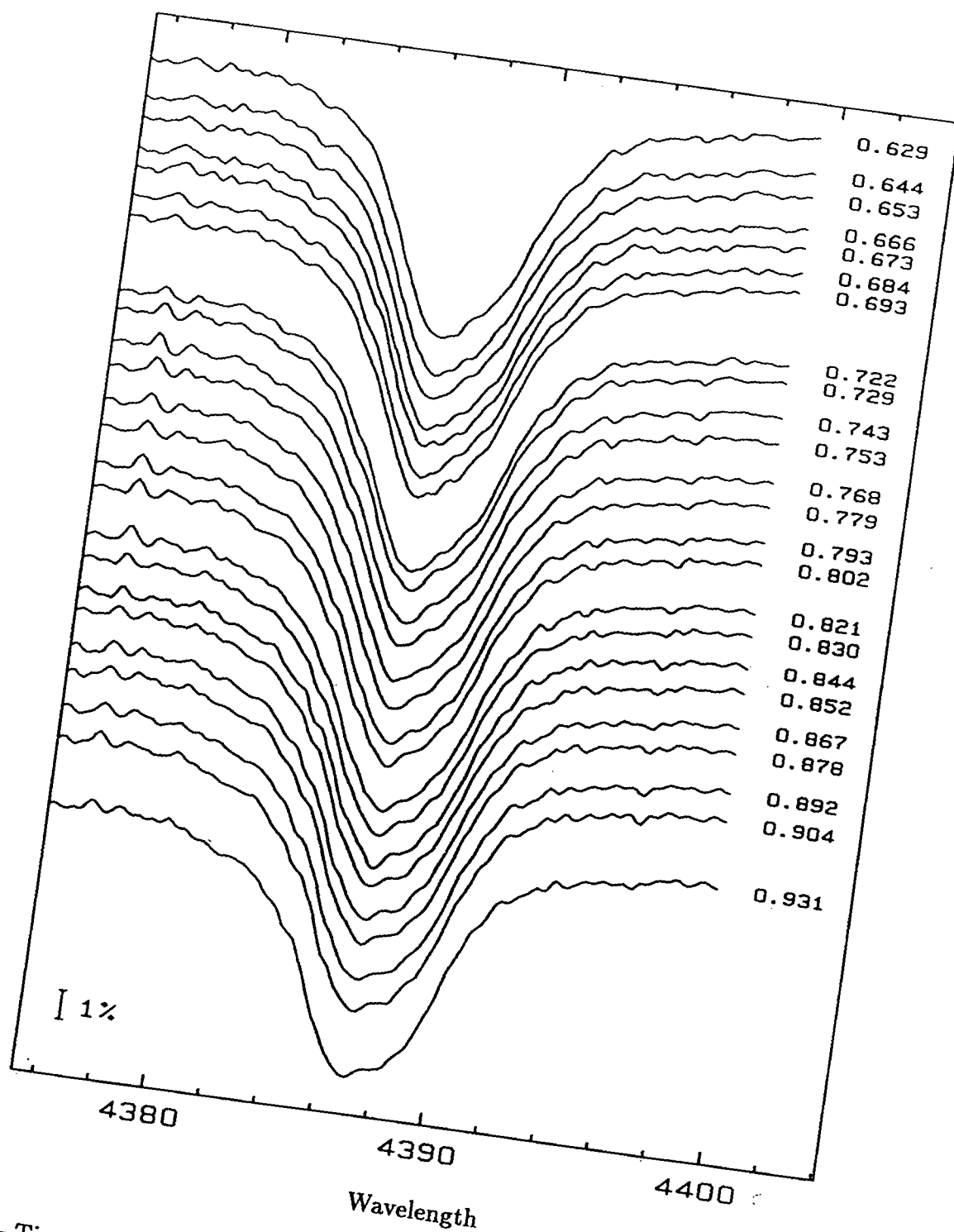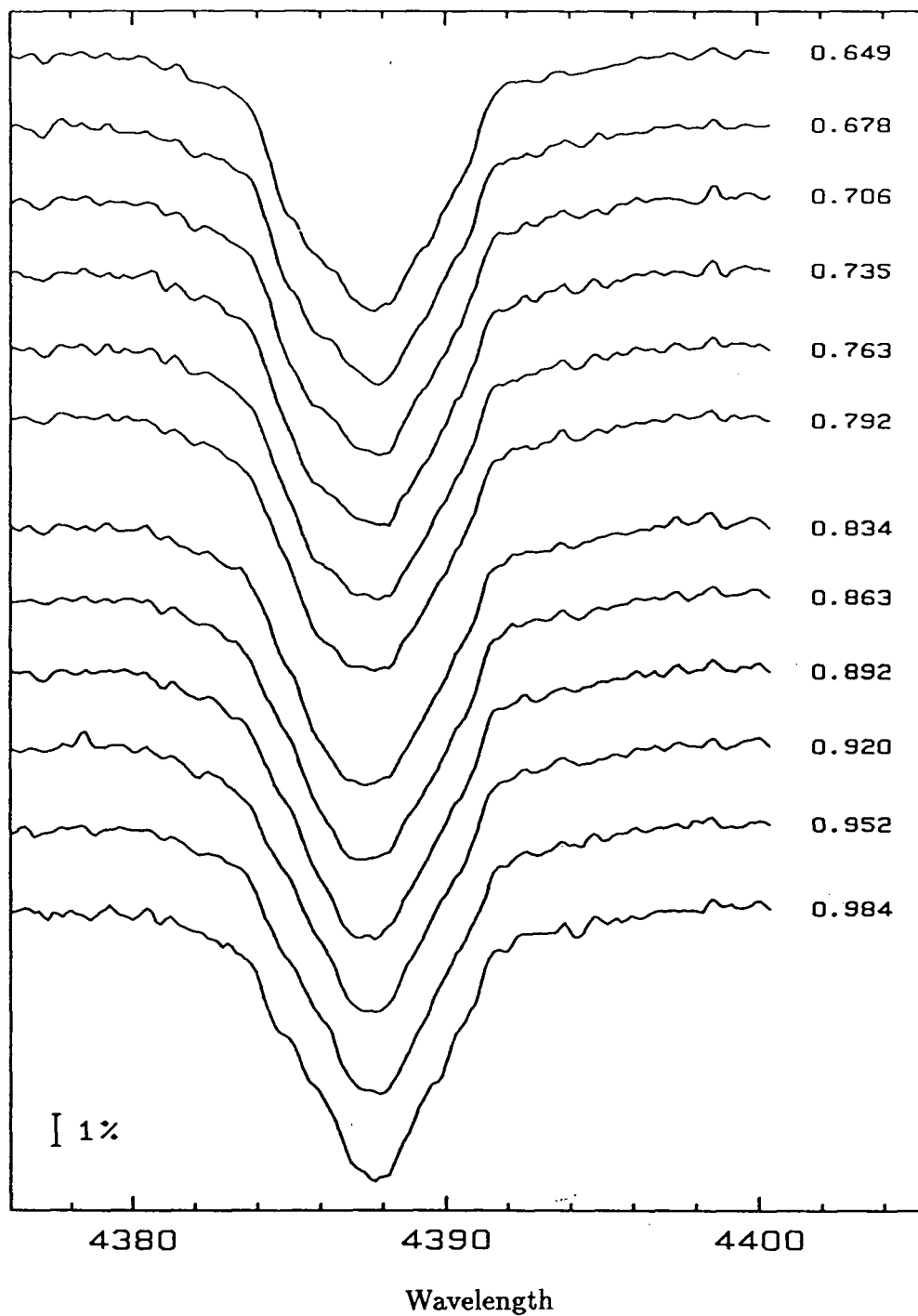
Fig. 31 — Time series of spectra showing He I λ 4388 line profiles obtained on 20 October 1986 (UT). The number at the right of each spectrum is the corresponding mid-exposure time in fractions of a day from BJD 2446723.
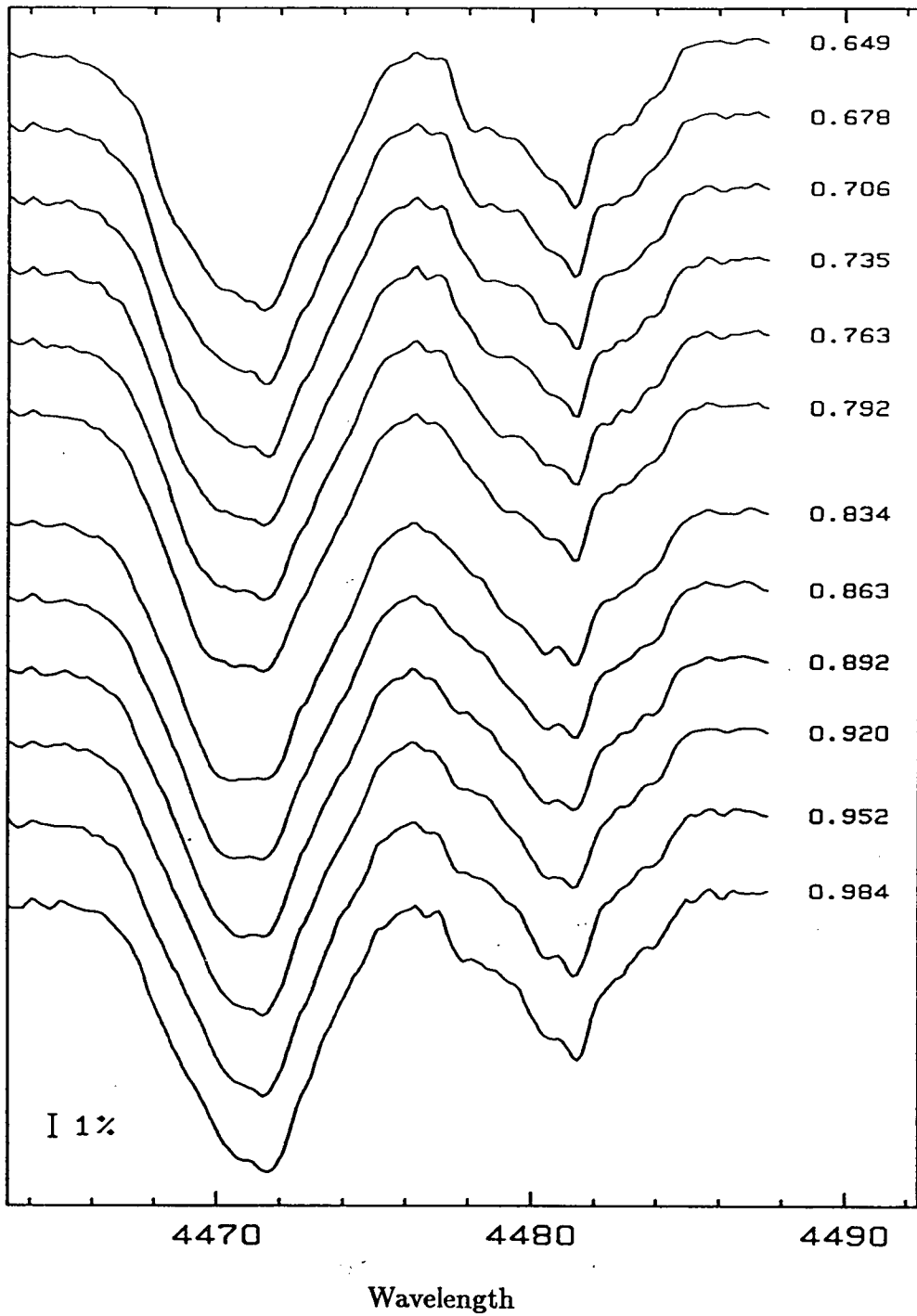
85
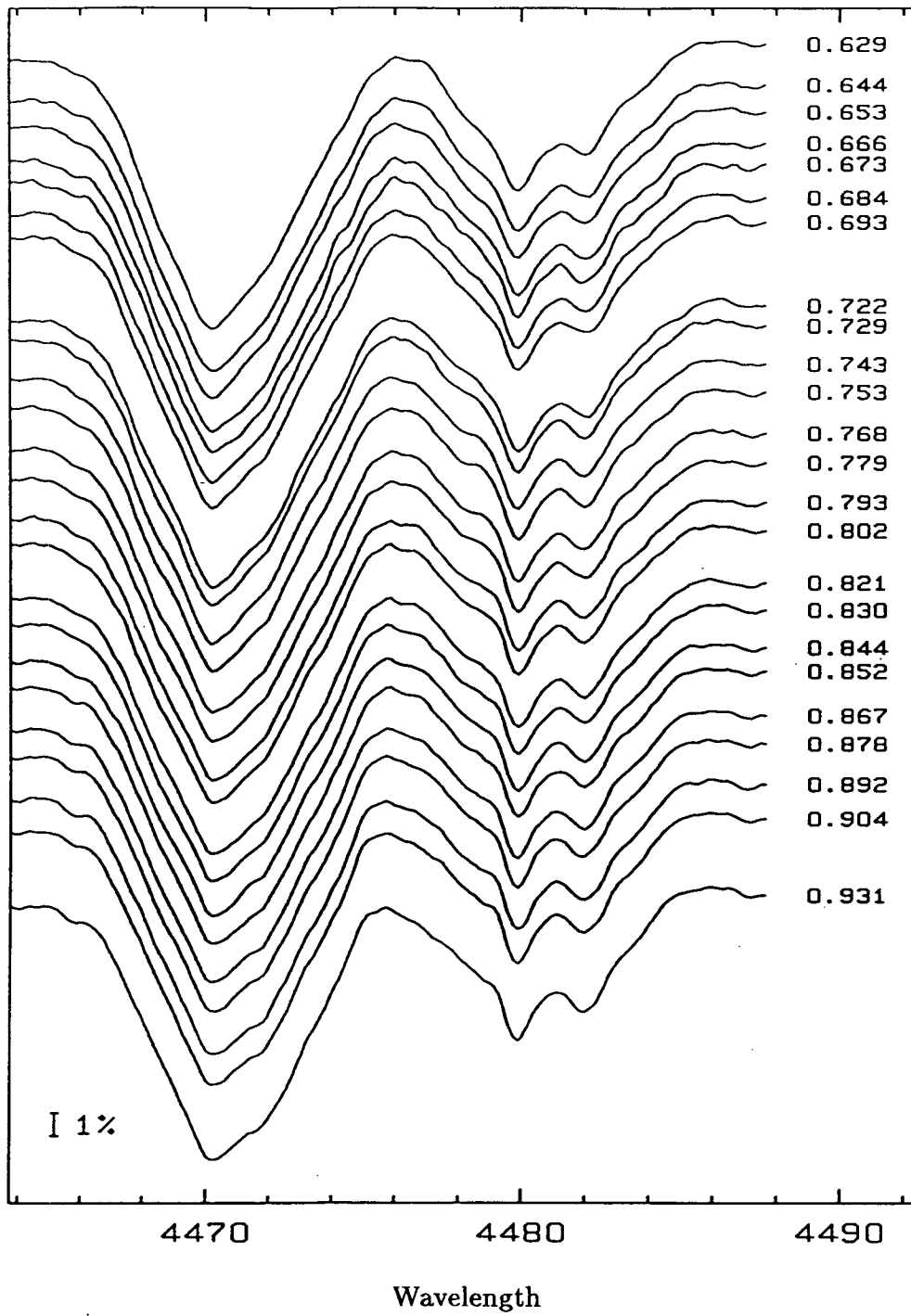
Fig. 32 — Time series of spectra showing He I λ 4471 and Mg II λ 4481 line profiles obtained on 20 October 1986 (UT). The number at the right of each spectrum is the corresponding mid-exposure time in fractions of a day from BJD 2446723.
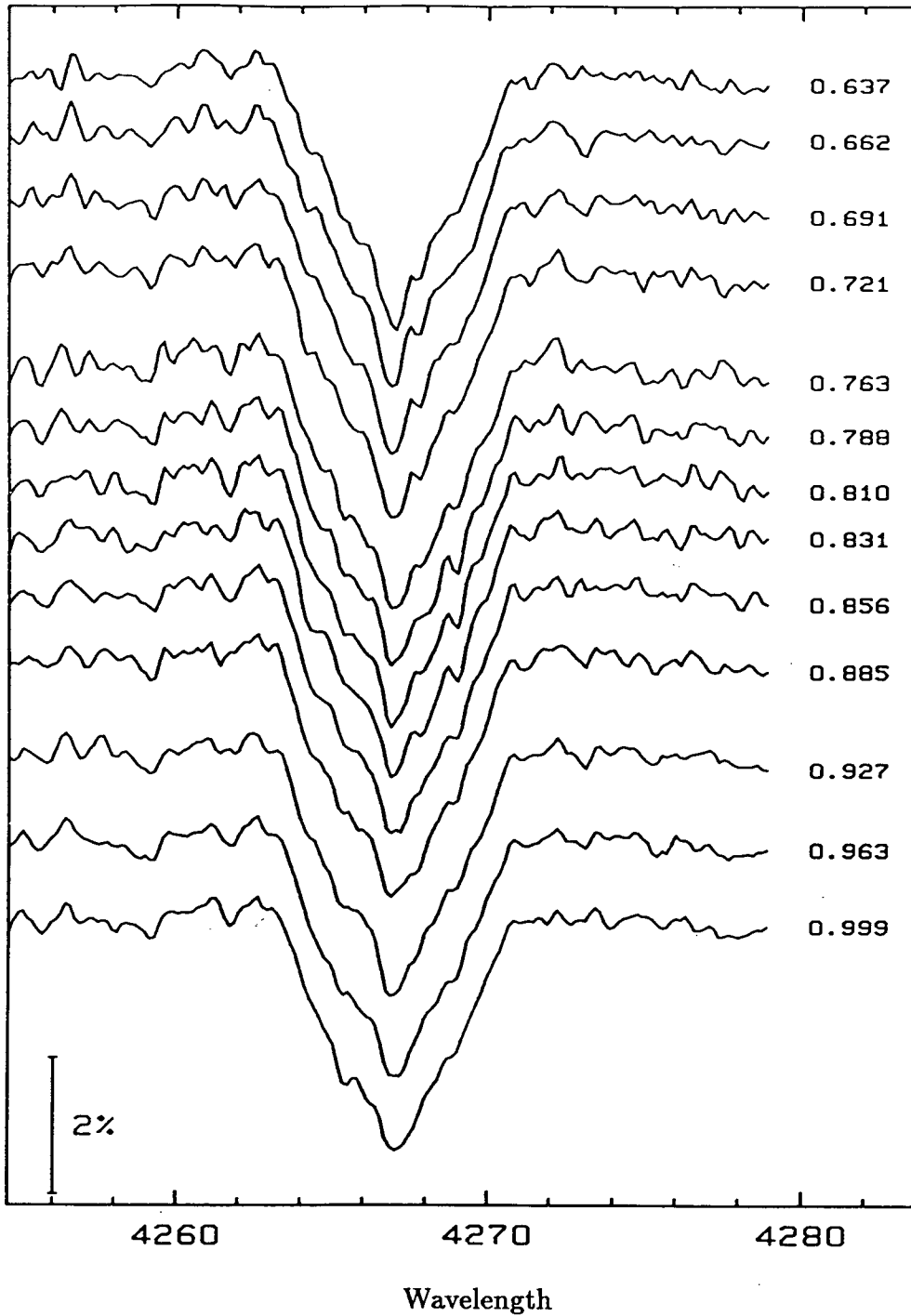
Fig. 33 — Time series of spectra showing C II λ 4267 line profiles obtained on 22 September 1987 (UT). The number at the right of each spectrum is the corresponding mid-exposure time in fractions of a day from BJD 2447060.
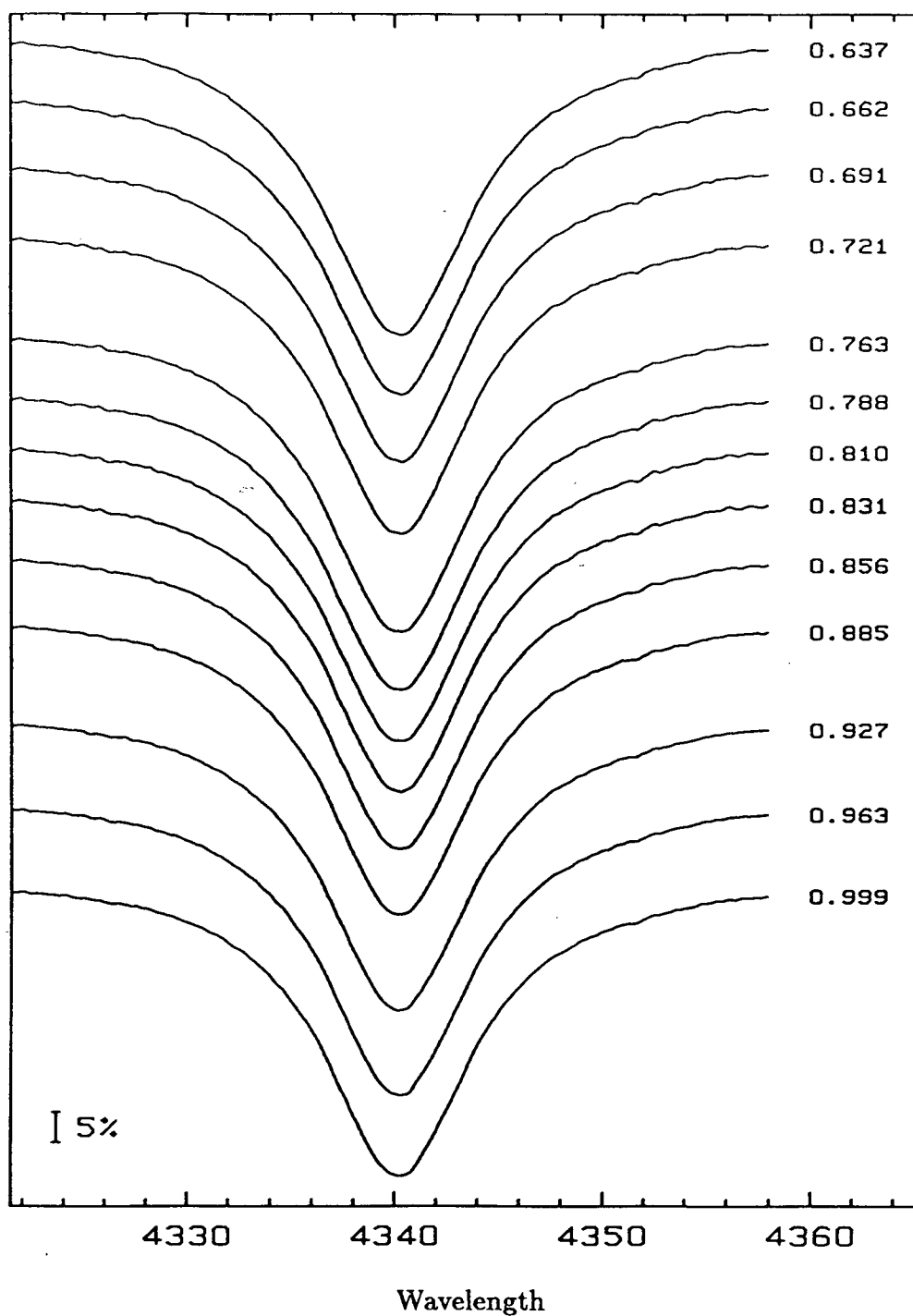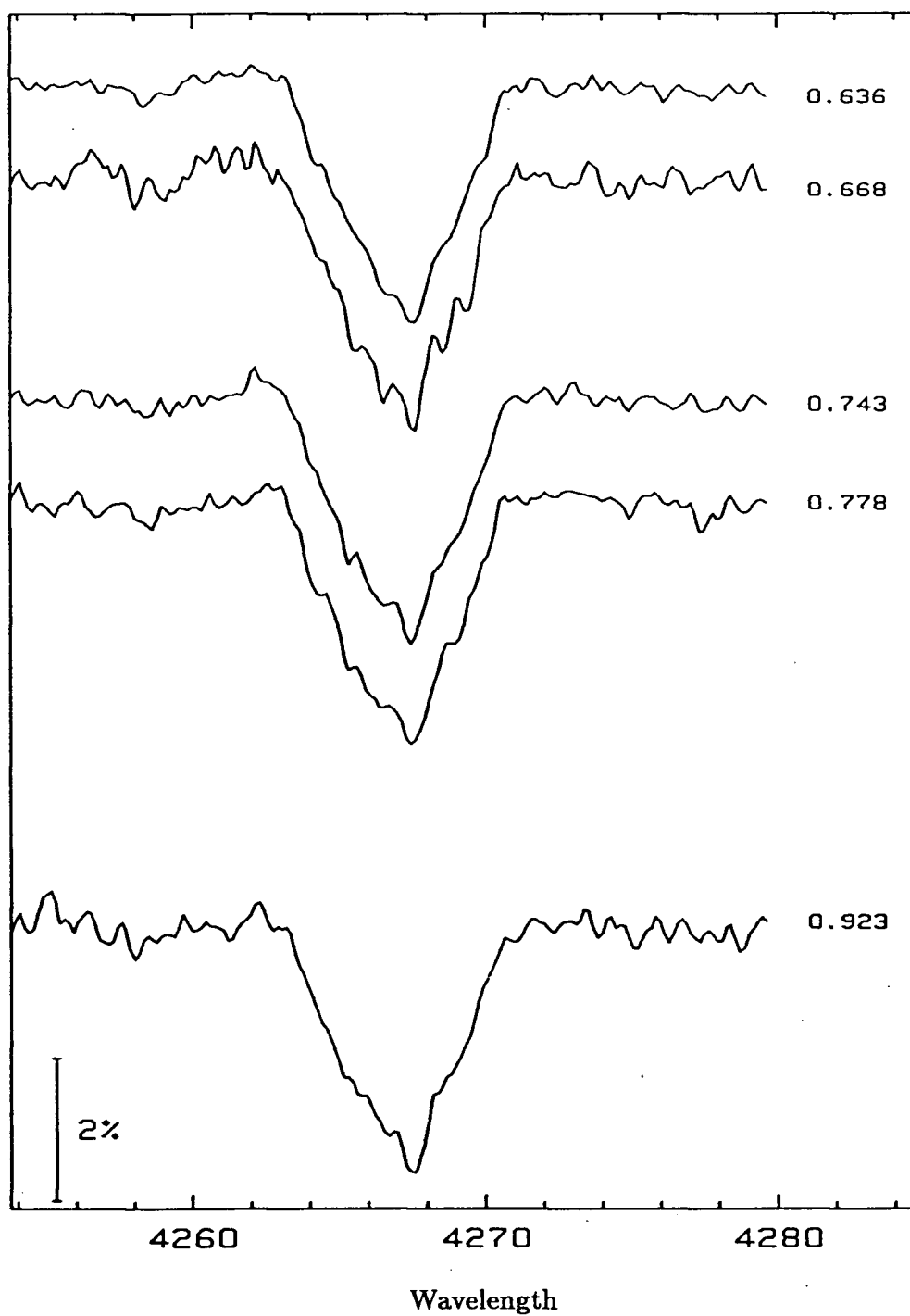
Fig. 34 — Time series of spectra showing Hγ line profiles obtained on 22 September 1987 (UT). The number at the right of each spectrum is the corresponding mid-exposure time in fractions of a day from BJD 2447060.
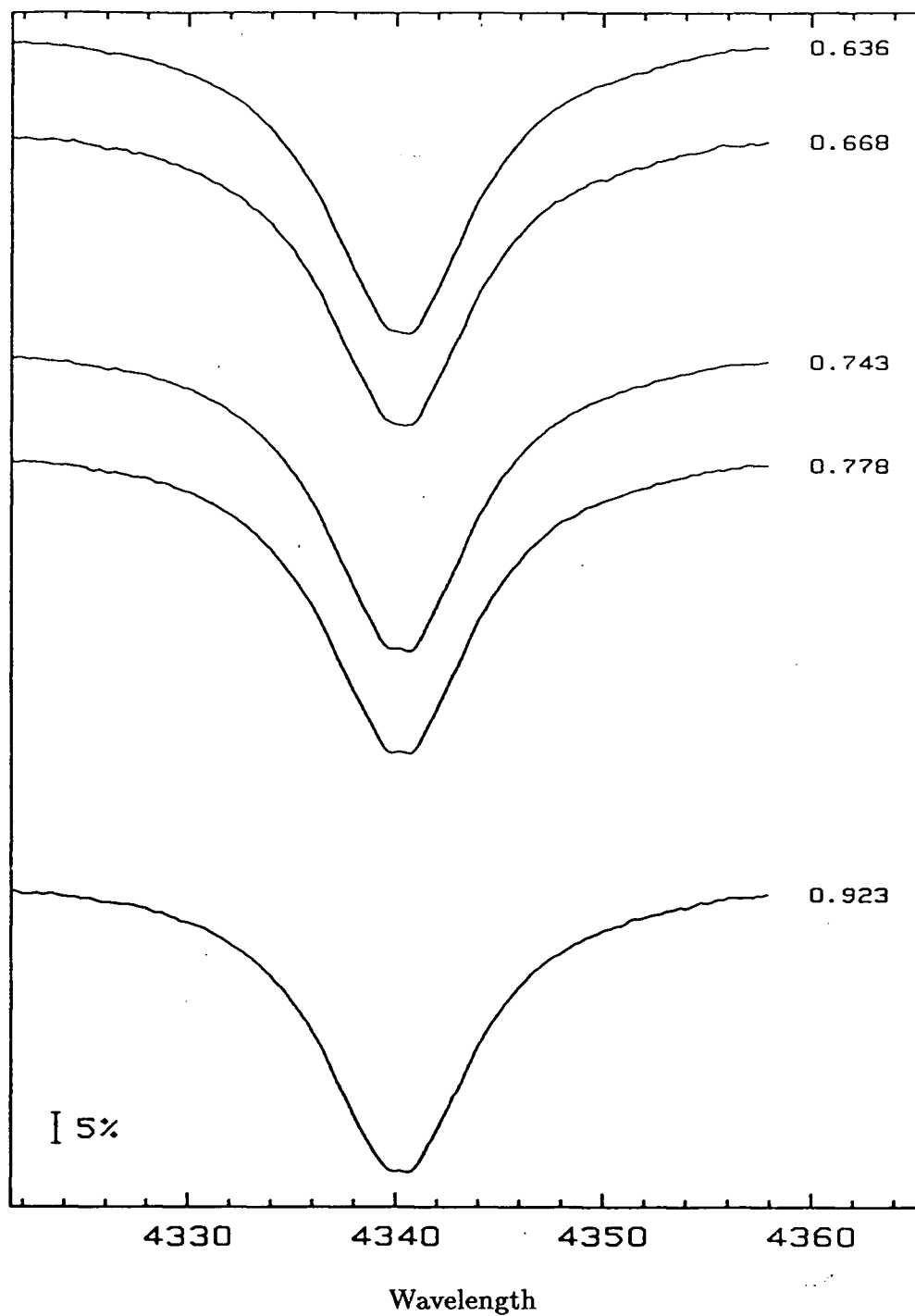
Fig. 35 — Time series of spectra showing He I λ 4388 line profiles obtained on 22 September 1987 (UT). The number at the right of each spectrum is the corresponding mid-exposure time in fractions of a day from BJD 2447060.

0.637
0.662
0.691
0.721

0.763
0.788
0.810
0.831
0.856
0.885

0.927

0.963

0.999

3%

4470   4480   4490

Wavelength
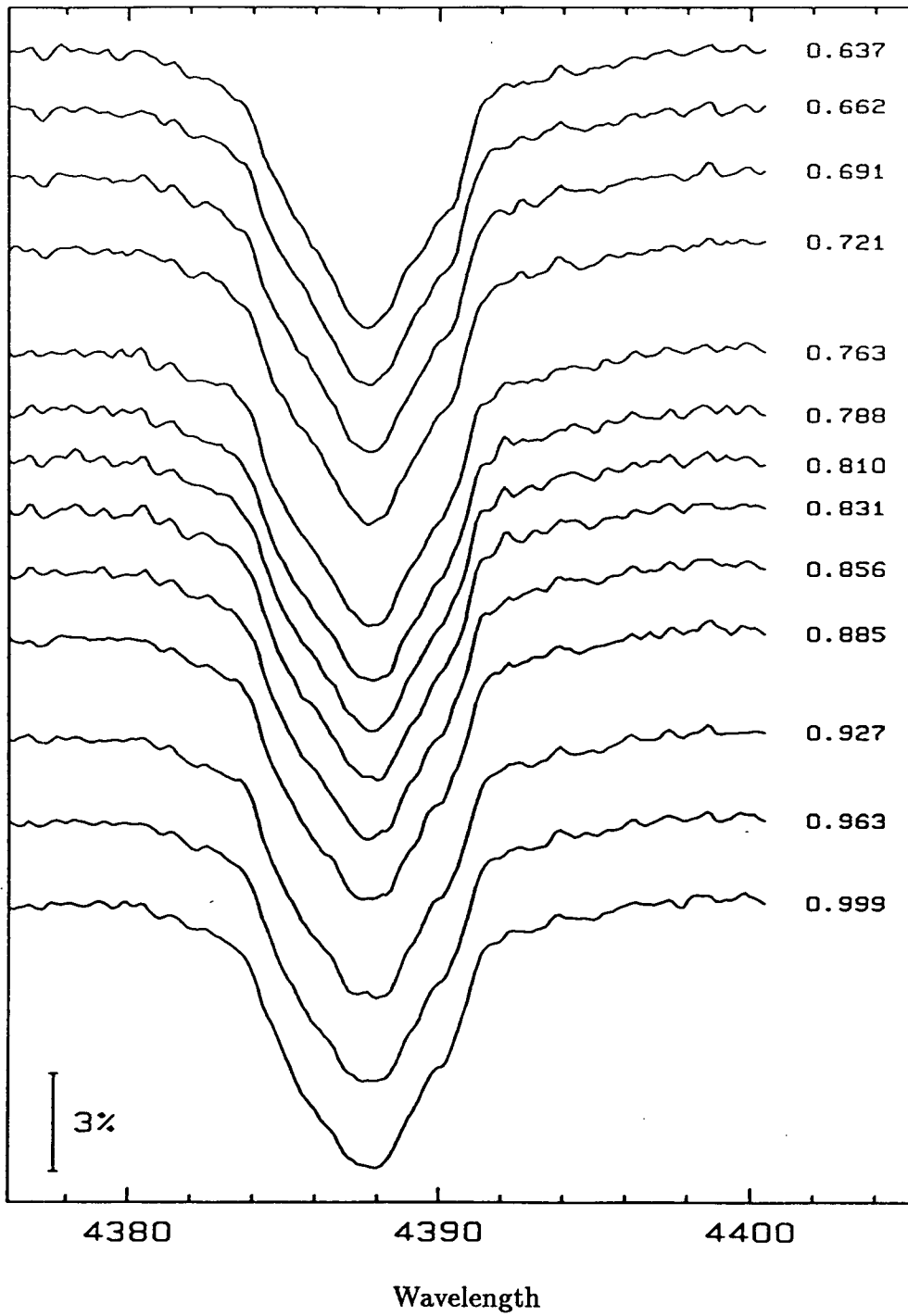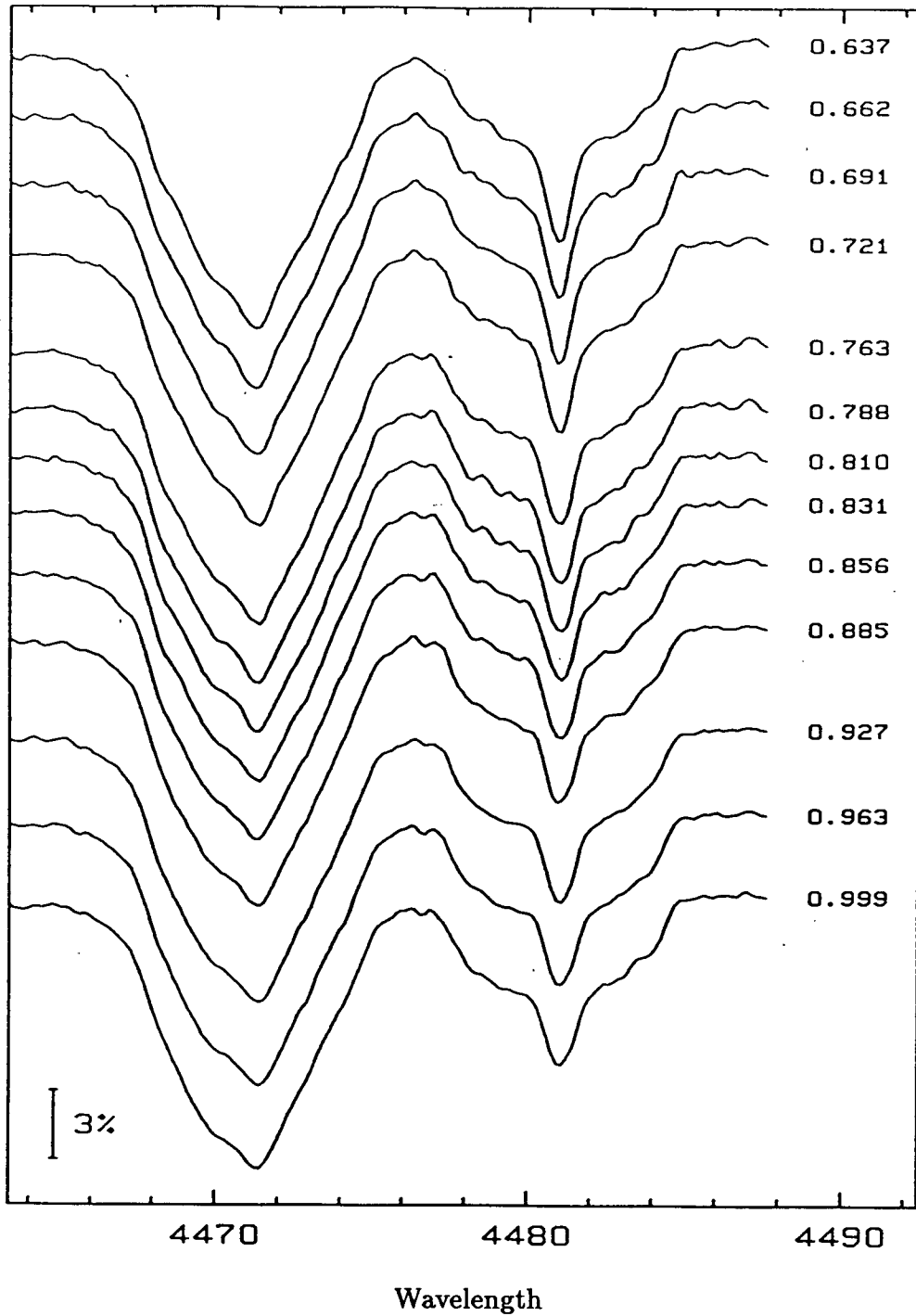
Fig. 36 — Time series of spectra showing He I λ 44471 and Mg IIλ 4481 line profiles obtained on 22 September 1987 (UT). The number at the right of each spectrum is the corresponding mid-exposure time in fractions of a day from BJD 2447060.
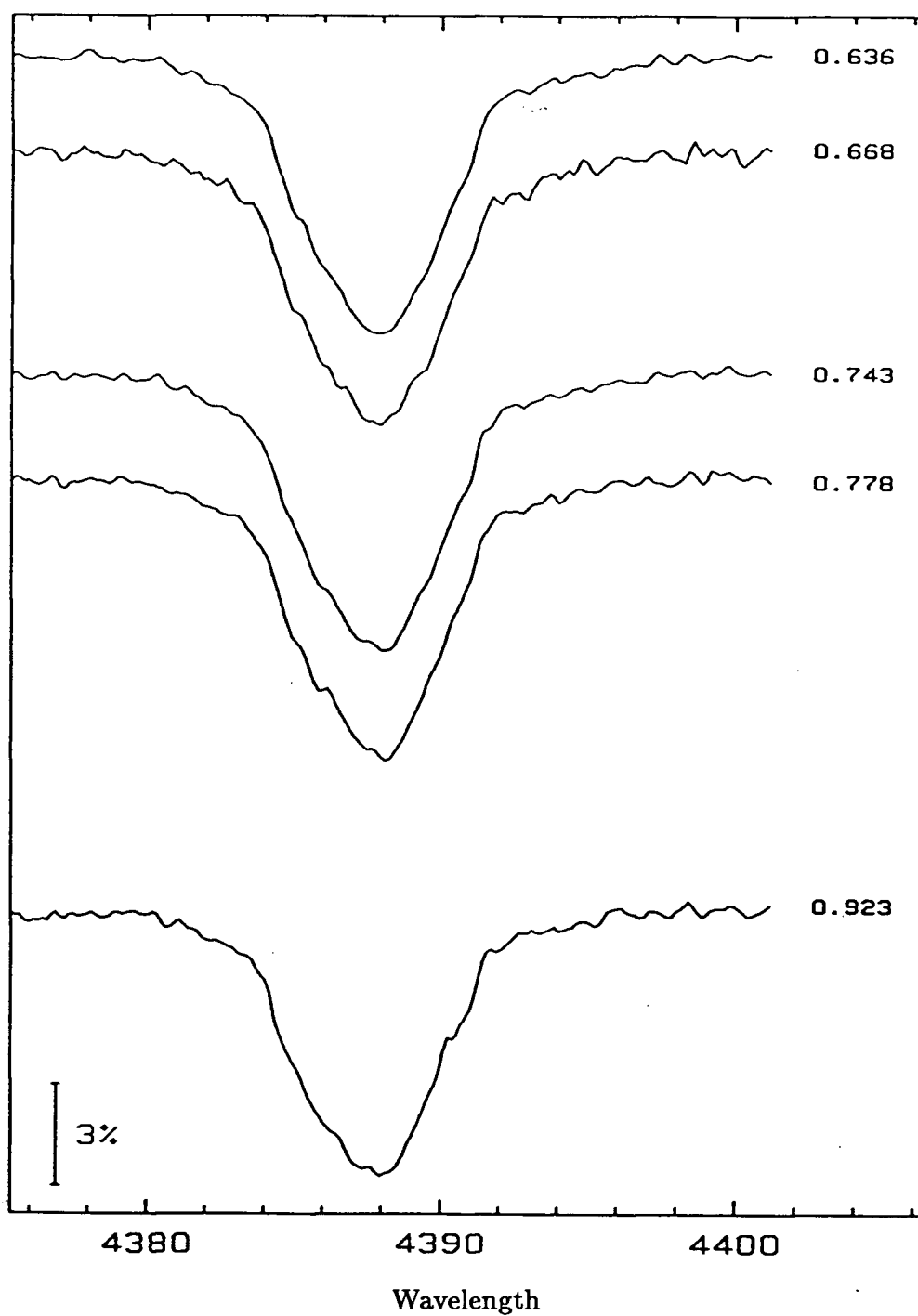
Fig. 37 — Time series of spectra showing C II λ 4267 line profiles obtained on 23 September 1987 (UT). The number at the right of each spectrum is the corresponding mid-exposure time in fractions of a day from BJD 2447061.
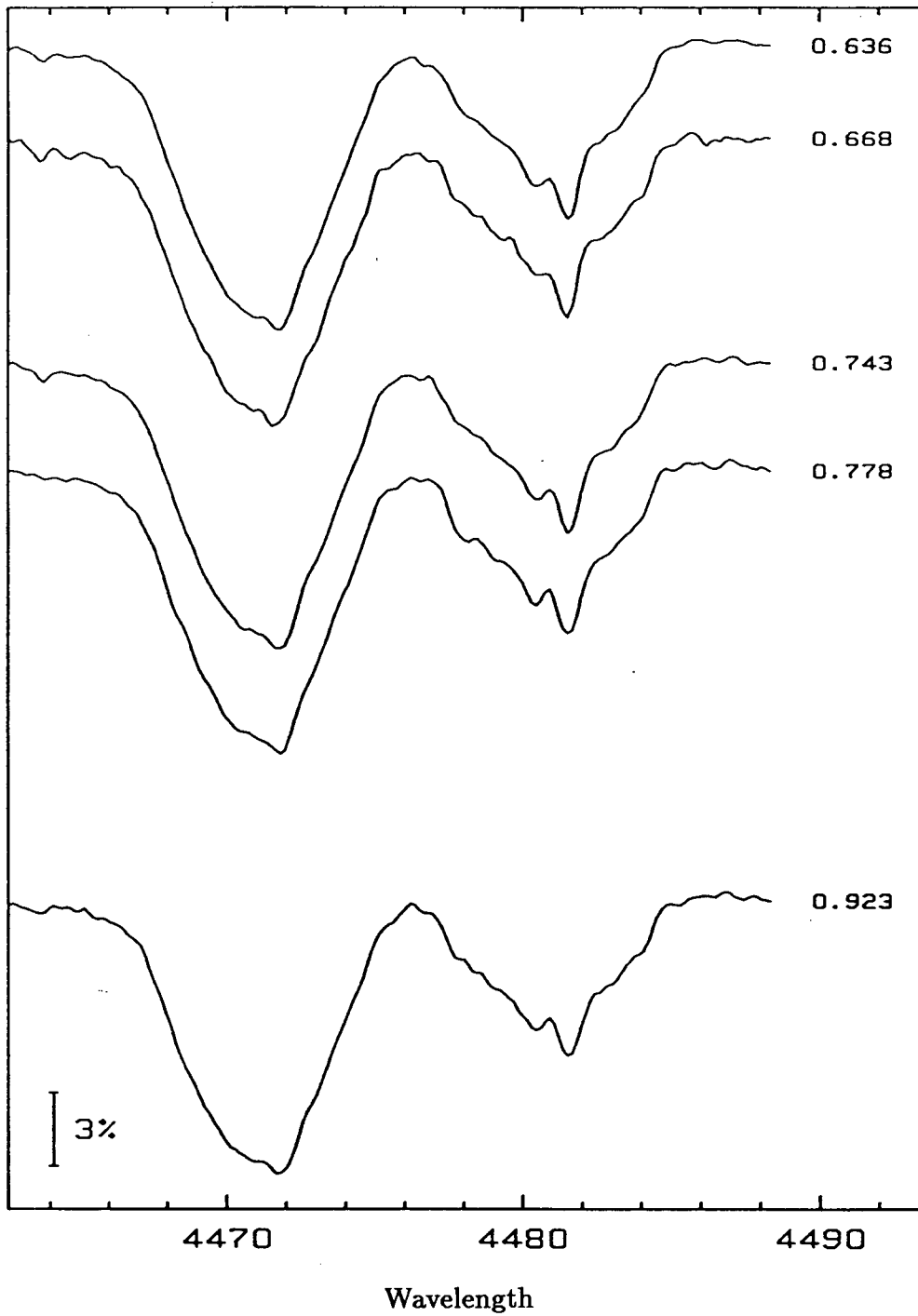
Fig. 38 — Time series of spectra showing Hγ line profiles obtained on 23 September 1987 (UT). The number at the right of each spectrum is the corresponding mid-exposure time in fractions of a day from BJD 2447061.
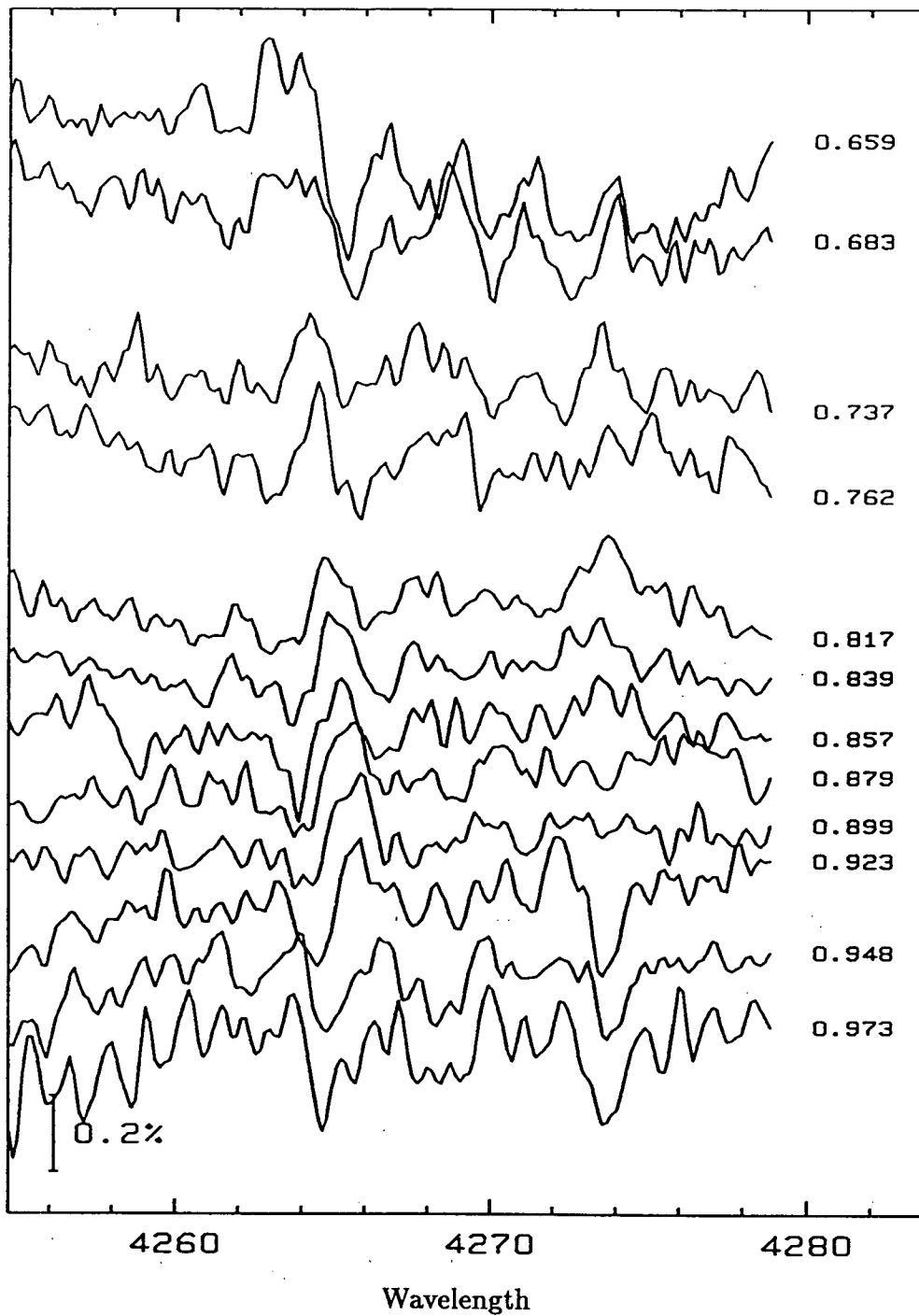
Fig. 39 — Time series of spectra showing He I λ 4388 line profiles obtained on 23 September 1987 (UT). The number at the right of each spectrum is the corresponding mid-exposure time in fractions of a day from BJD 2447061.

Fig. 40 — Time series of spectra showing He I λ 4471 and Mg II λ 4481 line profiles obtained on 23 September 1987 (UT). The number at the right of each spectrum is the corresponding mid-exposure time in fractions of a day from BJD 2447061.

Fig. 41 — Time series of spectra showing C II λ 4267 line profiles obtained on 24 September 1987 (UT). The number at the right of each spectrum is the corresponding mid-exposure time in fractions of a day from BJD 2447062.

Fig. 42 — Time series of spectra showing Hγ line profiles obtained on 24 September 1987 (UT). The number at the right of each spectrum is the corresponding mid-exposure time in fractions of a day from BJD 2447062.

Fig. 43 — Time series of spectra showing He I λ 4388 line profiles obtained on 24 September 1987 (UT). The number at the right of each spectrum is the corresponding mid-exposure time in fractions of a day from BJD 2447062.

Fig. 44 — Time series of spectra showing He I λ 4471 and Mg II λ 4481 line profiles obtained on 24 September 1987 (UT). The number at the right of each spectrum is the corresponding mid-exposure time in fractions of a day from BJD 2447062.

Fig. 45 — Time series of spectra showing C II λ 4267 line profiles obtained on 25 September 1987 (UT). The number at the right of each spectrum is the corresponding mid-exposure time in fractions of a day from BJD 2447063.

Fig. 46 — Time series of spectra showing Hγ line profiles obtained on 25 September 1987 (UT). The number at the right of each spectrum is the corresponding mid-exposure time in fractions of a day from BJD 2447063.

100

Fig. 47 — Time series of spectra showing He I λ 4388 line profiles obtained on 25 September 1987 (UT). The number at the right of each spectrum is the corresponding mid-exposure time in fractions of a day from BJD 2447063.

Fig. 48 — Time series of spectra showing He I λ 4471 and Mg II λ 4481 line profiles obtained on 25 September 1987 (UT). The number at the right of each spectrum is the corresponding mid-exposure time in fractions of a day from BJD 2447063.

0.659

0.683

0.737

0.762

0.817
0.839
0.857
0.879
0.899
0.923
0.948
0.973

0.2%

4260   4270   4280

Wavelength

Fig. 49 — The residuals formed by subtracting the mean of the 17 October 1986 C II λ 4267 line profiles presented in figure 21.
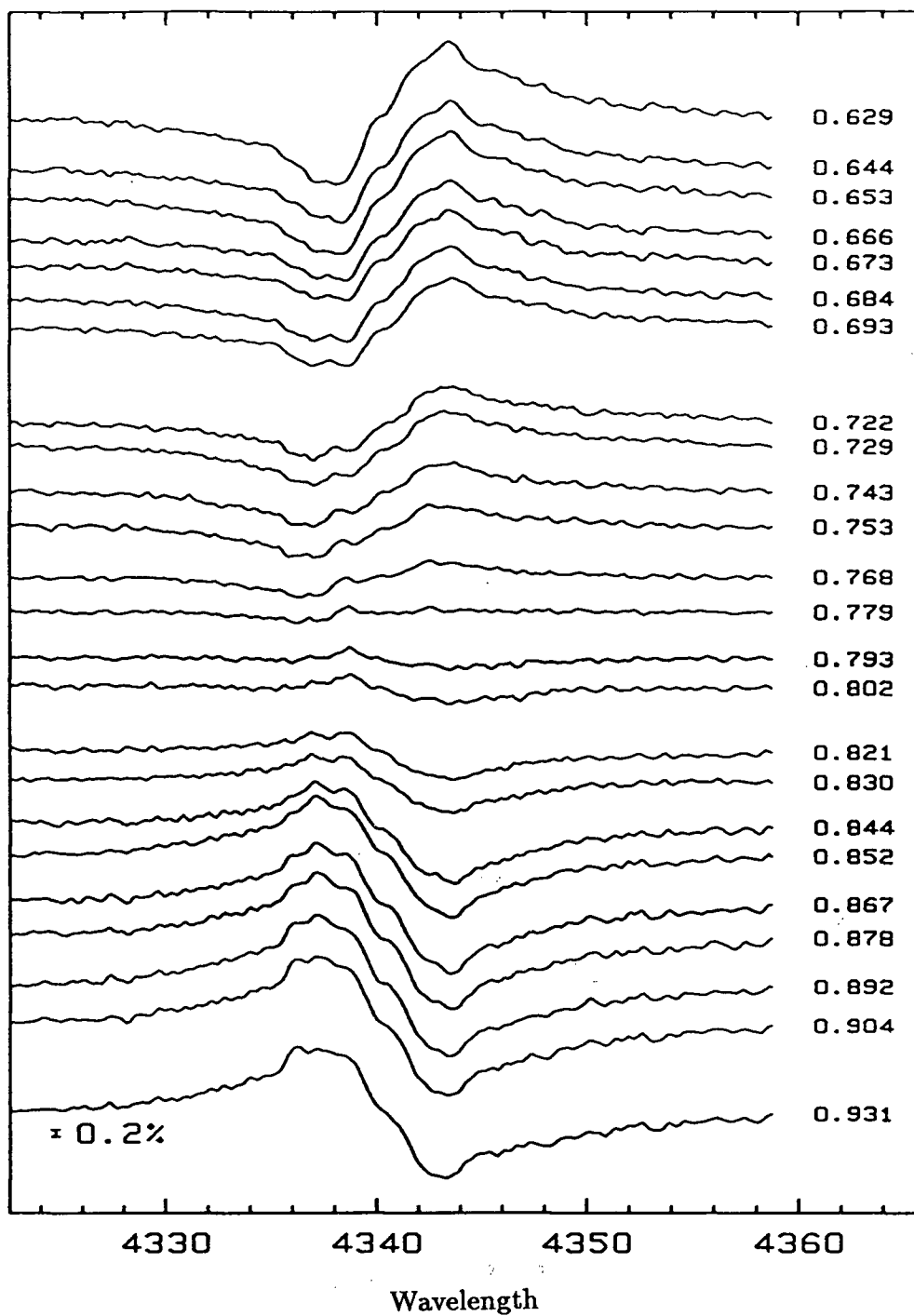
103
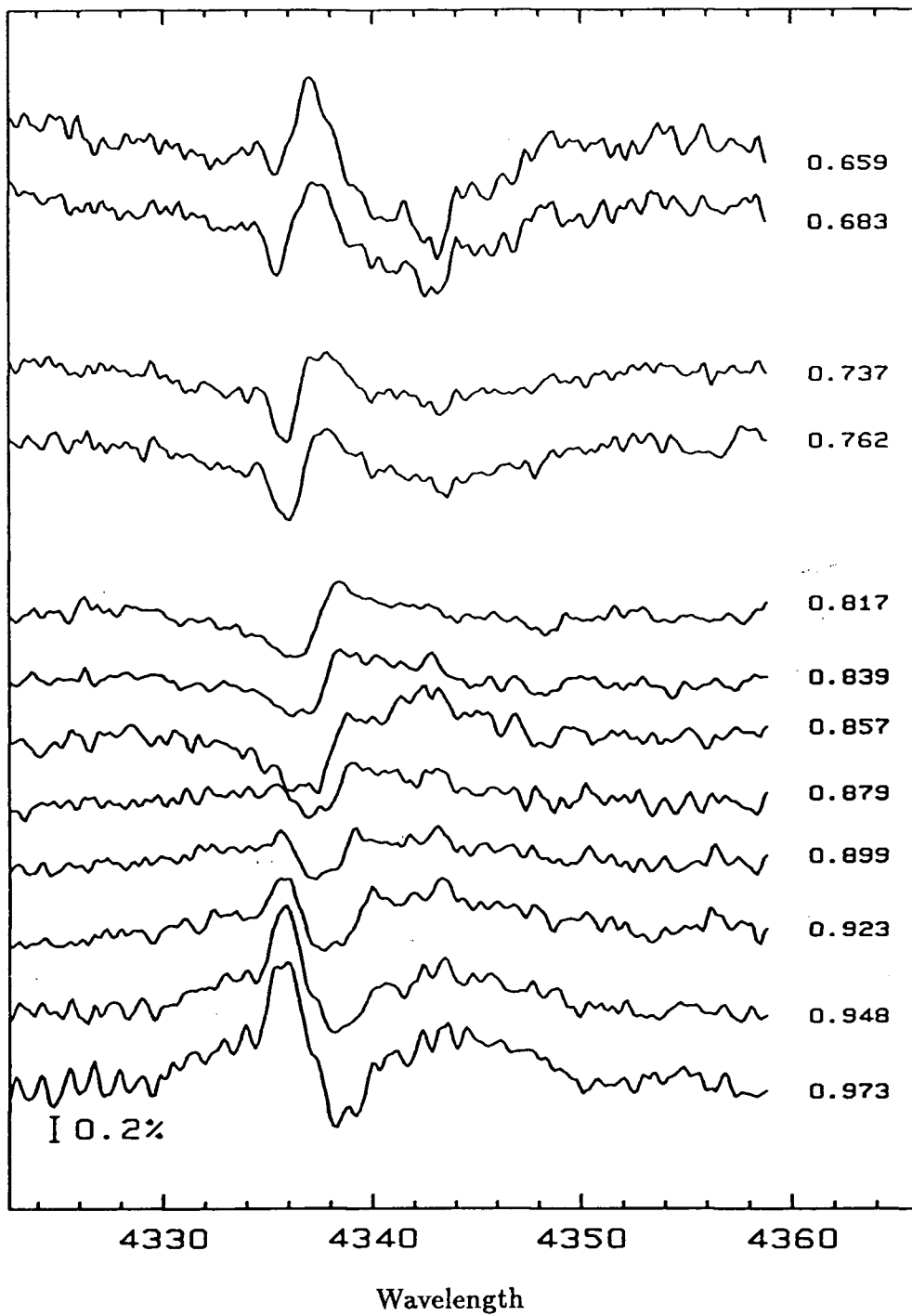
Fig. 50 — The residuals formed by subtracting the mean of the 17 October 1986 Hγ line profiles presented in figure 22.
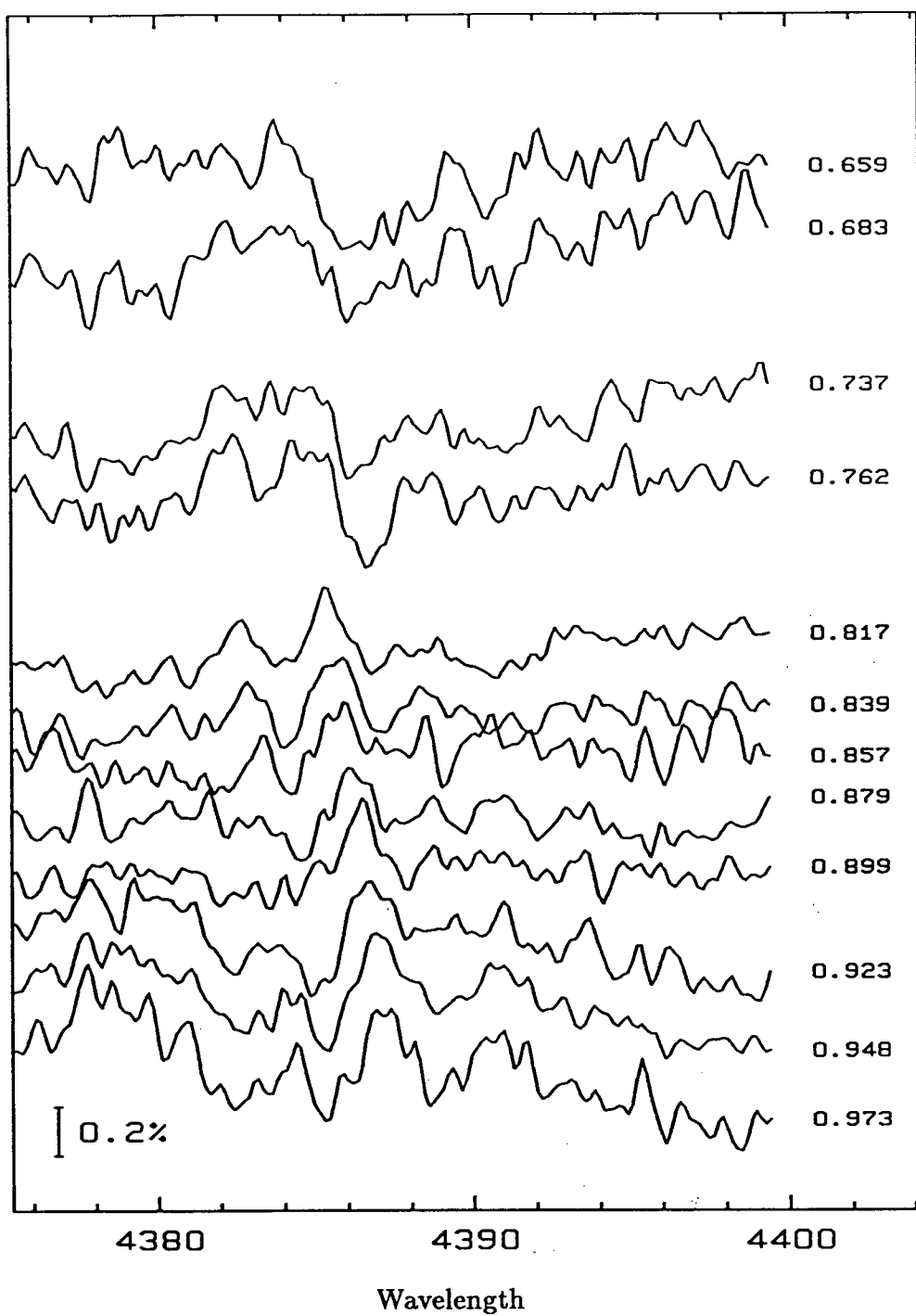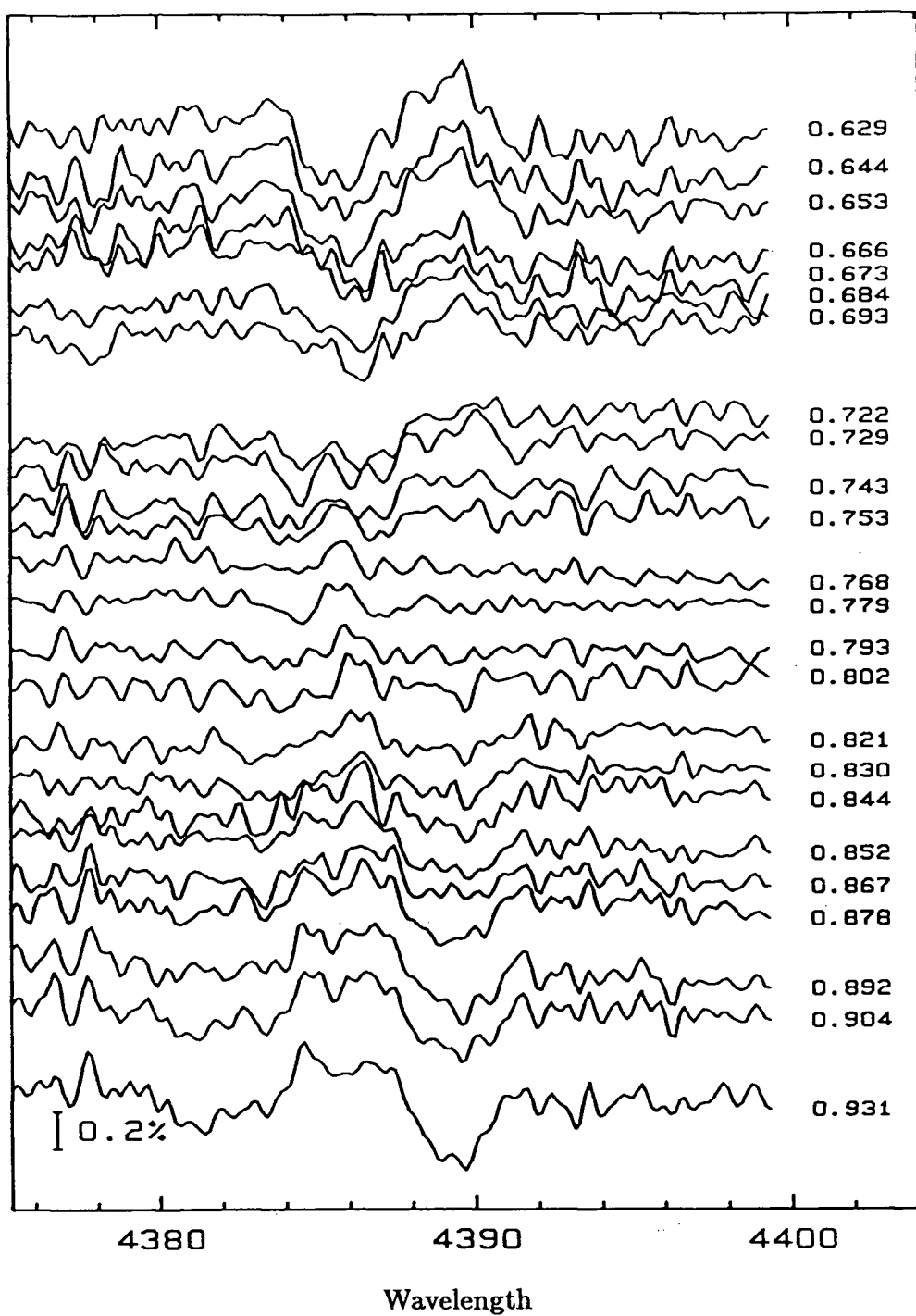
Fig. 51 — The residuals formed by subtracting the mean of the 17 October 1986 He I λ 4388 line profiles presented in figure 23.
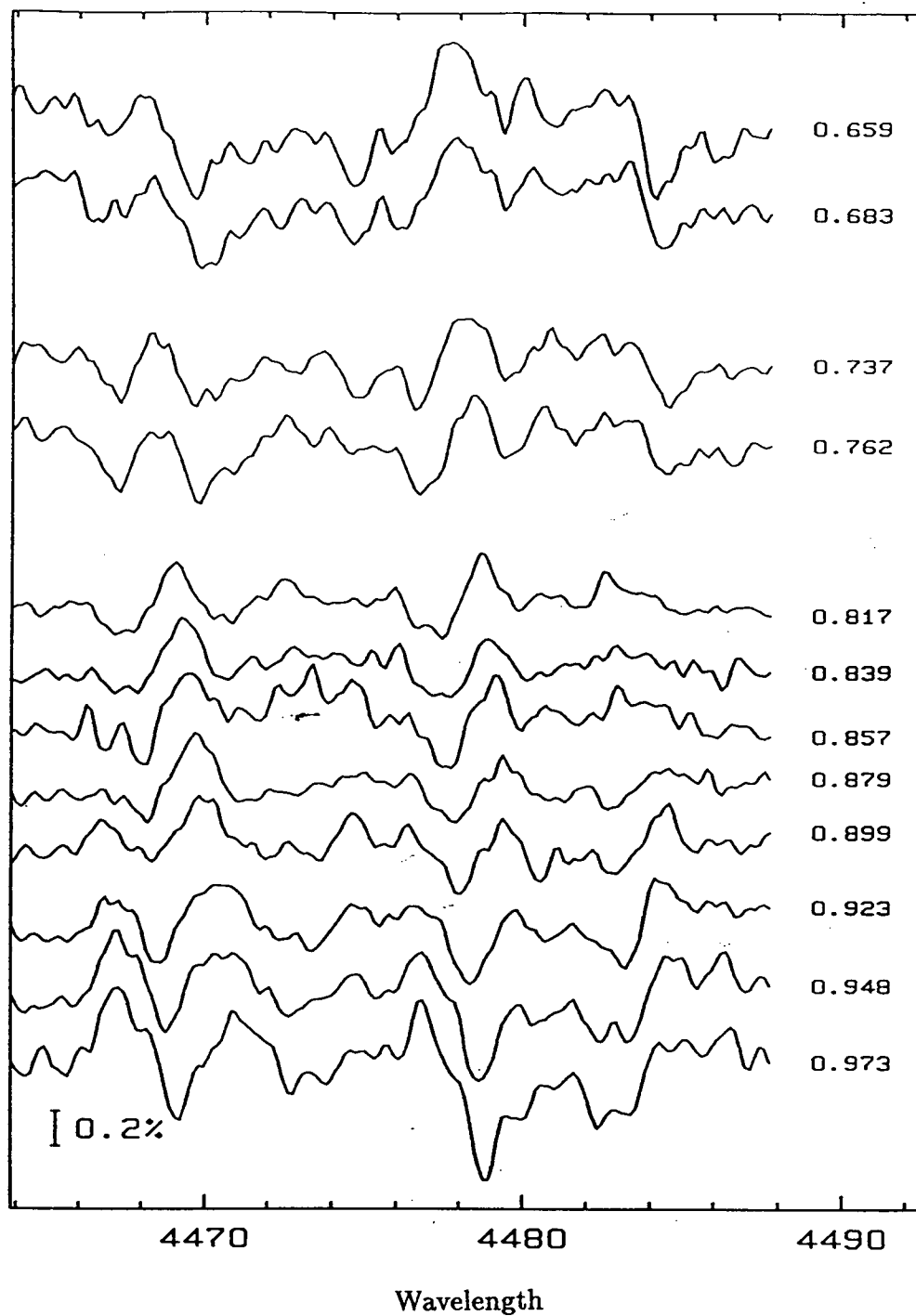
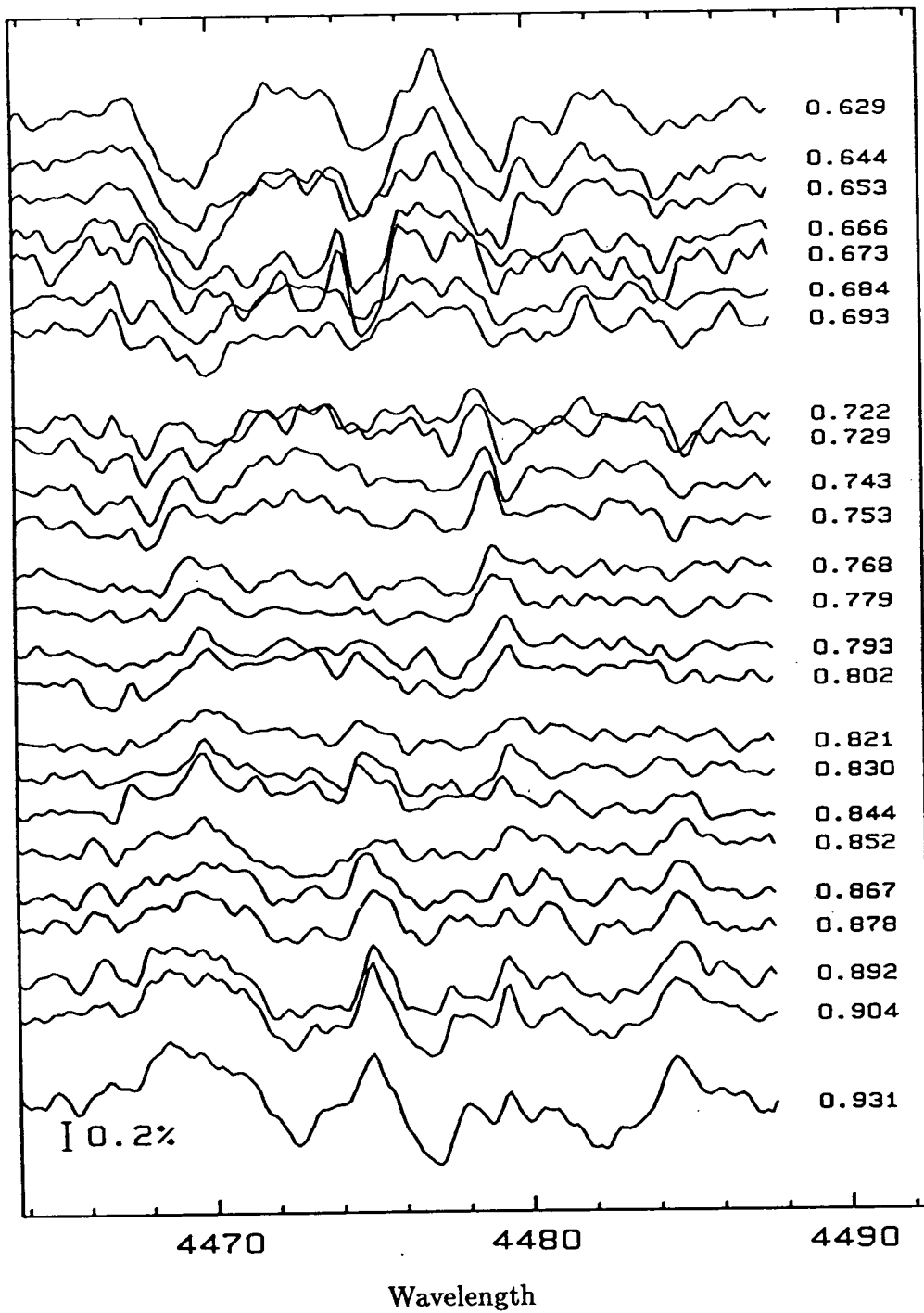Fig. 52 — The residuals formed by subtracting the mean of the 17 October 1986 He I λ 4471 and Mg II λ 4481 line profiles presented in figure 24.

0.593
0.609
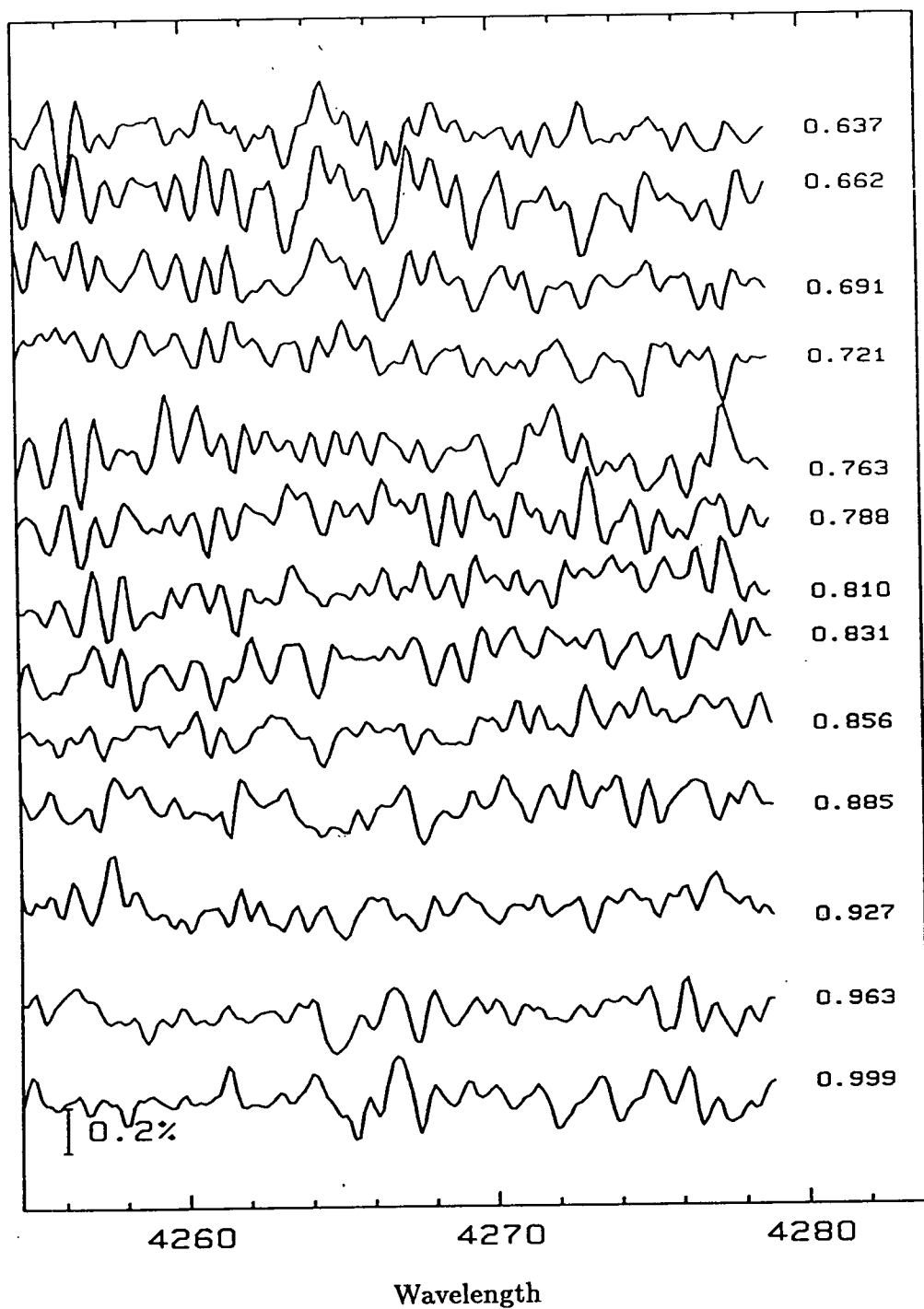0.620

0.731
0.747
0.766

0.806
0.825
0.843
0.865
0.894
0.921
0.943
0.964

0.2%

4260   4270   4280

Wavelength
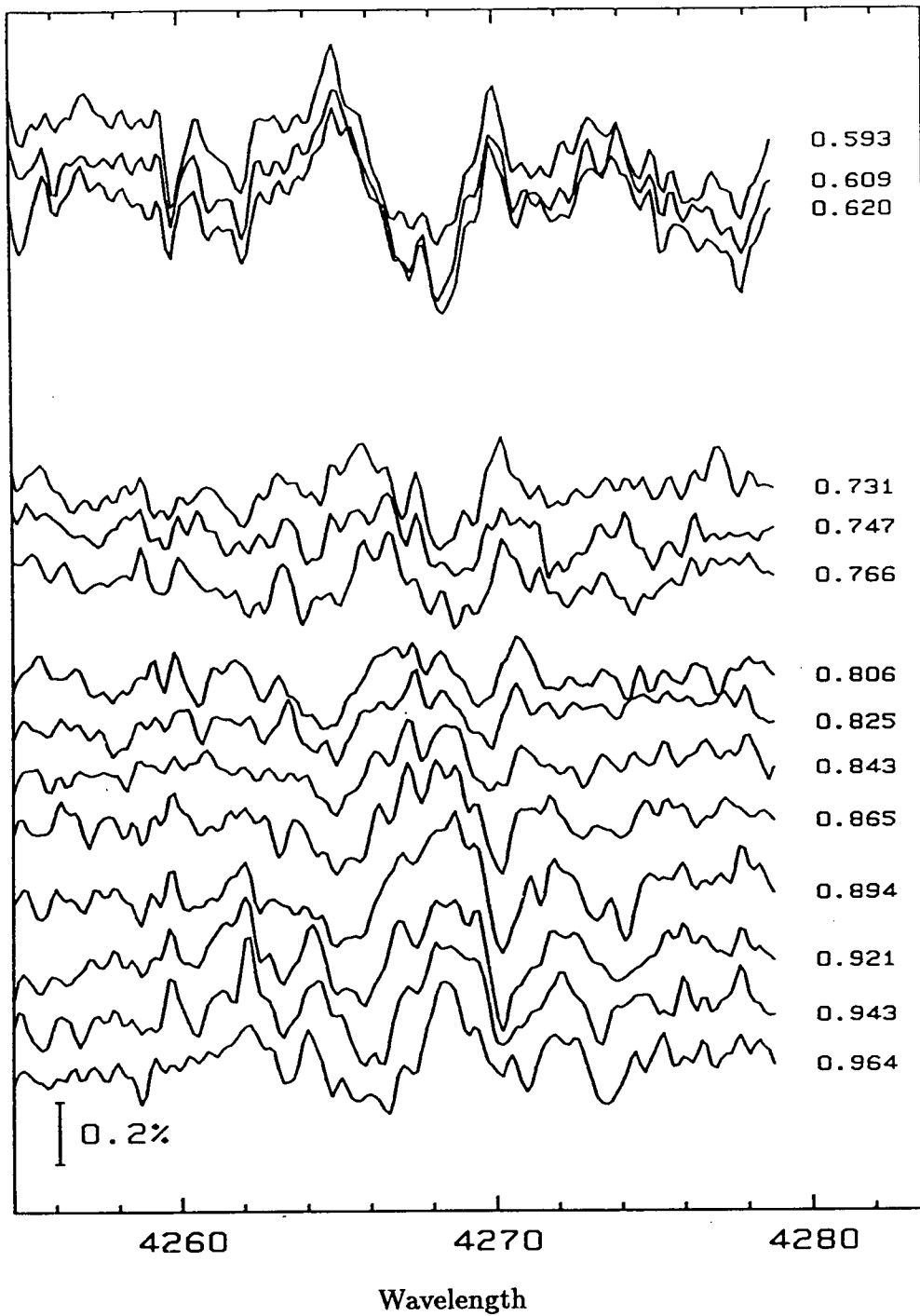
Fig. 53 — The residuals formed by subtracting the mean of the 19 October 1986 C II λ 4267 line profiles presented in figure 25.
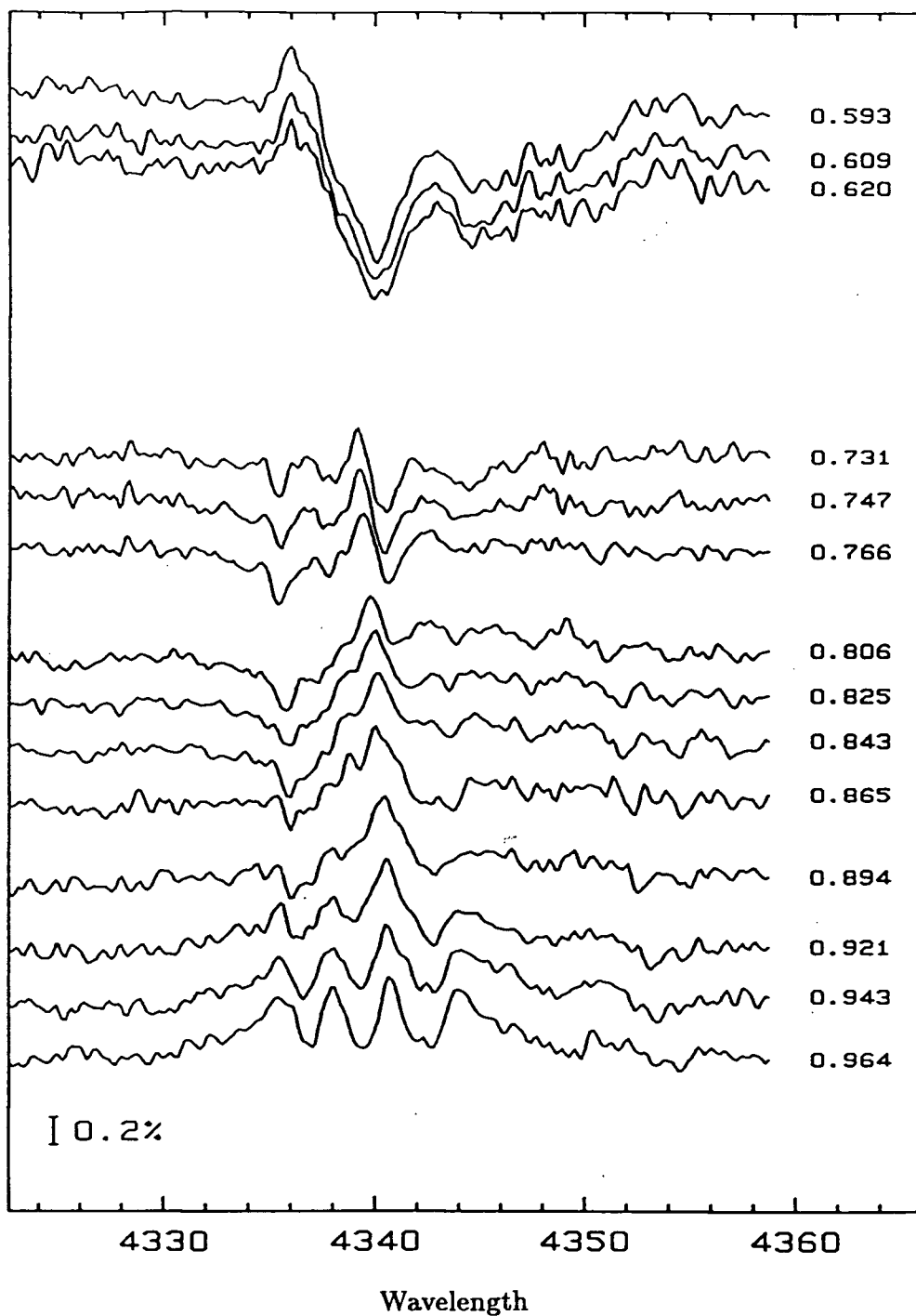
Fig. 54 — The residuals formed by subtracting the mean of the 19 October 1986 Hγ line profiles presented in figure 26.
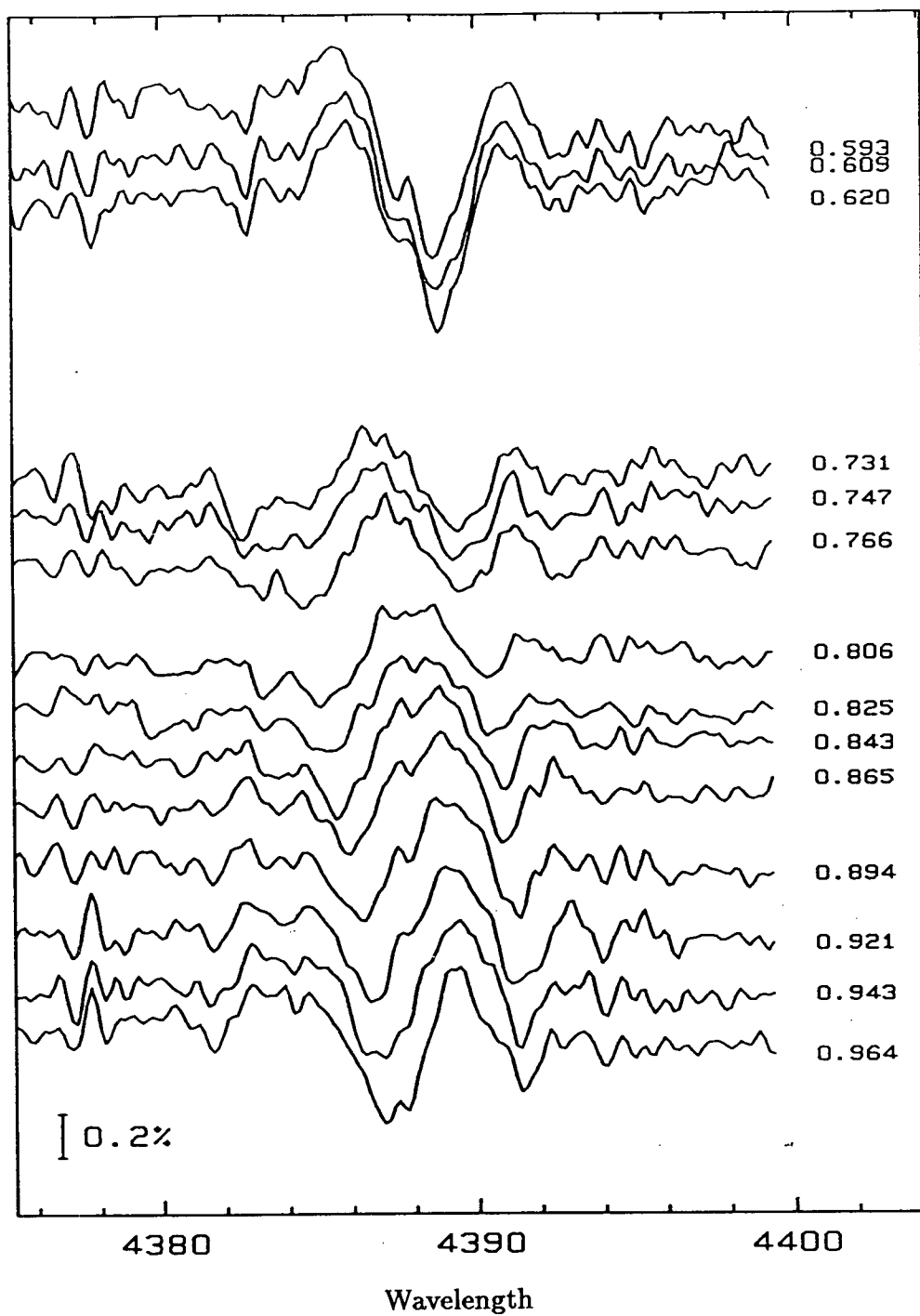
Fig. 55 — The residuals formed by subtracting the mean of the 19 October 1986 He I λ 4388 line profiles presented in figure 27.
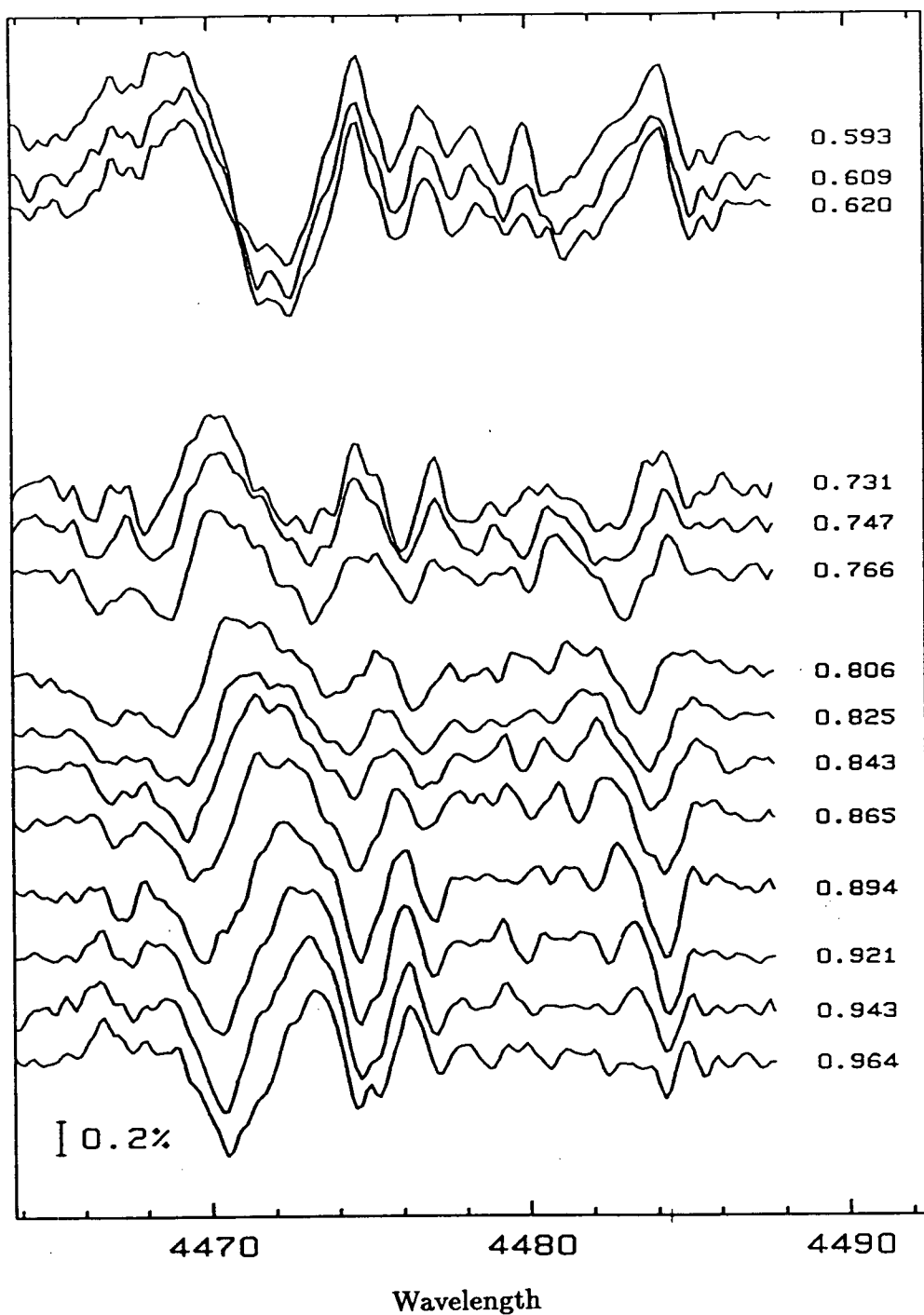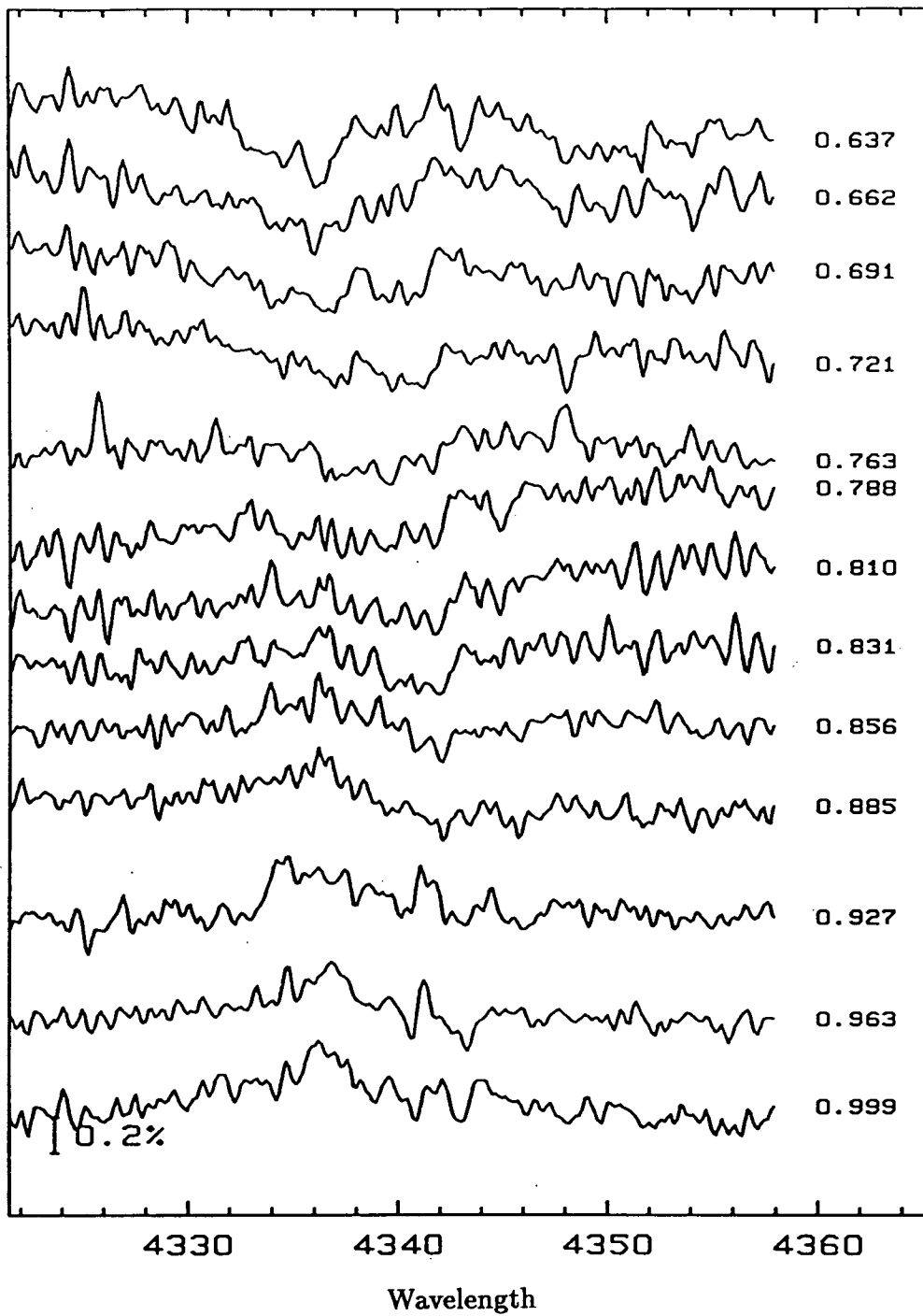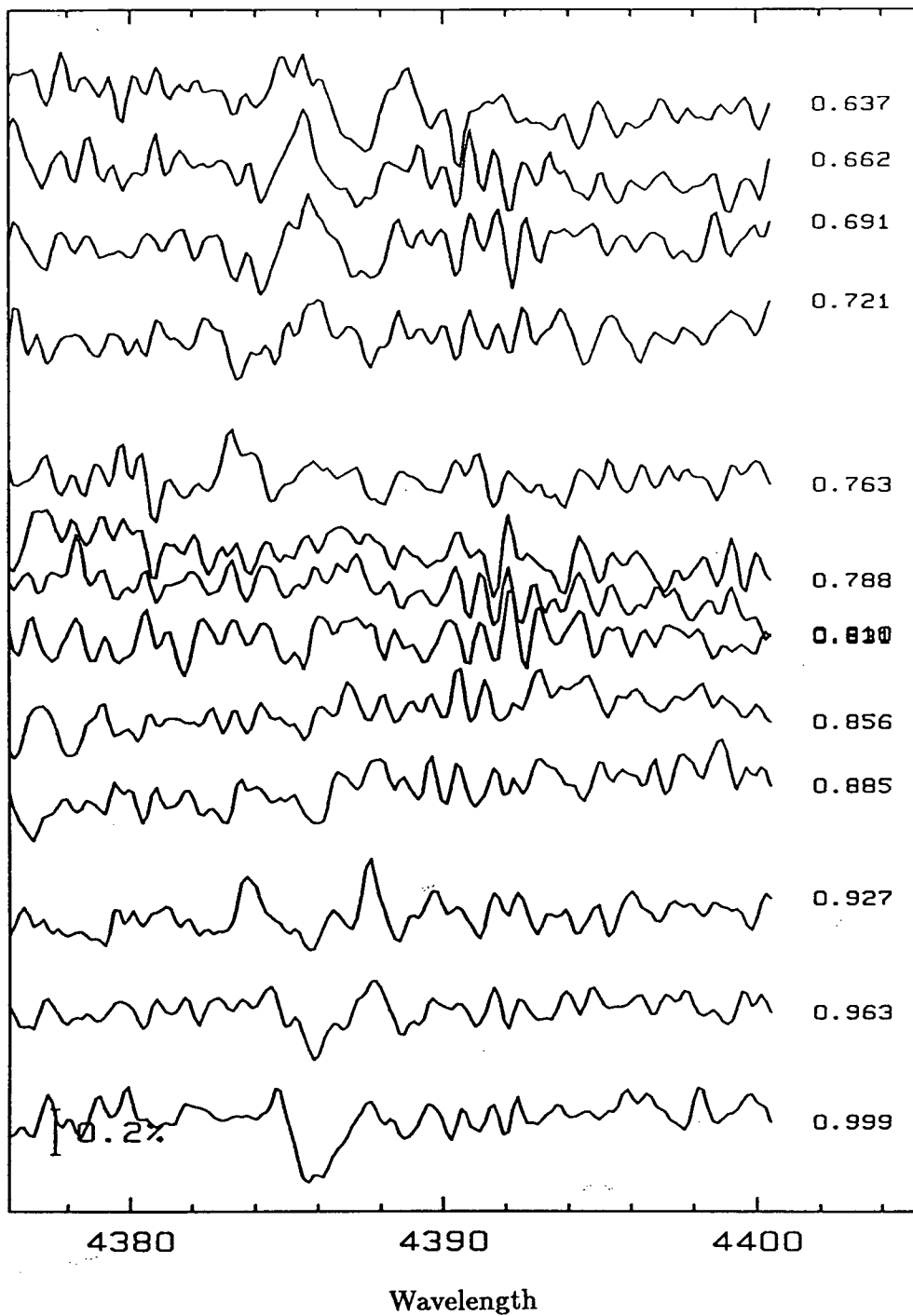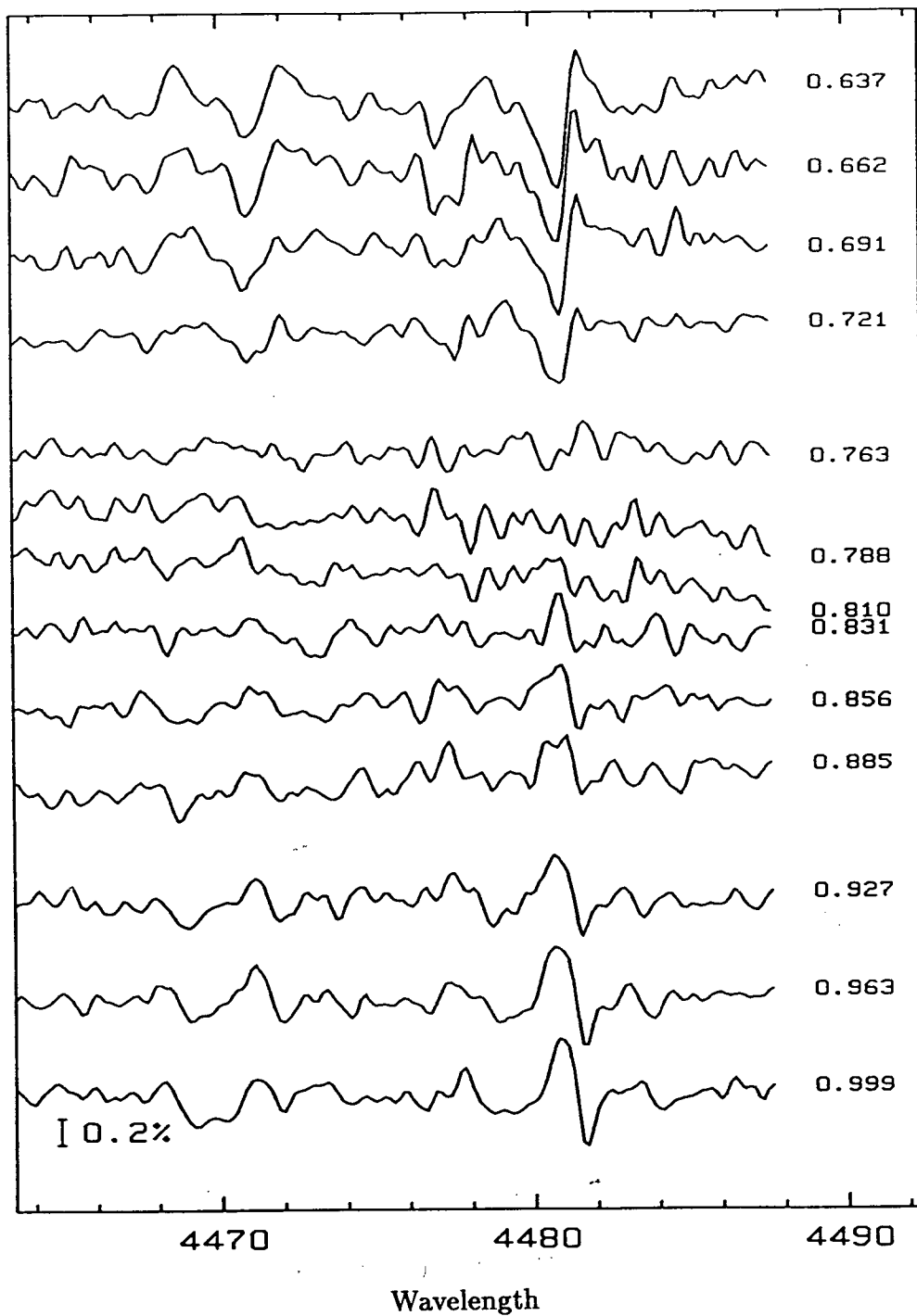
Fig. 56 — The residuals formed by subtracting the mean of the 19 October 1986 He I λ 4471 and Mg II λ 4481 line profiles presented in figure 28.

0.629

0.644
0.653

0.666
0.673

0.684
0.693

0.722
0.729

0.743
0.753

0.768
0.779

0.793
0.802

0.821
0.830

0.844
0.852

0.867
0.878

0.892

0.904

0.931

0.2%

4260   4270   4280

Wavelength
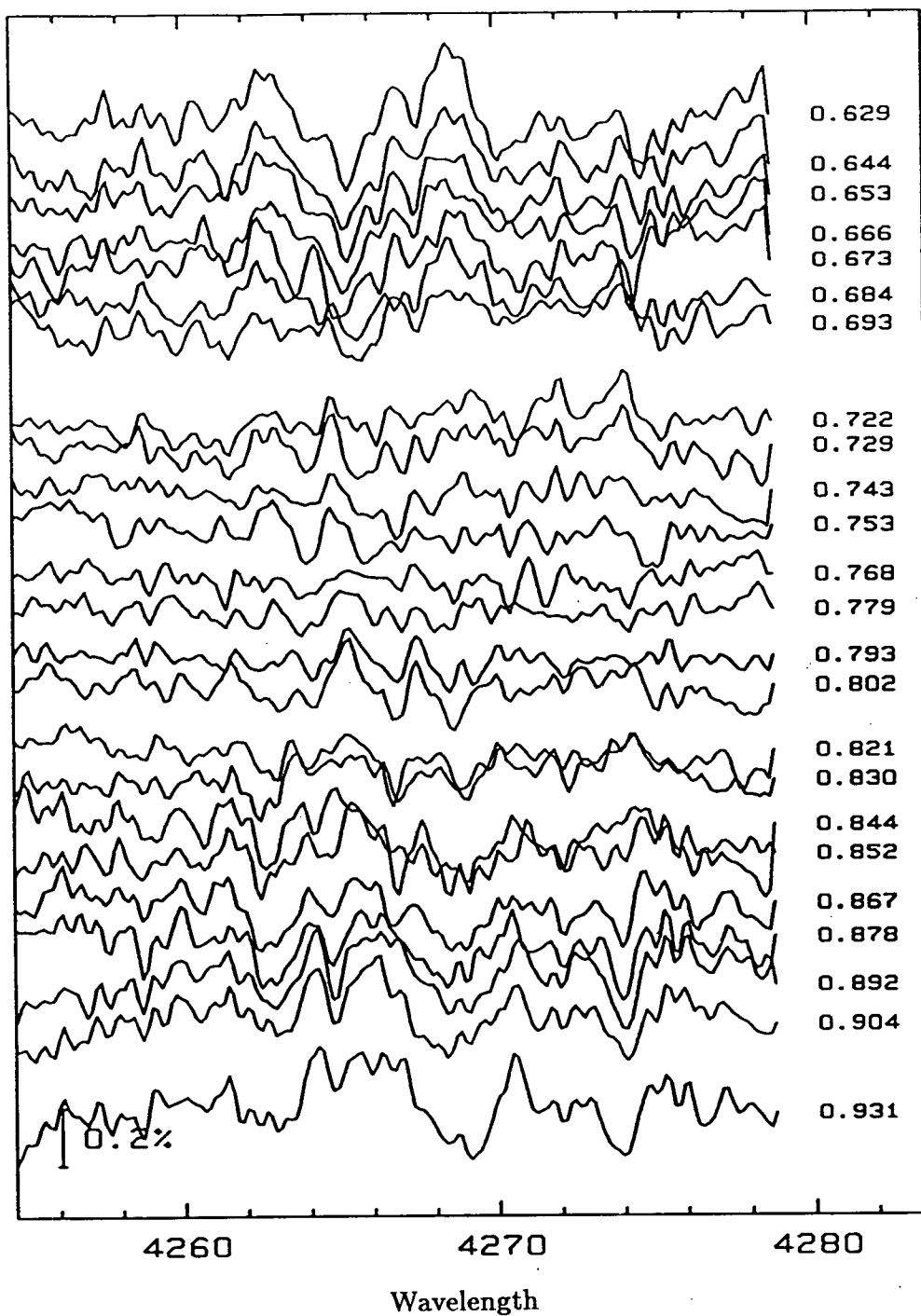
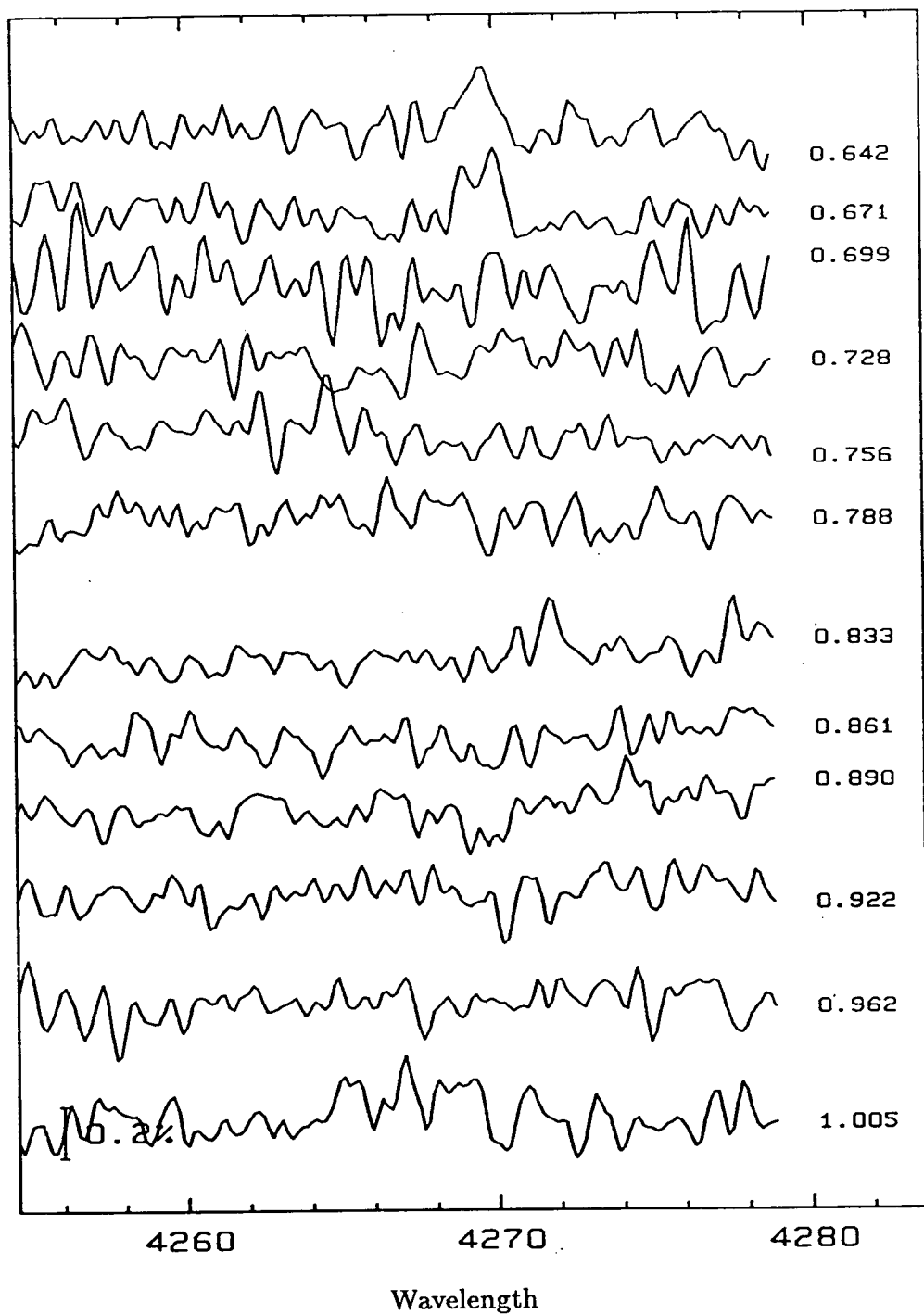Fig. 57 — The residuals formed by subtracting the mean of the 20 October 1986 C II λ 4267 line profiles presented in figure 29.

Fig. 58 — The residuals formed by subtracting the mean of the 20 October 1986 Hγ line profiles presented in figure 30.

0.629
0.644
0.653
0.666
0.673
0.684
0.693

0.722
0.729
0.743
0.753
0.768
0.779
0.793
0.802
0.821
0.830
0.844
0.852
0.867
0.878
0.892
0.904

0.931

0.2%

4380   4390   4400

Wavelength

Fig. 59 — The residuals formed by subtracting the mean of the 20 October 1986 He I λ 4388 line profiles presented in figure 31.

Fig. 60 — The residuals formed by subtracting the mean of the 20 October 1986 He I λ 4471 and Mg II λ 4481 line profiles presented in figure 32.

0.637
0.662
0.691
0.721
0.763
0.788
0.810
0.831
0.856
0.885
0.927
0.963
0.999

0.2%

4260   4270   4280

Wavelength

Fig. 61 — The residuals formed by subtracting the mean of the 22 September 1987 C II λ 4267 line profiles presented in figure 33.
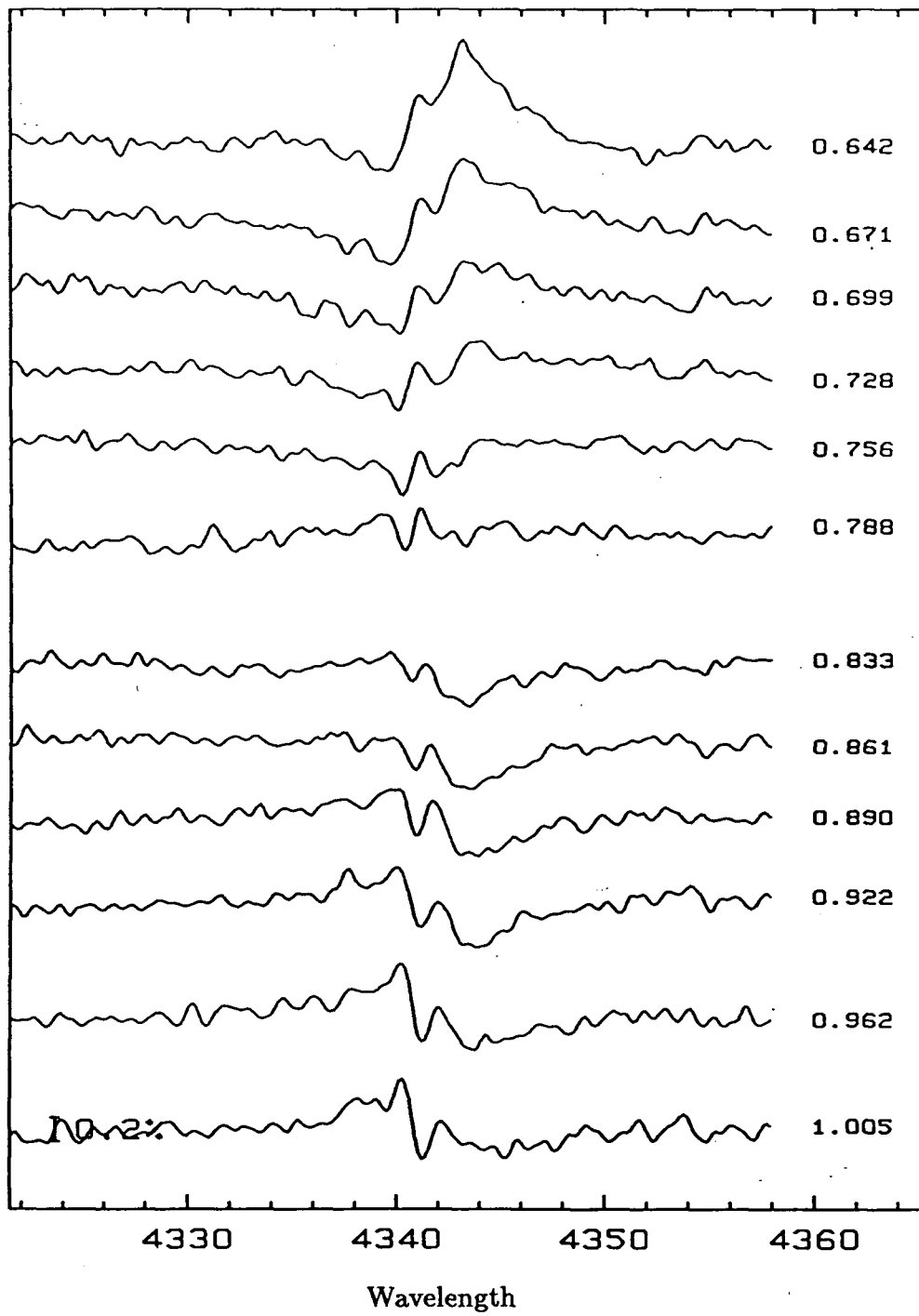
115

Fig. 62 — The residuals formed by subtracting the mean of the 22 September 1987 Hγ line profiles presented in figure 34.
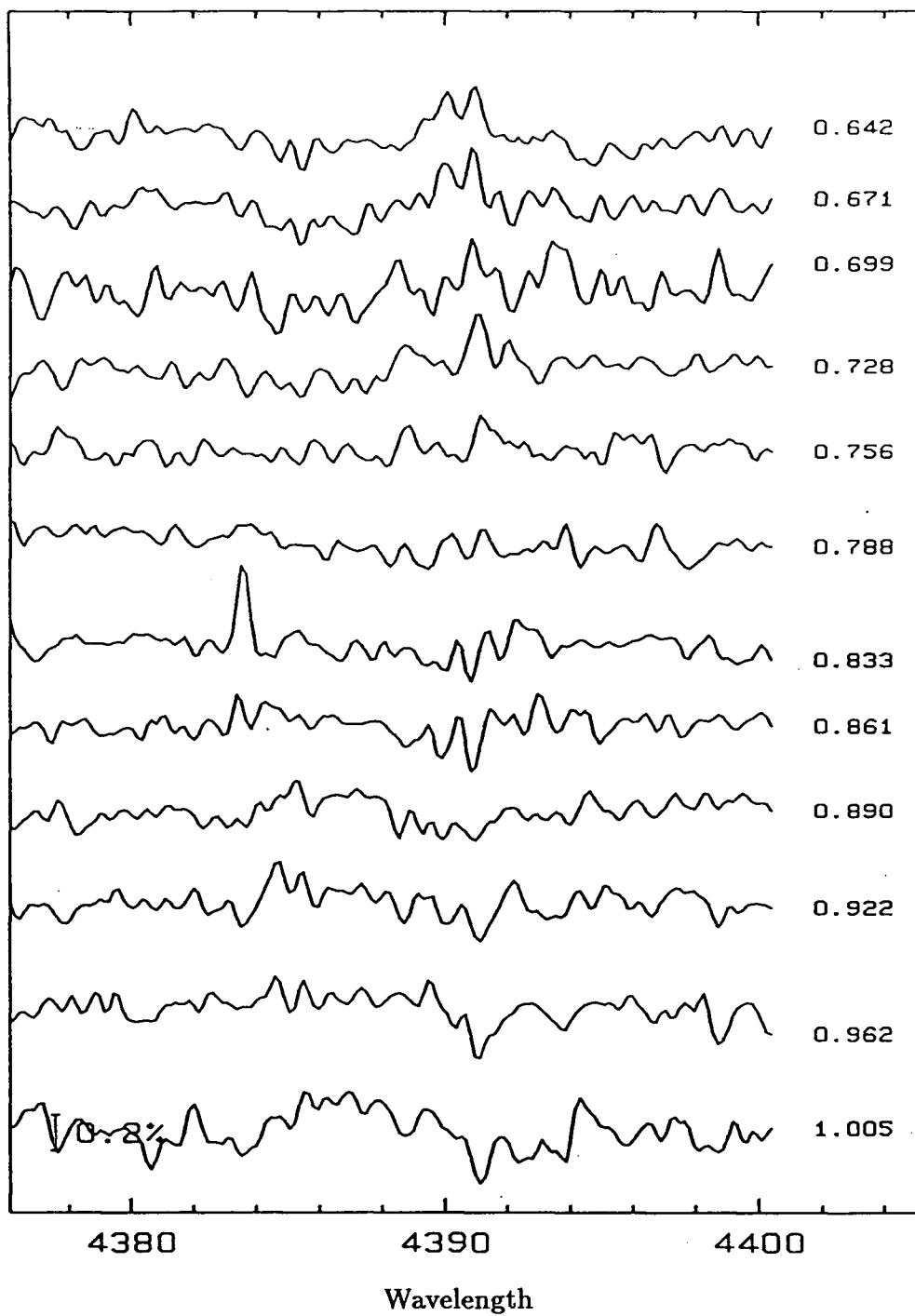
Fig. 63 — The residuals formed by subtracting the mean of the 22 September 1987 He I λ 4388 line profiles presented in figure 35.
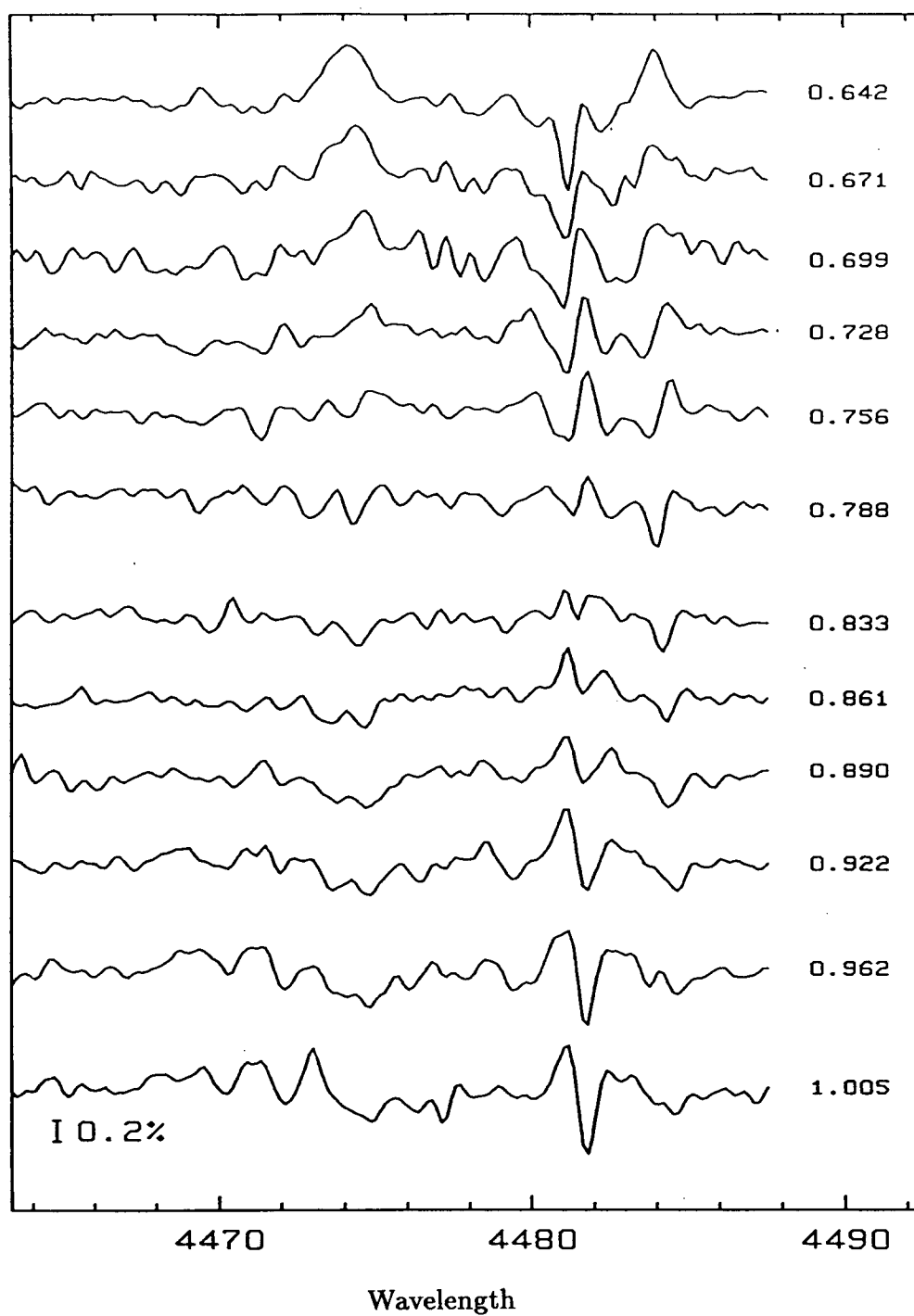
Fig. 64 — The residuals formed by subtracting the mean of the 22 September 1987 He I
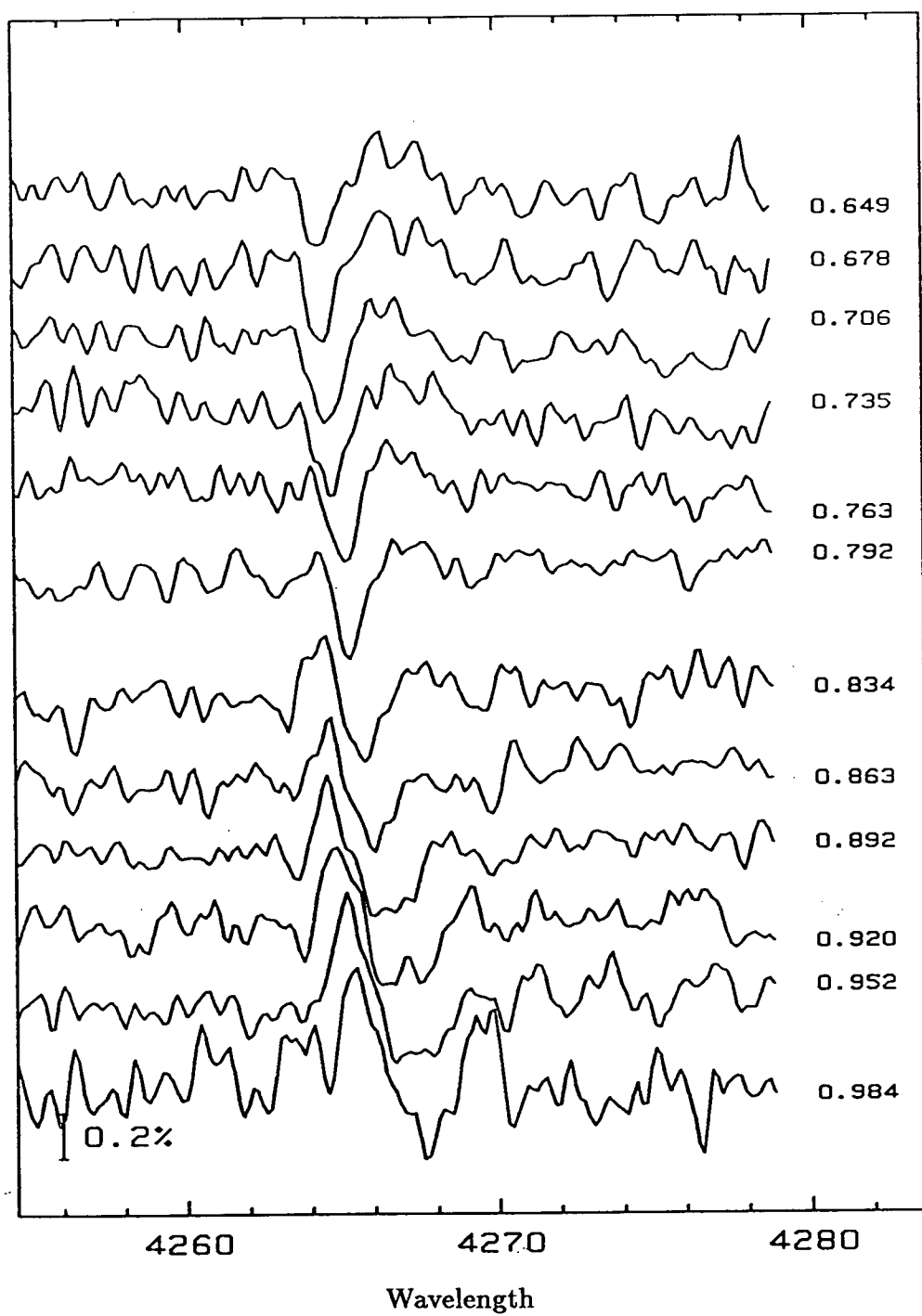λ 4471 and Mg II λ 4481 line profiles presented in figure 36.

Fig. 65 — The residuals formed by subtracting the mean of the 23 September 1987 C II λ 4267 line profiles presented in figure 37.

Fig. 66 — The residuals formed by subtracting the mean of the 23 September 1987 Hγ line profiles presented in figure 38.

120

Fig. 67 — The residuals formed by subtracting the mean of the 23 September 1987 He I λ 4388 line profiles presented in figure 39.

Fig. 68 — The residuals formed by subtracting the mean of the 23 September 1987 He I λ 4471 and Mg II λ 4481 line profiles presented in figure 40.

Fig. 69 — The residuals formed by subtracting the mean of the 24 September 1987 C II λ 4267 line profiles presented in figure 41.
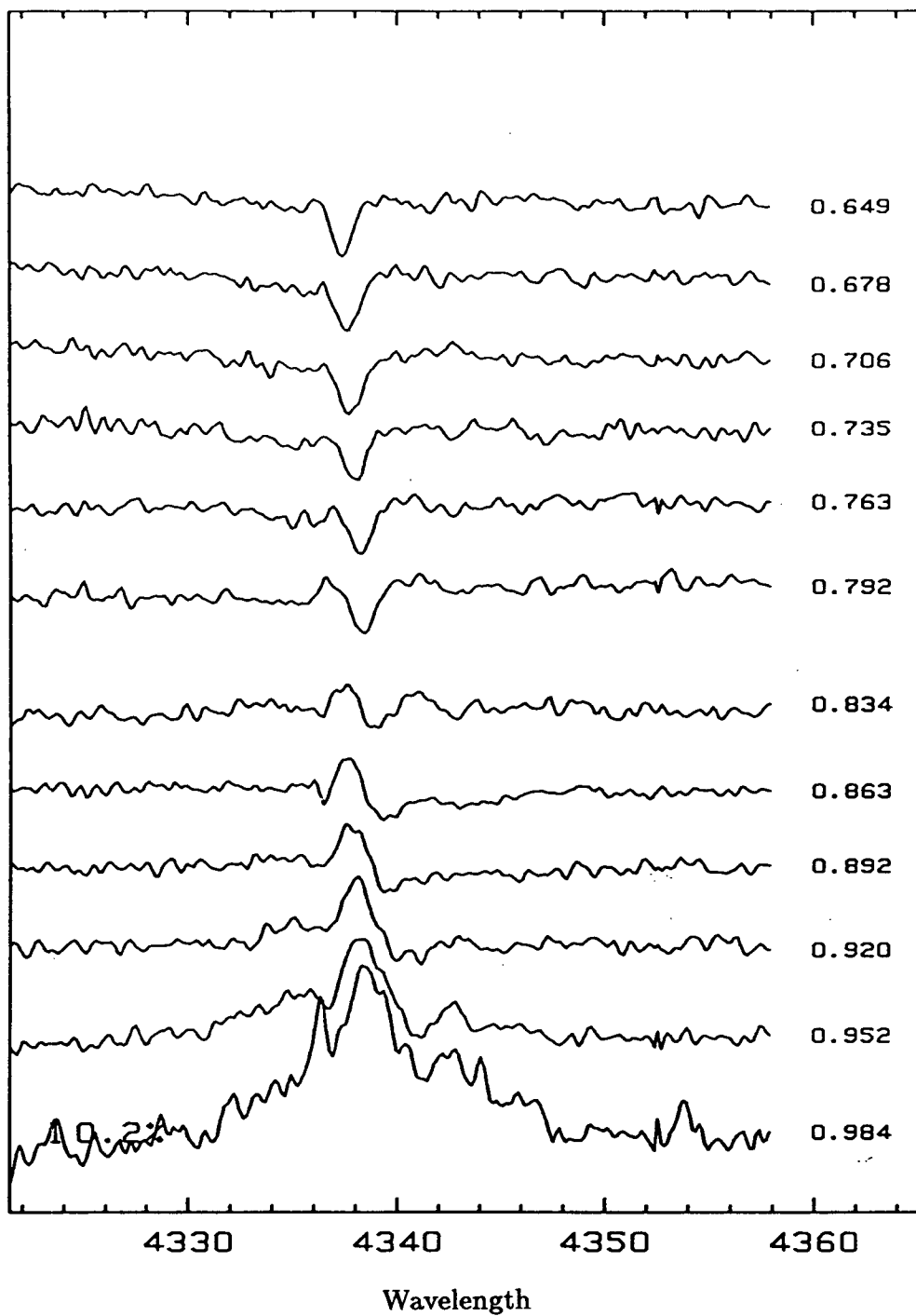
Fig. 70 — The residuals formed by subtracting the mean of the 24 September 1987 Hγ line profiles presented in figure 42.

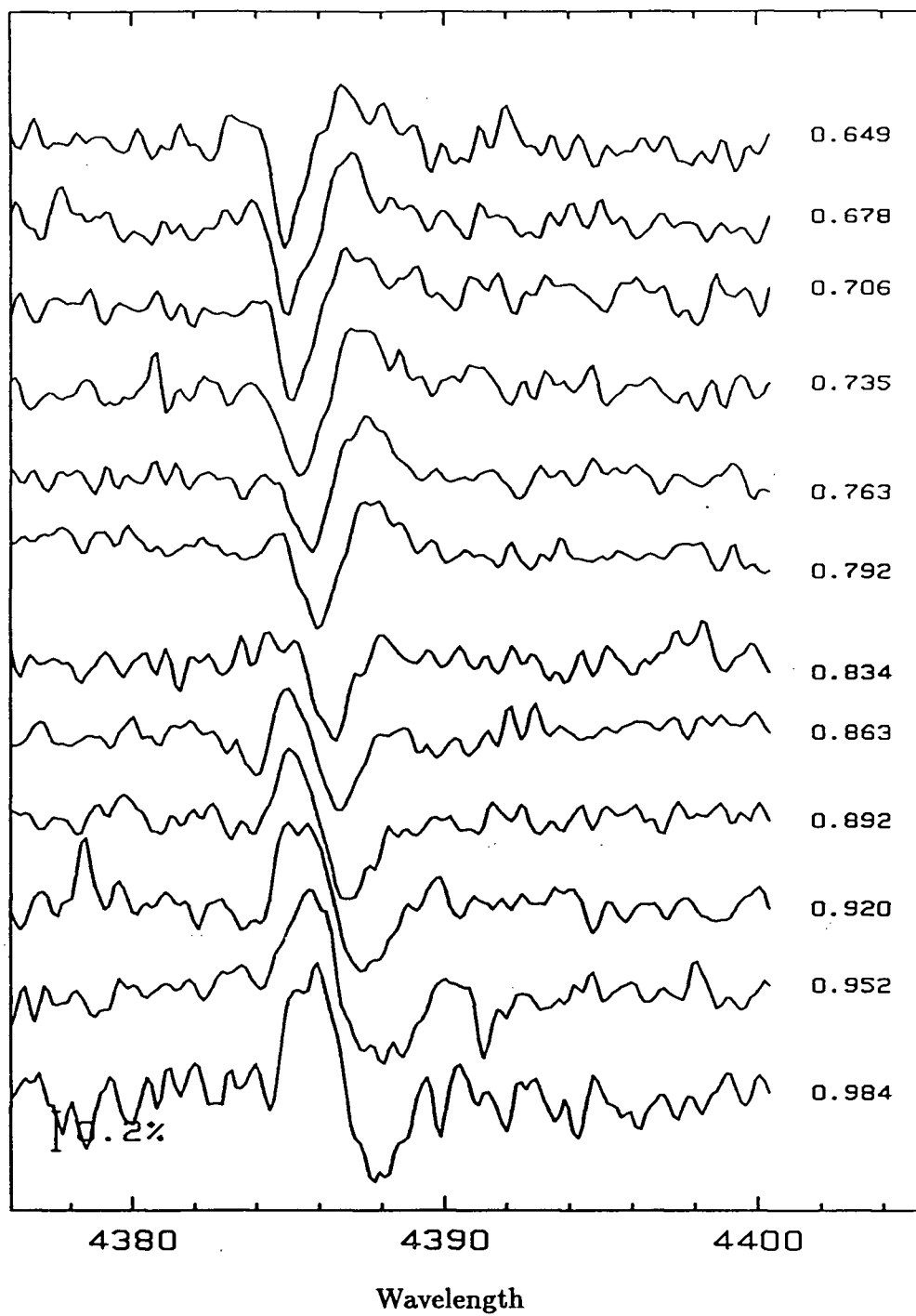Fig. 71 — The residuals formed by subtracting the mean of the 24 September 1987 He I
λ 4388 line profiles presented in figure 43.

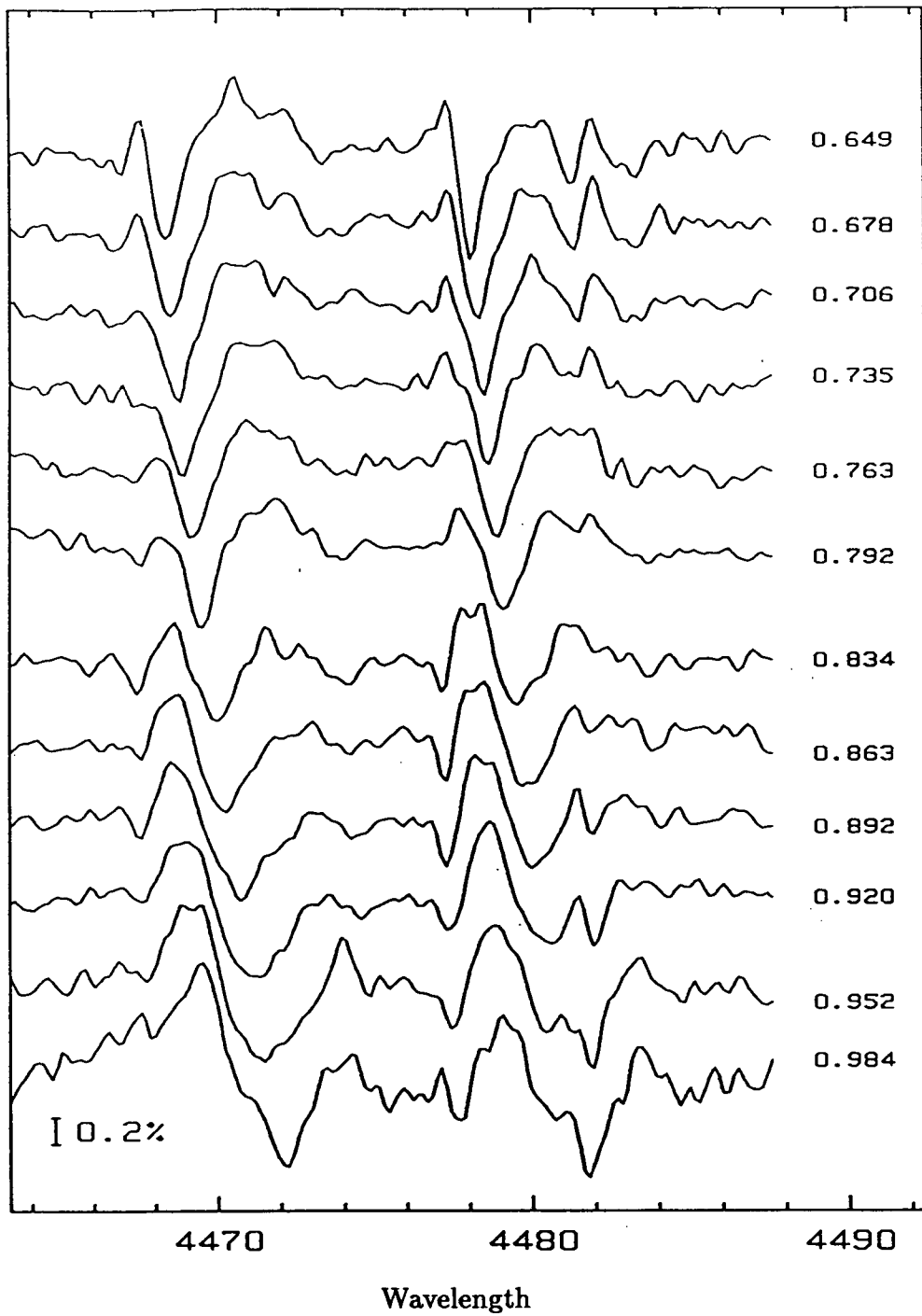Fig. 72 — The residuals formed by subtracting the mean of the 24 September 1987 He I λ 4471 and Mg II λ 4481 line profiles presented in figure 44.